

Alma Mater Studiorum – Università di Bologna

DOTTORATO DI RICERCA IN

Ingegneria Civile, Ambientale e dei Materiali

Ciclo XXVII

Settore Concorsuale di afferenza: 08/A1

Settore Scientifico disciplinare: ICAR 01

Dynamics of coastal aquifers: data-driven forecasting and risk analysis

Presentata da: Giada Felisa

Coordinatore Dottorato

Prof. Alberto Lamberti

Relatore

Prof. Vittorio Di Federico

Correlatori

Prof. Daniel M. Tartakovsky

Dott. Ing. Valentina Ciriello

Esame finale anno 2015

Contents

Abstract	7
1 Introduction	9
1.1 Saltwater intrusion in coastal aquifers	9
1.2 Methodology	11
1.3 Research outline	14
2 Analytical models for saltwater intrusion	17
2.1 Saltwater intrusion models	17
2.2 Estimation of saltwater wedge	19
2.2.1 Saltwater intrusion and natural recharge.....	21
2.2.2 Saltwater intrusion and pumping wells	23
2.3 Risk analysis of saltwater intrusion.....	25
2.3.1 Risk assessment for coastal vegetation due to saltwater intrusion (natural recharge).....	26
2.3.1.1 Problem formulation	26
2.3.1.2 Approach validation.....	28
2.3.1.3 Results and discussion.....	29
2.3.2 Risk assessment for coastal vegetation due to saltwater intrusion (pumping wells).....	32
2.3.2.1 Problem formulation.....	32
2.3.2.2 Results and discussion.....	36
2.4 Conclusions	44

3	Characterization of the study area	47
3.1	Coastal phreatic aquifer of Emilia-Romagna.....	47
3.2	Main characteristics of Ravenna phreatic aquifer.....	48
3.2.1	Geological evolution.....	51
3.2.2	Stratigraphic evolution.....	52
3.2.3	Surface geology and paleodunes.....	54
3.2.4	Recent evolution of coastline.....	55
3.2.5	Topography and subsidence.....	57
3.2.5.1	Land subsidence.....	58
3.2.5.2	Land use.....	60
3.2.6	Hydrology of the area.....	61
3.3	Monitoring of the aquifer.....	66
3.3.1	Emilia-Romagna Region survey network.....	66
3.3.2	University of Bologna (Ravenna) survey network.....	71
3.4	Focus on south Ravenna.....	77
4	Methodology	81
4.1	Time series analysis	81
4.2	Time series as a stochastic process.....	83
4.3	Stationary stochastic process	86
4.3.1	Invertibility assumption.....	89
4.3.2	Ergodicity and estimation of the moments of a stationary process.....	90
4.4	From non-stationary to stationary time-series.....	91
4.4.1	Estimating and removing trend component.....	93
4.4.2	Estimating and removing seasonal component.....	94
4.5	Main stationary stochastic process	95

4.5.1	Autoregressive processes AR(p).....	95
4.5.2	Moving average processes MA(q).....	96
4.5.3	Autoregressive moving average processes ARMA(p,q).....	96
4.6	Box-Jenkins procedure.....	98
4.6.1	Model identification and parameters estimation...	98
4.6.2	Testing goodness-of-fit of the model.....	100
4.7	Time series analysis with linear model.....	101
4.7.1	Static linear models.....	101
4.7.1.1	Simple linear regression model.....	101
4.7.1.2	Multiple linear regression model.....	103
4.7.2	Dynamic models.....	105
4.7.2.1	Distributed lag model.....	105
4.7.2.2	Autoregressive distributed lag model.....	108
5 Results and discussion		109
5.1	Application of time series analysis	109
5.2	Time delay among natural recharge and phreatic level....	110
5.3	Characteristics of the area.....	116
5.4	Stationarity of time series.....	117
5.5	Application of the ARDL model on time series: rainfalls - phreatic level.....	123
5.5.1	Testing residuals and stability of the process.....	127
5.5.2	Comparison between other rainfall/water table time series.....	129
5.6	Application of the ARDL model on time series: pumping - phreatic level and rainfalls - pumping.....	132
5.6.1	ARDL between phreatic level and pumping time series.....	133

6 | Contents

5.6.2 ARDL between rainfall and pumping time series.....	135
5.7 Application of the generic static model on time series: phreatic level - top salinity.....	137
5.8 Forecasting time series.....	139
6 Conclusions	145
Appendix A	147
Appendix B	153
References	169
Ringraziamenti	183

Abstract

This work is focused on the study of saltwater intrusion in coastal aquifers, and in particular on the realization of conceptual schemes to evaluate the risk associated with it.

Saltwater intrusion depends on different natural and anthropic factors, both presenting a strong aleatory behaviour, that should be considered for an optimal management of the territory and water resources. Given the uncertainty of problem parameters, the risk associated with salinization needs to be cast in a probabilistic framework. On the basis of a widely adopted sharp interface formulation, key hydrogeological problem parameters are modeled as random variables, and global sensitivity analysis is used to determine their influence on the position of saltwater interface. The analyses presented in this work rely on an efficient model reduction technique, based on Polynomial Chaos Expansion, able to combine the best description of the model without great computational burden.

When the assumptions of classical analytical models are not respected, and this occurs several times in the applications to real cases of study, as in the area analyzed in the present work, one can adopt data-driven techniques, based on the analysis of the data characterizing the system under study. It follows that a model can be defined on the basis of connections between the system state variables, with only a limited number of assumptions about the "physical" behaviour of the system.

1. Introduction

1.1 SALTWATER INTRUSION IN COASTAL AQUIFERS

Groundwater contamination caused by saltwater intrusion in coastal aquifers is a global issue, affecting water quality, vegetation, and soil conditions [Rodriguez *et al.*, 2007; Antonellini and Mollema, 2010]. Freshwater stored in coastal aquifers is particularly vulnerable to degradation due to (i) its close proximity to seawater, and (ii) the significant water demand associated with coastal areas, whereby groundwater is often the main source of drinking water [Werner *et al.*, 2013].

The fragile equilibrium of coastal environments is mainly compromised by climate changes and anthropic activities, that strongly affect groundwater levels. According to the IPCC's forecasts, the expected rising temperatures, during the 21st century, are contributing to sea level rise, thus encouraging the advance of saltwater wedge and increasing the salinization of soil [IPCC, 2007; Watson *et al.*, 2010; Werner *et al.*, 2009]. Furthermore, variation of rainfall regimes plays a key role in modifying the natural recharge of the aquifer, as reported in many hydrological records provided by several Environmental Agencies [e.g. ARPA - Regional Agency for Environmental Protection, Italy; NOAA - National Oceanic and Atmospheric Administration, USA] and scientific studies [e.g., Henry *et al.*, 2011; Mollema *et al.*, 2013]. Regarding to human activities, increasing urbanization along coastal areas and over-exploitation of natural resources,

enhance these effects and may induce a strong subsidence. This phenomenon is part of the natural development of floodplains and represents the result of deep downward tectonic movement and compaction of geologically recent deposits [Kooi, De Vries, 1998; Meckel *et al.*, 2007]; nevertheless, it is also produced by groundwater and gas extraction [Teatini *et al.*, 2006; Gambolati *et al.*, 1999]. Anthropogenic subsidence is usually predominant, with rates up to three times compared with the natural component, leading many areas exposed to several hazards, as flooding by river inundations or sea storms, local inversion of water flow within river and artificial channels, loss of land and consequently variations of coastline. Different land uses and the spatial variability of hydraulic parameters, e.g. hydraulic conductivity and porosity of the aquifer, can also enhance the risk of increase in salinity, creating preferential flow paths [Yang *et al.*, 2014; Vandenbohede *et al.*, 2014]. Climate variations, groundwater pumping and fluctuating sea levels impose dynamic hydrologic conditions, which are interrelated with the distribution of dissolved salts through water density-salinity relationships.

Over the last several decades, saltwater intrusion has become a crucial issue in Italy, as denoted by many studies conducted on different coastal areas [Capaccioni *et al.*, 2005; De Luca *et al.*, 2004]. This phenomenon represents a serious threat along the coast of Emilia-Romagna, as it is combined with a strong anthropogenic subsidence, only partially limited in recent years. The presence of vegetation and complex ecosystems in such areas (i.e., lagoons, marshes, and pine forests), also increases potential adverse impacts from an ecological point of view: understanding the mechanisms whereby these sensitive environments/ecosystems can be affected by saltwater intrusion represents a critical research challenge, as evidenced by recent literature findings [Manfreda, Caylor, 2013].

1.2 METHODOLOGY

For more than 50 years, intensive research effort has been focused on understanding better coastal aquifer flow and transport processes, enhancing coastal water security, and avoiding environmental degradation of coastal systems [Werner *et al.*, 2013, and references therein]. Coastal hydrogeology spans many fields, e.g. saltwater intrusion, submarine groundwater discharge, beach-scale hydrology, sub-seafloor hydrogeology, and studies on geological timescales involving coastline geomorphology. However, coastal aquifer hydrodynamics and saltwater intrusion remain challenging to measure and quantify, as commonly used models and field data are difficult to reconcile, and predictions of future coastal aquifer functioning are relatively uncertain across both regional and local scales [e.g. Sanford, Pope, 2010].

The velocity fields characterizing the two fluids, i.e. freshwater and saltwater, can be modelled following two different methodologies [Bolster *et al.*, 2007]. The first postulates the existence of a sharp interface separating the fresh and saltwater, with results strictly valid for advection-dominated systems. This assumption allows the use of potential theory to derive analytical solutions for the location of this interface [e.g., Strack, 1976; Huppert, Woods, 1995; Najii *et al.*, 1998; Kacimov and Obnosov, 2001]. The second methodology explicitly accounts for the existence of a transitional zone, with a model consisting of a variable density (Darcy) flow equation coupled with the advection-diffusion equation for the transport of salt. Even for the simplest geometries of a flow domain, this coupling makes it difficult to obtain analytical solutions, which are essential for the testing and validation of numerical codes. To the best of our knowledge, the Henry [Henry, 1964] formulation of variable density

flow in coastal aquifers provides the only mathematical setting for which analytical solutions are available.

Risk assessment related to saltwater intrusion represents a big challenge due to the complexity of the problem. Mathematical models of subsurface flow and transport are routinely used to describe the phenomenon, but heterogeneity of the aquifer and an incomplete knowledge of the data, combined with structural uncertainties of the models themselves, represent important and essential issues. The model predictions are consequently affected by uncertainties, whose evaluation is fundamental in order to describe correctly the environmental systems.

Different models can be used to describe saltwater intrusion as good as possible. The most suitable approach is to rely on full stochastic models, able to consider all the parameters involved in the problem as random variables, but this leads to great computational burdens. In order to decrease this computational effort and maintain high levels of description of the problem, simplified probabilistic models have been proposed in several studies [*Winter and Tartakovsky, 2008; Tartakovsky, 2007; Neumann, 2003; Neumann et al., 2012*]. To combine accuracy and improvement of computation burden, a good alternative is represented by the adoption of model reduction techniques, i.e. surrogate models that simplify the original model maintaining interpretive features [*Sudret, 2008; Ciriello et al., 2013; Xiu and Karniadakis, 2002*].

Structural and parametric uncertainties ensure that risk assessment of saltwater intrusion should be evaluated following a stochastic approach, introducing simplified models able to conserve a suitable descriptive level of the phenomenon [*Tartakovsky, 2012; Tartakovsky, 2007*]. This methodology is applied in several fields, from nuclear and aerospace

engineering to subsurface hydrology recently [Tartakovsky, 2007; Bolster et al., 2009; Jurado et al., 2012].

Characterizing ground water salinization and recognizing the important driving processes in a low coastal plain is challenging given the number of factors involved. Among these factors, the most critical are: low water table level, insufficient aquifer recharge, sea water encroachment along rivers and canals, land reclamation drainage, water pumping from wells, up-welling of connate water from the bottom of the aquifer, evapotranspiration, natural and anthropogenic land subsidence (Bear et al. 1999; Post et al. 2003; Antonellini et al. 2008).

Analytical and numerical modeling [Bear et al., 1999; Cheng et al., 2001; Langevin et al., 2007] are among the methods usually employed to identify the driving mechanisms and their contributions to the process of ground water salinization. Many published works show how these methods work well if the factors controlling ground water salinization are few and constrained [Bear et al., 1999] or the amount of data available is extensive [Post et al., 2003; Oude Essink et al., 2010]. When these situations do not occur, e.g. as in the case of Ravenna aquifer, the applications of analytical and numerical modelling have only limited success in characterizing the phenomenon. For this reason, other approaches can be properly adopted, as data driven techniques based on the analysis of the data characterizing the system under study, in order to understand the fundamental processes controlling salinization of a coastal shallow aquifer where multiple drivers are at work [Solomatine, Ostfeld, 2008]. In this framework, time series analysis plays a key role, able to define the history of each parameter involved in the process, and to describe the link among them [Machiwal, Jal, 2012; Hanson et al., 2006; Koutsoyiannis, Montanari, 2007].

1.3 RESEARCH OUTLINE

The overall aim of this thesis is the study of the phenomenon of saltwater intrusion in coastal aquifers, and in particular the realization of conceptual schemes related to the risk associated with it.

Chapter 2 illustrates analytical models describing saltwater intrusion, i.e. the movement of seawater inland, under the assumption of sharp interface. In this section, two typical situations are presented in order to estimate the extension of saltwater wedge, and consequently the risk associated to an undesired event, e.g. an elevation of the interface between the two fluids that can affect coastal vegetation. The first considers only the presence of natural recharge, while the second case represents the risk associated with the presence of a pumping field, at a certain distance from the coast. In these studies, the parameters involved in the model are modelled as random variables. In particular, model reduction techniques, e.g. Polynomial Chaos Expansion, have been used to compute the first two moments associated with the response of the model and to provide informations about the importance of each parameters, relying on Global Sensitivity Analysis.

Chapter 3 presents the area object of study, i.e. the coastal phreatic aquifer of Ravenna, Emilia-Romagna, a very young territory where the process of salinization, both due to saltwater intrusion and to dissolved salts in the aquifer itself, is particularly intensive, threatening precious and protected environments. In this context, the physical approach provided by analytical models do not work, because of an inverse flow from sea to inland that is not included in the assumptions of classical models.

To achieve the goal of representing the relationships among the factors describing the salinization process, data driven techniques, i.e. time

series analysis, are illustrated in Chapter 4. Considering every time series of the parameters involved as a single realization of a stochastic process, it is possible to model the parameters, i.e. rainfalls, water table of the aquifer, pumping discharge, salinization at water table level, and to describe the relationships among them.

Chapter 5 shows the results of these analyses. Once time series have been turned into stationary processes, models are first calibrated and then validated, with the aim to understand the dependence of water table, and consequently the salinization, from driving forces, i.e. natural recharge and pumping discharge of wells.

Chapter 6 presents the conclusion of the dissertation.

2. Analytical models for saltwater intrusion

2.1 SALTWATER INTRUSION MODELS

In general, in coastal aquifers a hydraulic gradient exists toward the sea, that serves as a recipient for the excess of fresh groundwater [Bear, 1979]. The presence of seawater in the aquifer formation under the sea bottom is responsible for the creation of a zone of contact with freshwater, due to the different specific weights of fluids. Indeed, there exists a body of seawater, often in a form of a wedge, underneath the freshwater.

The fluids are actually miscible, consequently the zone of contact among them takes the form of a transition zone governed by hydrodynamic dispersion, where the density of mixed water varies from freshwater to seawater. However, under certain conditions, the width of this zone is small compared with the thickness of the aquifer, hence it is possible to assume the abrupt interface approximation to model the dynamic of fluids.

While under natural undisturbed conditions the interface maintains a state of equilibrium, water extraction in excess of replenishments lowers the water table with respect to its initial position, allowing the interface to move inland. This phenomenon is called seawater intrusion, or encroachment. As the pumping rate increases, the interface between the fluids advances towards the well, until an unstable critical situation is reached. Any further increase in the pumping rate causes a jump of the toe

position landward of the well, which thereby becomes contaminated by saltwater.

In recent years, numerical approaches have been increasingly adopted to represent the detailed and complex processes involved in saltwater intrusion [Werner *et al.*, 2013]. The characterization of the mixing zone as well as the evolution of intrusion temporally represent some applications in which the adoption of numerical models is relevant [Henry, 1959; Servan-Camas *et al.*, 2010]. Similarly, analytical formulations can provide a prompt insight into relevant physical processes involved and, for this reason, a significant number of studies have been conducted in this realm [Cheng *et al.*, 2000; Mantoglou, 2003; Mantoglou *et al.*, 2008; Werner *et al.*, 2012]. In particular, the theory developed by Strack [1976] based on the sharp interface approximation, has been widely adopted to predict the extension of saltwater intrusion in steady-state flow under the Dupuit-Forchheimer assumption [Najii *et al.*, 1998; Lu *et al.*, 2012].

In the overall discussion, we refer to sharp interface assumption to predict the position of saltwater-freshwater interface.

2.2 ESTIMATION OF SALTWATER WEDGE

In the following, the theory developed by *Strack* [1976] is used to predict the extension of saltwater intrusion into a coastal phreatic aquifer, for the case of steady state flow under the Dupuit - Forchheimer assumption, whereby it is possible to neglect the vertical component of the specific flow vector.

The sharp interface approximation and the homogeneity assumption allow for the derivation of a closed form solution that describes the main processes involved in saltwater intrusion. Consider a semi-infinite domain bounded by a straight coastline and divided into two zones, as depicted in Figure 2.1, with freshwater in zone 1 and freshwater and saltwater in zone 2. The aquifer thickness b [L] is:

$$b = h_f \quad \text{zone 1} \quad (2.1a)$$

$$b = h_f - d + \xi \quad \text{zone 2} \quad (2.1b)$$

where d [L] is the mean sea level with respect to the bottom of the aquifer, ξ [L] the interface depth with respect to mean sea level, h_f [L] the hydraulic head, and q [L^2T^{-1}] represents the uniform discharge to the sea per unit width of aquifer [*Cheng and Ouazar, 1999*]. In zone 2, the Ghyben-Herzberg assumption, i.e. $h_f - d = ((\gamma_s - \gamma_f)/\gamma_f) \xi$, is imposed to express the relationship between hydraulic head and interface depth, with respect to mean sea level.

Following the theory of *Strack* [1976] for an unconfined aquifer, the potential ϕ [L^2] is defined as:

$$\phi = \frac{1}{2} \left[h_f^2 - \frac{\gamma_s}{\gamma_f} d^2 \right] \quad \text{zone 1} \quad (2.2a)$$

$$\phi = \frac{1}{2} \frac{\gamma_s}{\gamma_s - \gamma_f} (h_f - d)^2 \quad \text{zone 2} \quad (2.2b)$$

These functions and their first derivatives are continuous across the multiple-zone aquifer and satisfy the Laplace equation, $\nabla^2 \phi = 0$, in the x - z plane. At the interface, substituting in Equation (2.2a) or (2.2b) the condition $\xi = d$, hence $h_f = (\gamma_s/\gamma_f) \xi$, the potential is:

$$\phi_{toe} = \frac{1}{2} \frac{\gamma_s(\gamma_s - \gamma_f)}{\gamma_f^2} d^2 \quad (2.3)$$

The estimation of saltwater intrusion needs additional conditions to be characterized, as discussed in the following Sections.

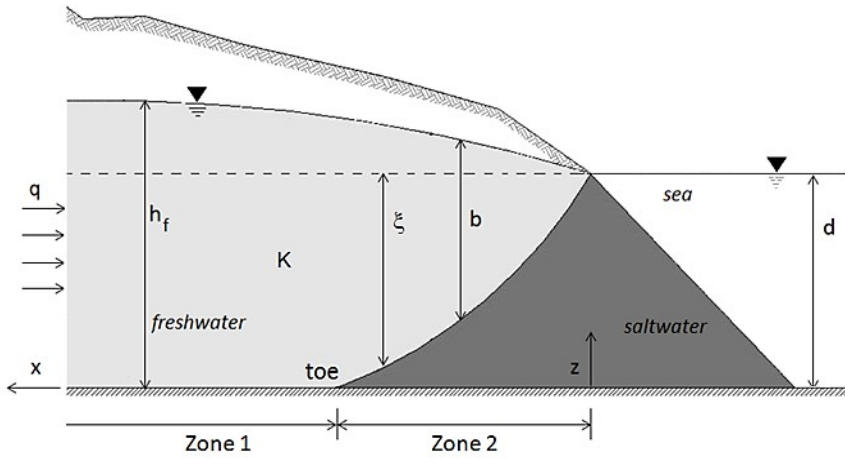


Figure 2.1 Reference unconfined aquifer with saltwater wedge.

2.2.1 SALTWATER INTRUSION AND NATURAL RECHARGE

Consider a vertical section of a phreatic aquifer, with constant natural recharge, as depicted in Figure 2.2, where q [L^2T^{-1}] is the uniform discharge to the sea per unit width of aquifer, W [LT^{-1}] is the natural recharge, and K is the hydraulic conductivity [LT^{-1}].

In this situation, the governing equation of the phenomenon and the boundary conditions result:

$$\frac{d^2\phi}{dx^2} = -\frac{W}{K} \tag{2.4}$$

$$\phi(0) = 0 \tag{2.5}$$

$$\frac{d\phi}{dx}(L) = \frac{q}{K} \tag{2.6}$$

The resulting solution is obtained as:

$$\phi_{res} = -\frac{W}{2K}x^2 + \left(\frac{q}{K} + \frac{WL}{K}\right)x \tag{2.7}$$

By combining Equations (2.7) and (2.3), it is possible to estimate the resulting position of the toe from the coast, i.e. x_{toe} , for this case study:

$$x_{toe} = \frac{q}{W} + L - \sqrt{\left(\frac{q}{W} + L\right)^2 - \frac{K}{W} \frac{\gamma_s(\gamma_s - \gamma_f)}{\gamma_f^2} d^2} \tag{2.8}$$

Similarly, considering the expressions for the potential in zone 1 and zone 2 [Strack, 1976] allows to define the elevation of the hydraulic head above the mean sea level:

$$h_f - d = \sqrt{2\left(\frac{q + WL}{K}\right)x - \frac{W}{K}x^2 + \frac{\gamma_s}{\gamma_f}d^2} - d \quad \text{zone 1} \tag{2.9a}$$

$$h_f - d = \sqrt{\frac{\gamma_s - \gamma_f}{\gamma_s} \left[2 \left(\frac{q + WL}{K} \right) x - \frac{W}{K} x^2 \right]} \quad \text{zone 2} \quad (2.9b)$$

Finally, the depth of the interface results:

$$\xi = d \quad \text{zone 1} \quad (2.10a)$$

$$\xi = \frac{\gamma_f}{\gamma_s - \gamma_f} (h_f - d) \quad \text{zone 2} \quad (2.10b)$$

where the latter derives from Ghyben-Herzeber assumption.

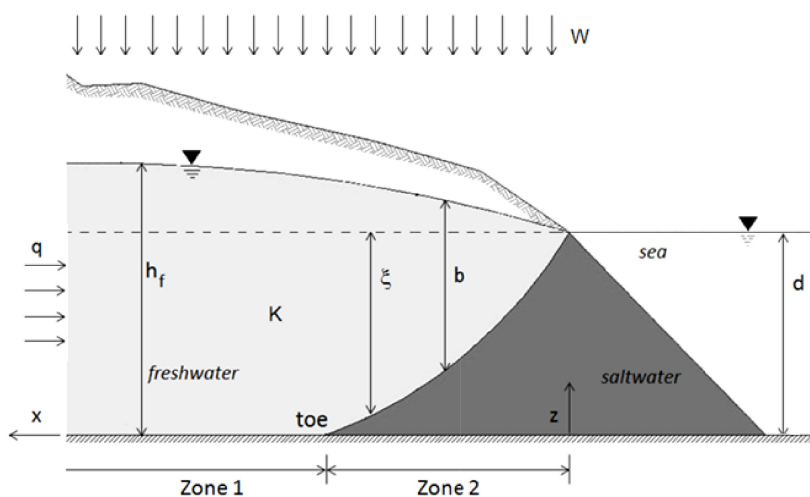


Figure 2.2 Reference scheme of a vertical section of phreatic aquifer, with constant natural recharge.

2.2.2 SALTWATER INTRUSION AND PUMPING WELLS

In the following, the presence of a pumping/recharging well with discharge Q_w [L^3T^{-1}], located at a distance x_w from the coast is considered, as depicted in Figures 2.3(a), 2.3(b).

The solution of the problem, in terms of potential, can be found by resorting to the superposition principle and the method of images as [Strack, 1976]:

$$\phi = \frac{q}{K}x + \frac{Q_w}{4\pi K} \ln \left[\frac{(x - x_w)^2 + y^2}{(x + x_w)^2 + y^2} \right] \quad (2.11)$$

The location of the leading edge, or “toe”, of the saltwater wedge can be computed from Equations (2.3) and (2.11) as:

$$\phi_{toe} = \frac{q}{K}x_{toe} + \frac{Q_w}{4\pi K} \ln \left[\frac{(x_{toe} - x_w)^2 + y^2}{(x_{toe} + x_w)^2 + y^2} \right] \quad (2.12)$$

Finally, combining expressions (2.2a) and (2.2b) with (2.11) allows for the determination of the elevation of the hydraulic head above mean sea level, for zone 1 and 2 respectively:

$$h_f - d = \sqrt{\frac{2q}{K}x + \frac{Q_w}{2\pi K} \ln \left[\frac{(x - x_w)^2 + y^2}{(x + x_w)^2 + y^2} \right] + \frac{\gamma_s}{\gamma_f}d^2} - d \quad (2.13)$$

$$h_f - d = \sqrt{\frac{\gamma_s - \gamma_f}{\gamma_s} \left[\frac{2q}{K}x + \frac{Q_w}{2\pi K} \ln \left[\frac{(x - x_w)^2 + y^2}{(x + x_w)^2 + y^2} \right] \right]} \quad (2.13b)$$

Utilizing the Ghyben-Herzberg assumption, the interface depth is evaluated with Equations (2.13a) and (2.13b), as in the previous discussion.

For multiple pumping wells, Equation (2.11) can be extended to:

$$\phi = \frac{q}{K}x + \sum_{i=1}^n \frac{Q_i}{4\pi K} \ln \left[\frac{(x-x_i)^2 + (y-y_i)^2}{(x+x_i)^2 + (y-y_i)^2} \right] \quad (2.14)$$

where (x_i, y_i) are the coordinates, and Q_i is the pumping rate of well i , which can be taken as positive or negative to represent pumping and recharging mode, respectively. With these assumptions, Equations (2.13a) and (2.13b) become for zone 1 and 2, respectively:

$$h_f - d = \sqrt{\frac{2q}{K}x + \sum_{i=1}^n \frac{Q_i}{2\pi K} \ln \left[\frac{(x-x_i)^2 + (y-y_i)^2}{(x+x_i)^2 + (y-y_i)^2} \right] + \frac{\gamma_s}{\gamma_f}d^2 - d} \quad (2.15a)$$

$$h_f - d = \sqrt{\frac{\gamma_s - \gamma_f}{\gamma_s} \left[\frac{2q}{K}x + \sum_{i=1}^n \frac{Q_i}{2\pi K} \ln \left[\frac{(x-x_i)^2 + (y-y_i)^2}{(x+x_i)^2 + (y-y_i)^2} \right] \right]} \quad (2.15b)$$

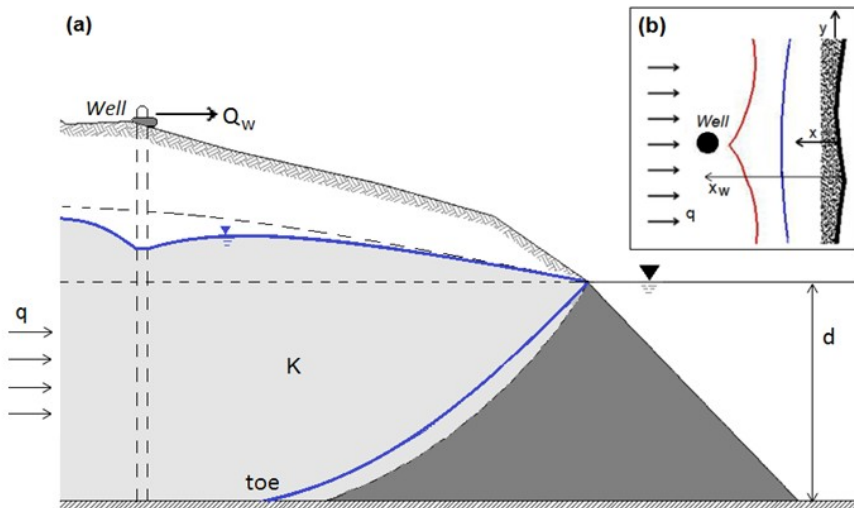


Figure 2.3 (a) Effect of a pumping well on saltwater wedge, in a reference scheme; (b) saltwater intrusion fronts near the pumping well (blue and red lines), in the x - y plane, for different values of pumping rate.

2.3 RISK ANALYSIS OF SALTWATER INTRUSION

The literature on seawater intrusion is rich with several simple analytical models describing situations of potential engineering interest, to be re-examined under the viewpoint of risk analysis [*De Barros et al., 2011; Tartakovsky, 2012*]. These approaches combine, in a different fashion and with diverse boundary conditions, (i) a constant discharge towards the sea, (ii) pumping by single or multiple wells, (iii) the presence of recharge, either distributed (due to surface infiltration) or concentrated (due to a canal to protect groundwater abstraction). Further, the analysis can be conducted in phreatic or confined aquifers.

A rigorous application of risk analysis (RA) in environmental problems has been promoted by several environmental agencies and institutions [*US National Research Council, 1997; European Committees, 2003*]. In the context of climate change, taking into account the uncertainty affecting hydrological parameters is even more important to make accurate predictions. In general, uncertainties are linked to (i) the incomplete knowledge of system dynamics (epistemic uncertainty), and (ii) the randomness which is inherent to natural phenomena (aleatory uncertainty) [*Tartakovsky, 2007; Rubin, 2003*]. This uncertainty, propagating towards the state variables of interest through a selected analytical or numerical model, has to be properly considered in a probabilistic framework.

In the following two different situations, i.e. (i) natural recharge and (ii) the presence of a well field, are considered, in order to assess model sensitivity to random input parameters and evaluate the probability of an undesired event, i.e. the risk that interface reaches a sensitive area below coastal vegetation. Model sensitivity is carried out relying on model

reduction techniques, i.e. Polynomial Chaos Expansion (PCE) [see Appendix A].

2.3.1 RISK ASSESSMENT FOR COASTAL VEGETATION DUE TO SALTWATER INTRUSION (NATURAL RECHARGE)

2.3.1.1 Problem formulation

The analytical solution developed by *Strack* [1976] is considered here to predict the extension of saltwater intrusion in the case of steady state flow under the Dupuit-Forchheimer and the Ghyben-Herzberg assumptions, as discussed in Section 2.2.1. In order to evaluate the impact of saltwater intrusion on coastal vegetation, the simplified scheme depicted in Figure 2.4 is adopted, in which saltwater intrusion threatens a sensitive area below coastal vegetation. This situation is typical in the coastal region of Emilia-Romagna, Italy.

In a probabilistic framework, the extension of saltwater wedge, and all dependent variables linked to it, is a function of the most significant hydro-geological parameters involved, represented as random variables, e.g.:

$$x_{toe} = \Phi(d, q, W, K) \quad (2.16)$$

The aim of the study consists in the identification of the probability that sensitive area below vegetation roots, having a thickness equal to w , comes next to saltwater interface under a fixed security distance, f . Identifying the corner of the sensitive area closer to the saltwater/freshwater interface through its coordinates (x^*, z^*) , the resulting depth of the bottom of the sensitive area at x^* is $z^* - w$ (Figure 2.4).

To solve the problem, first it is necessary to define an hypothetic future scenario of interest related to sea level rise in order to attain a value for mean sea level, \tilde{d} , with a certain associated probability, i.e. $P(d = \tilde{d})$. For the results presented in the following, this first step is substituted with the attribution of a deterministic value for d . Consequently, defined the probability distribution functions *pdf* for the parameters retained uncertain, i.e. q, W, K , it is possible to evaluate the *pdf* associated with x_{toe} , resorting to Strack theory (Sections 2.2.1) and PCE methodology, and to compute the probability that plant roots belong to zone 2:

$$P(x^* < x_{toe}) \tag{2.17}$$

The *pdf* associated with $d - \xi(x^*)$ is computed following the same approach for x_{toe} , and then the probability that the distance between the bottom of the sensitive area and saltwater interface is less than f is evaluated as:

$$\begin{aligned} P(z^* - w - f < d - \xi(x^*) | x^* < x_{toe}) = \\ = P(z^* - w - f < d - \xi(x^*)) \cdot P(x^* < x_{toe}) \end{aligned} \tag{2.18}$$

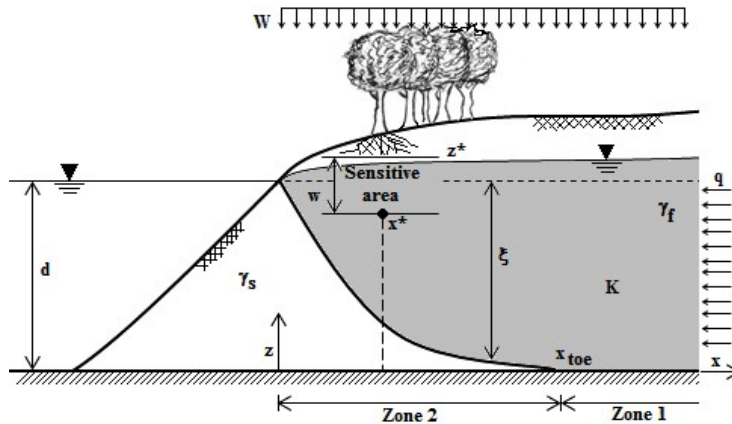


Figure 2.4 Reference scheme of the case study, with natural recharge W .

2.3.1.2 Approach validation

Starting from the formulation reported in Section 2.2.1, *Cheng and Ouazar* [1999] resort to the Small Perturbation Theory (SPT) in order to derive analytical expressions for the first two statistical moments associated with x_{toe} [*Naji et al.*, 1998]. Here, q , W , and K are modeled as independent random variables. In the following these first-order analytical expressions are compared with results obtained with the PCE theory, free of the small perturbation assumption, in order to assess the quality of the results obtainable with the PCE theory. To define the PCE, normal distributions are associated with the three input parameters. Mean values and variation coefficient (equal for all the parameters) are the same of *Cheng and Ouazar* [1999].

Figure 2.5 depicts, for different values of coefficient of variation (CV), the relative error (RE) committed in the computation of the mean and standard deviation of x_{toe} through the PCE of second order with respect to the analytical derivations in *Cheng and Ouazar* [1999]. Analyzing the results, it is possible to observe the accurate agreement attained for small values of CV (< 0.15), i.e. when the SPT represents an acceptable approximation. As expected, for increasing values of CV, the PCE method deviates from the SPT results. Furthermore, the RE in the mean value is always appreciably smaller than that one in the standard deviation. This effect is presumably caused by the fact that, for the development of the PCE, it is necessary to define the full *pdf* while the expressions in *Cheng and Ouazar* [1988] are simply functions of the first two moments. Therefore it is possible to infer that the PCE approximation is able to return accurate results for this case study even if the minimum order is adopted and high CVs are considered.

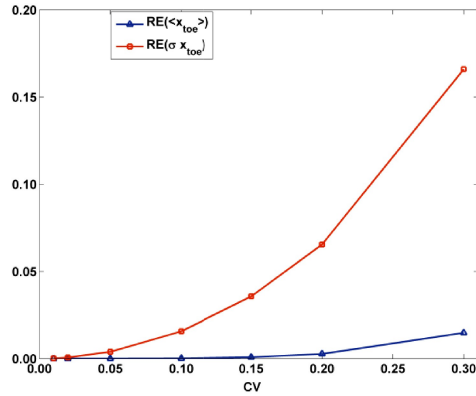


Figure 2.5 Relative error (RE) committed in the computation of the mean and standard deviation of x_{toe} through the PCE of second order with respect to the analytical derivations in *Cheng and Ouazar* [1999].

2.3.1.3 Results and discussion

Let consider the case study whose main characteristic parameters (deterministic and uncertain) are reported in Table 2.1 [*Cheng and Ouazar*, 1999]. The PCE approximation of the model response x_{toe} , expressed by Equation (2.10), is computed by resorting to the *Hermite Chaos* suitable for Gaussian processes.

Parameter	Value / Distribution
d (m)	20
L (m)	1000
q (m ² /day)	$N(\mu_q=1; CV=0.1)$
W (m/day)	$N(\mu_w=5 \cdot 10^{-3}; CV=0.1)$
K (m/day)	$N(\mu_K=70; CV=0.1)$

Table 2.1. Deterministic and uncertain parameters involved in the problem.

In Table 2.2, the Total Sensitivity Indices of Sobol, the mean and standard deviation, computed on the basis of the selected case study, are

collected. The hydraulic conductivity, K , results the most influent parameter while the effect of the uncertainty associated with the flux, q , is not significant.

Uncertain and Sensitivity Analysis on x_{toe}	Results
μ (m)	61.85
σ (m)	8.37
$S_T(q)$	0.017
$S_T(W)$	0.416
$S_T(K)$	0.570

Table 2.2. Total Sensitivity Indices of Sobol, mean and standard deviation, for the extension of saltwater wedge.

Figure 2.6 depicts the cumulative distribution function CDF, $F_{x_{toe}}$, of x_{toe} , that is Normal distributed. Considering a reasonable value for x^* of $30m$, it is possible to define the probability that the vegetation fall into the zone interested by saltwater intrusion (zone 2). For this case study results:

$$P(x^* < x_{toe}) = 1 - F_{x_{toe}}(x^*) \cong 1 \tag{2.19}$$

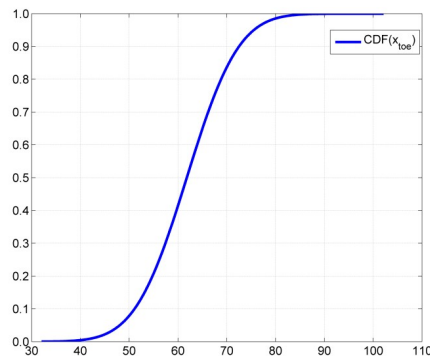


Figure 2.6 Cumulative distribution function of x_{toe} .

The same results have been derived for the vertical position of saltwater interface in x^* , i.e. $z(x^*)=d - \zeta(x^*)$. Note that the sensitivity indices for $d - \zeta(x^*)$ are qualitatively similar to those derived for x_{toe} when the relative influence of the uncertain parameter is considered (Table 2.3). In Figure 2.7 the resulting CDF of $z(x^*)$ are reported, that is again Normal distributed.

Uncertain and Sensitivity Analysis on $d-\zeta(x^*)$	Results
μ (m)	5.88
σ (m)	0.94
$S_T(q)$	0.016
$S_T(W)$	0.392
$S_T(K)$	0.592

Table 2.3. Total Sensitivity Indices of Sobol, mean and standard deviation, for the elevation of the interface.

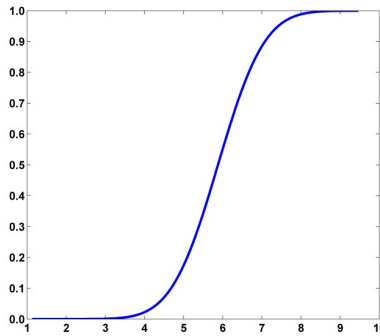


Figure 2.7 Cumulative distribution function of $z(x^*)=d - \zeta(x^*)$.

Upon fixing $z^* = 18\text{m}$, $w = 10\text{m}$, and $f = 1\text{m}$, the probability of vegetation being compromised by saltwater intrusion results:

$$P(z^* - w - f < z(x^*)) = 1 - F_{z(x^*)}(z^* - w - f) = 0.115 \tag{2.20}$$

In this simplified case study, in which the CDF functions are Normal, the computational cost associated with the PCE definition is the one strictly necessary in order to obtain the first two moments of model responses (this correspond to 10 model runs for each response). If the output distribution is unknown, it is possible to obtain the CDF functions in a Monte Carlo framework applied to the PCE surrogate model, again with a negligible associated computational cost.

2.3.2 RISK ASSESSMENT FOR COASTAL VEGETATION DUE TO SALTWATER INTRUSION (PUMPING WELLS)

2.3.2.1 Problem formulation

In order to evaluate the effects of saltwater intrusion on coastal vegetation due to both natural and anthropogenic causes, a simplified conceptualization representing specific areas of the Emilia-Romagna coast is configured (Figure 2.8) [Felisa *et al.*, 2013].

An ‘environmentally sensitive area’ representing a pinewood forest (an infinitely long strip) is located at a minimum $x^* = 50$ m from the coastline. The lower limit of the plants capture zone (the volume of soil affected by water uptake by roots) is defined such that the sensitive zone surrounding the plant is not impacted by the intruding saltwater and any adverse effects on the plants are prevented. The extension of this zone depends on both the length of roots and the width of the transpiration zone; its minimum elevation from the bottom of the aquifer is set to $z_{lim} = 12$ m in the present case. A well field established for agricultural purposes is located inland of the pinewood, as depicted in Figure 2.8. The well field is comprised of three wells, each located in the middle of an area

of dimensions $b \cdot e$, distant a from the coast. Between every pumping area there are non-overlapping zones of width equal to c , to reduce mutual interactions among the wells. The total discharge Q is equally divided among the wells. Values assumed for the design parameters of the well field are summarized in Table 2.4.

Following a probabilistic approach, the hydrogeological parameters K , q and d are modeled as independent random variables. Based on previous studies [Cheng *et al.*, 1999], all parameters are assumed to follow a normal distribution, characterized by the average values and the coefficients of variation reported in Table 2.5. Note that the coefficient of variation of d is selected according to the prediction of annual sea level rise [Preti *et al.*, 2009] and subsidence for the area of interest.

Once the uncertain parameters are defined, the extension x_{toe} of saltwater intrusion in the x - y plane is evaluated through Equations (2.3) and (2.14). The computed values of x_{toe} are affected by the uncertainty propagated from the input parameters through the selected model equations. Since the domain considered is symmetric, the maximum value of x_{toe} occurs along the middle, at $y = y_{crit}$. The extent of intrusion can be determined in the x - z plane corresponding to y_{crit} by computing the elevation of the interface z_i with respect to the bottom of the aquifer via Equation (2.15b). This is also a random variable. The risk for the vegetation, here considered as the probability that the saltwater interface reaches the sensitive zone below the plants roots, is then derived following two steps. First, the probability that plant roots occur in the zone impacted by saltwater intrusion (i.e., zone 2 in Figure 2.9) is computed as:

$$P_1 = P(x^* < x_{toe}) = 1 - F_{x_{toe}}(x^*) \tag{2.21}$$

where $F_{x_{toe}}(x^*)$ is the cumulative distribution function of the random variables x_{toe} . According to the data results $P_1 \approx 1$, *i.e.*, the vegetation falls into zone 2 almost certainly within the selected case study. Secondly, the probability that the saltwater interface reaches the sensitive zone below the plants roots is evaluated in correspondence of the maximum intrusion, *i.e.*, $y = y_{crit}$. This probability is conditional on the previous one as follows:

$$P_2 = P(z_i(x^*; y_{crit}) > z_{lim} | x^* < x_{toe}) \quad (2.22)$$

In this selected case study, as $P_1 \approx 1$, Equation (2.22) reduces to $P_2 = P(z_i(x^*; y_{crit}) > z_{lim}) = 1 - F_{z_i}(z_{lim})$, where F_{z_i} is the cumulative distribution function of the random variable z_i . Consequently, in the following section the simplified formulation for the computation of the risk, *i.e.*, $R = P_2$, is considered.

The proposed methodology is suitable to predict the risk to which coastal vegetation is subjected, considering the uncertainty of the parameters involved. For this purpose, the evaluation of the mean position of the toe (considering the schematic scenario described above) and its variance, applying Global Sensitivity Analysis [Sudret, 2008], must be conducted in order to evaluate the influence (sensitivity) of each uncertain parameter. Subsequently, the risk affecting the vegetation is computed for different scenarios defined through the parameters that characterize the well field and modifying their values with respect to those reported in Table 2.4. In particular, variations in (i) the overall pumping discharge, Q ; (ii) the distance of wells from the coast, a ; and (iii) the width of non-overlapping zones, c , are considered.

Parameters	Values
a (m)	650
b (m)	300
c (m)	100
e (m)	300
x_1 (m)	800
y_1 (m)	950
x_2 (m)	800
y_2 (m)	550
x_3 (m)	800
y_3 (m)	150
Q_1, Q_2, Q_3 (m ³ /day)	200
Q (m ³ /day)	600

Table 2.4. Design parameters of the well field, represented in Figure 2.8.

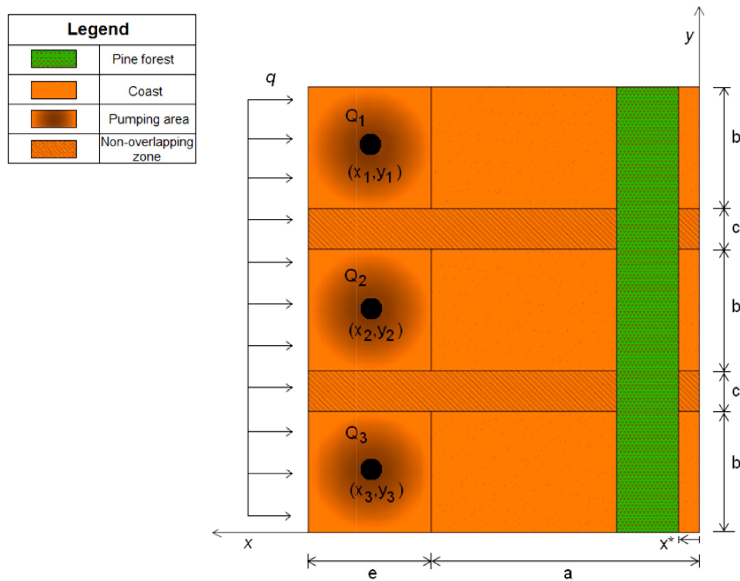


Figure 2.8 Well field and location of pine forest in x-y plane.

Parameters	Distribution
K (m/day)	$N(\mu_K = 40; cv_K = 0.1)$
q (m ² /day)	$N(\mu_q = 0.9; cv_q = 0.1)$
d (m)	$N(\mu_d = 20; cv_d = 0.001)$

Table 2.5. Main characteristic uncertain parameters of the model.

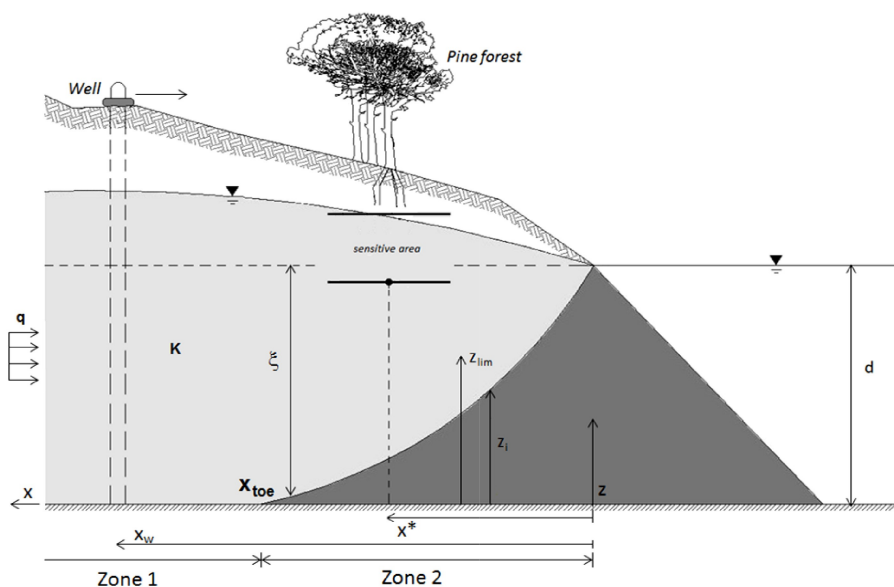


Figure 2.9 Simplified conceptualization of the problem, in x - z plane, for $y = y_{crit}$.

2.3.2.2 Results and discussion

Applying the methodology described previously, the extension of saltwater intrusion is first evaluated by using the values (parameters) collected in Table 2.4 to represent the well field. The uncertainty in the hydrogeological parameters is modeled using probability distributions as reported in Table 2.5. Under this framework, the first two moments

associated with x_{toe} and the global sensitivity indices are evaluated [See Appendix A].

The mean value of x_{toe} as a function of y is depicted in Figure 2.10(a), showing the intervals of width $\pm \sigma$ and $\pm 2\sigma$ surrounding it. The maximum value for the mean of x_{toe} (i.e., the leading edge of the intrusion) is reached at $y_{crit} = 3b/2 + c$, since the domain is symmetric. The maximum intrusion extent is equal to 303.6 m for the selected case study; this value is consistent with those typically observed for the area of Ravenna, and with results reported in numerical studies of the effects of subsidence on saltwater intrusion [Giambastiani *et al.*, 2007]. The uncertainty in the hydrogeological parameters results in a standard deviation of x_{toe} with a maximum of ~ 50 m (i.e., more than the 15% of the correspondent mean value).

The standard deviation σ of x_{toe} is illustrated in Figure 2.10(b) as a function of y , showing the individual contributions due to each random parameter value (K , q and d) in order to investigate how these different values influence saltwater intrusion. The results indicate that the primary influence is due to the variability in q , whereby, in contrast, the mean sea level, d , is relatively inconsequential. However, the impact of d is shown to produce significant effects on saltwater intrusion in a long-term period of time due to climatic changes and the combined increase in natural/anthropogenic subsidence. As expected, the effect of domain heterogeneity, exemplified through the variability of K , is also significant. These results highlight the importance of proper site characterization in order to obtain accurate predictions for the extension of the wedge. Other studies [e.g., Werner *et al.*, 2012] have relied on the theory presented by Strack [1976], whereby a sensitivity-based approach is adopted in order to define vulnerability indicators for saltwater intrusion. However, these

global sensitivity analysis models do not account for the simultaneous variability of all the parameters of interest when evaluating effects on the phenomenon.

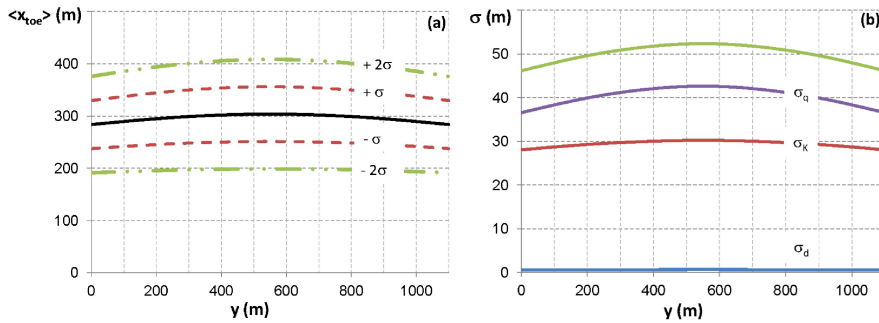


Figure 2.10 (a) Mean interface location x_{toe} (solid line) $\pm\sigma$ and $\pm 2\sigma$ (dashed line), versus y ; (b) Standard deviation σ of x_{toe} , and partial contribution of each individual parameter, i.e., σ_q , σ_K and σ_d .

This study also evaluates the influence of saltwater intrusion on the risk for vegetation health due to variations of the deterministic parameters Q (overall pumping discharge), a (distance of the well field from the coast), and c (width of non-overlapping zones).

The mean and the standard deviation of x_{toe} versus y for different values of total pumping rate Q are depicted in Figures 2.11(a) and 2.11(b) respectively. In particular, it is shown that the mean of x_{toe} reaches its maximum at $y = y_{crit}$, ranging between 280 and 365 m. This reveals a relatively high degree of variability for different values of Q_i ; specifically, the largest extent of saltwater intrusion is reached for the maximum pumping rate considered (i.e., $Q_i = Q/3 = 300 \text{ m}^3/\text{day}$) (Figure 2.11(a)). The standard deviation σ of x_{toe} follows the same trend (Figure 2.11(b)), whereby values range between 45.7 and 74.8 m, primarily as a function of the variability of domain properties, q and K , as described above.

A similar analysis is illustrated in Figure 2.12(a) and 2.12(b), with the exception that different values of a were considered to evaluate effects on saltwater intrusion. As previously noted, the results of this study reveals that the distance of the well field from the coast, within the range considered, seemed to be inconsequential, as the two moments of x_{toe} do not exhibit significant changes in the extent of the wedge. In particular, the maximum value of the mean of x_{toe} ranges between 294 and 308 m (i.e., trend increasing with a) (Figure 2.12(a)), and the associated standard deviation varies between 49.7 and 54 m (Figure 2.12(b)).

Finally, the influence of c , i.e. the width of the non-overlapping zones among the wells, on the first two moments of x_{toe} is depicted in Figures 2.13(a) and 2.13(b). By varying the width of the non-overlapping zones, the size of the entire domain is modified. For example, maximum values of mean x_{toe} and standard deviations are obtained for smaller values of c , whereby $y_{crit} = 3b/2 + c$ tends to decrease. For $c = 50$ m, $y_{crit} = 500$ m, with a mean value of x_{toe} equal to 307 m and an associated standard deviation of 53.6 m; for a value of $c = 200$ m, y_{crit} becomes 660 m, whereby the mean value of x_{toe} is reduced to 297 m with a standard deviation of 50.2 m.

For this analysis the design parameters of the well field demonstrate that saltwater intrusion is extremely sensitive to the pumping discharge Q , in contrast to the other parameters considered (i.e., a and c) which seem to have only a minimal influence on the optimization of groundwater extraction and effect on the phenomenon.

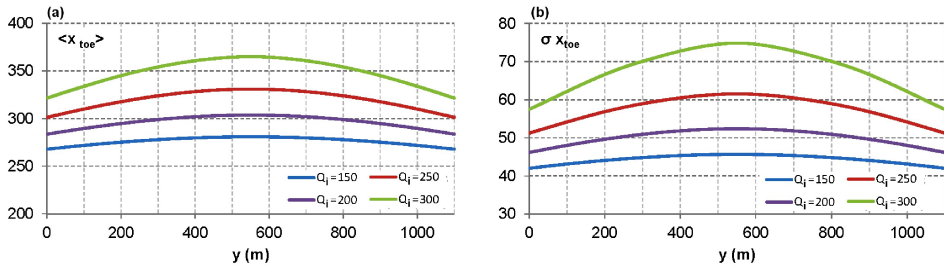


Figure 2.10 (a) Mean value of x_{toe} , for different values of Q_i ; (b) Standard deviation σ of x_{toe} .

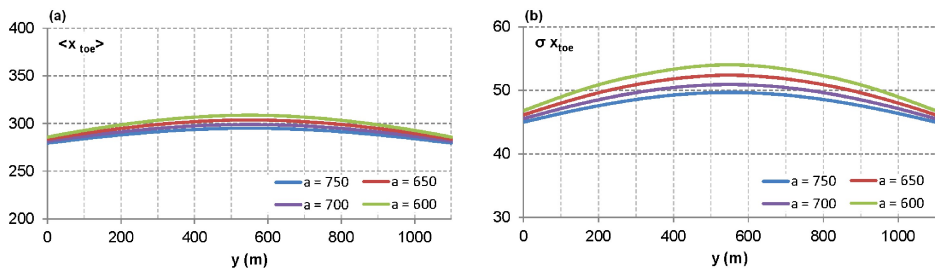


Figure 2.11 (a) Mean value of x_{toe} , for different values of a ; (b) Standard deviation σ of x_{toe} .

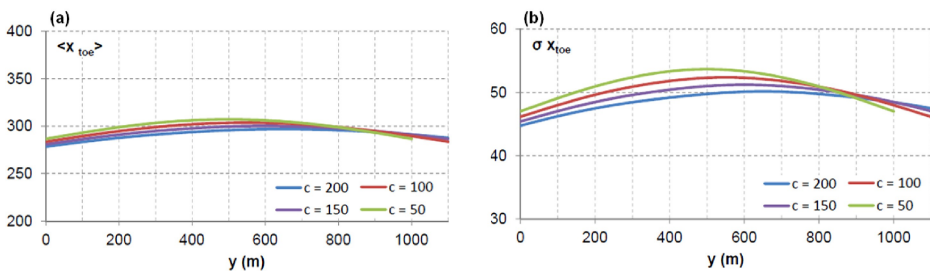


Figure 2.12 (a) Mean value of x_{toe} , for different values of c ; (b) Standard deviation σ of x_{toe} .

In order to complete the analysis, the effects of the variability in the parameters characterizing the well field on the risk of contamination are evaluated. The results obtained increasing Q_i are presented in Figure 2.13(a). It can be observed that the cumulative distribution functions of the

interface elevation computed in z_{lim} , $F_{z_i}(z_{lim})$, tend to decrease with higher values of Q_i and consequently the risk increases quasi-linearly (Figure 2.13(b)). When considering the value of $z_{lim} = 12$ m as a fixed variable herein, $F_{z_i}(z_{lim})$ ranges from 0.78 to 0.28, as Q_i varies between 150 and 300 m³/day. In Figure 2.14(a), obtained for different values of a , a different trend is revealed, whereby $F_{z_i}(z_{lim})$ increases and risk decreases, as expected for higher values of a (Figure 2.14(b)). In this case, $F_{z_i}(z_{lim})$ increases from 0.60 to 0.71, while varying a between 600–750 m. Finally, in the last simulation whereby different values of c are utilized, a similar trend to the one described above is observed, albeit less pronounced (Figures 2.15(a), 2.15(b)). For example, a value of $z_{lim} = 12$ m, produces a narrow range of values of $F_{z_i}(z_{lim})$ from 0.61 to 0.67 when varying c between 50 and 200 m.

Overall, when comparing all of the different simulation results obtained for the risk of saltwater intrusion (Figures 2.13(b), 2.14(b), 2.15(b)), the increase in Q seems to produce the most detrimental effects in terms of extent of saltwater wedge and risk to the preservation of vegetation health in coastal areas. For example, with values of $z_{lim} = 12$ m, the results show that risk ranges between 0.2 and 0.7 when varying parameter Q (Figure 2.13(b)), while values of risk lower than 0.4 result when parameters a and c are varied (Figures 2.14(b) and 2.15(b)).

It should be noted that the parameters of the well field can also be modeled as random variables and investigated via a global sensitivity analysis to appropriately understand their influence on the risk of contamination. This could be particularly useful for problems that require optimization solutions [e.g. *Mantoglou, 2003*]. Although the analyses herein primarily focuses on a risk assessment for vegetation in coastal areas

influenced by SI, this study also reveals that both the pumping rate and domain heterogeneity (i.e., permeability distribution) significantly influenced the extent of saltwater intrusion, consistent with findings reported by other studies [Mantoglou, 2003; Park, Aral, 2004].

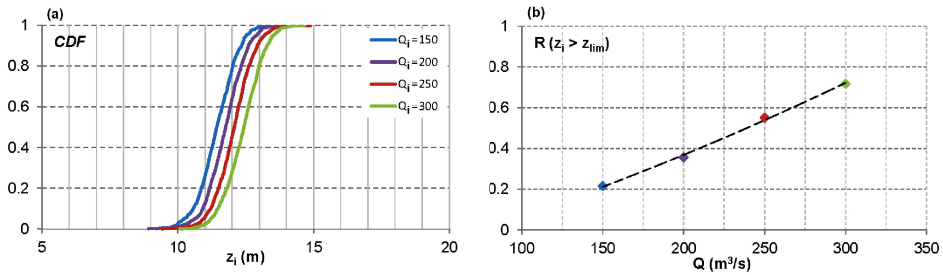


Figure 2.13 (a) Cumulative distribution function F_{z_i} of the surface elevation z_i computed in z_{lim} ; (b) Computed risk [see Equation (2.22)] resulting from different values of single pumping discharge Q_i .

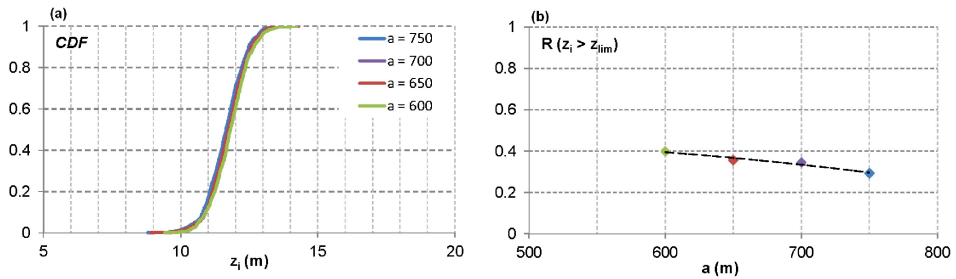


Figure 2.14 (a) Cumulative distribution function F_{z_i} of the surface elevation z_i computed in z_{lim} ; (b) Computed risk [see Equation (2.22)] resulting from different values of distance from the coast a .

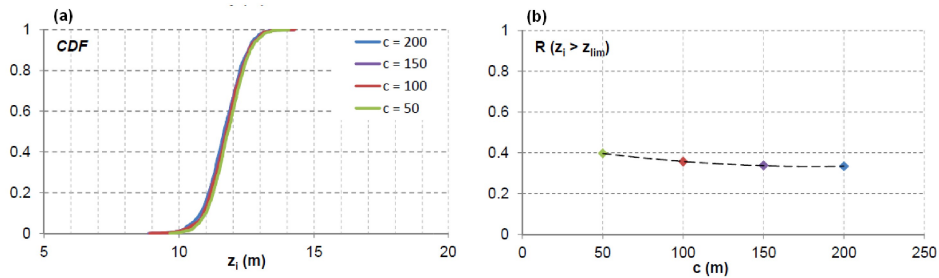


Figure 2.15 (a) Cumulative distribution function F_{z_i} of the surface elevation z_i computed in z_{lim} ; (b) Computed risk [see Equation (2.22)] resulting from different values of width of non-overlapping zones c .

2.4 CONCLUSIONS

The previous studies discussed in Sections 2.3.1 and 2.3.2 present a computationally efficient technique to evaluate risk to ecosystems (*i.e.*, vegetation health) along coastal regions that are impacted by saltwater intrusion processes. A stochastic approach to the problem was adopted to represent the random nature of the hydrogeological parameters. Computational efficiency was further increased by incorporating model reduction techniques via Polynomial Chaos Expansion theory for modeling saltwater intrusion effects and associated risk analyses.

A simplified analytical formulation was adopted to allow for the evaluation of the probability that the vegetation capture zone overlaps with the intruding saltwater wedge. Natural and anthropogenic influence on the risk to vegetation due to saltwater intrusion was modeled (i) through the contribution of a natural recharge, in order to evaluate the contribute of each parameters involved in the phenomenon, and (ii) through the presence of a well field, specifically accounted for through adjustment of pumping discharge, wells distance from the coast, and mutual distance between wells. For the simplified scenario representative of the Ravenna coast, the comprehensive results of the modeling analyses revealed the parameters most responsible for influencing the extent of saltwater intrusion. For example, in the second case study, increases in the overall pumping discharge of the well field produced the most significant increase in the probability that saltwater intrusion reaches the vegetation capture zone.

The computational methodology used herein can be applied to more complex systems whereby a closed-form solution is not available and would require more time-consuming numerical approaches, *i.e.* to resolve the shape and size of the intruding saltwater wedge. In such cases, the model reduction technique adopted for these analyses allowed for both excellent representation of the physical system and an increase of computational efficiency. Moreover, the current approach can assist in the

development of appropriate management strategies for coastal aquifers. These techniques allow the parameters describing the anthropogenic influences to be considered as random variables, which provide an improved means of discriminating the parameters most responsible for saltwater intrusion and for solving optimization problems that require a specific set of environmental constraints.

3. Characterization of the study area

3.1 COASTAL PHREATIC AQUIFER OF EMILIA-ROMAGNA

In the coastal plain of Emilia-Romagna many different and precious environments are present, which are strongly affected not only by the features of natural depositional systems and its geomorphology, but also by anthropic activities and management or protection practice of the territory [Bonzi *et al.*, 2010]

Recent and rapid urbanization of the coast, especially in densely populated areas, has modified natural equilibrium, concurring to the onset of some problems of water supply. The environmental risks associated with the processes of groundwater overexploitation are known and common, but what makes it a unique coastal aquifers is the risk of salinization water resource.

In the following, the discussion is focused on Ravenna coastal aquifer, with a focus on the southern part, where the complex ecosystem of this area is particularly threatened by salinization process.

3.2 MAIN CHARACTERISTICS OF RAVENNA PHREATIC AQUIFER

Emilia-Romagna coast faces Adriatic Sea, a shallow basin whose depth rises southwards and is characterized by a modest tidal excursion. The Adriatic coastline south of the Po River was originally part of its delta and alluvial plain.

The province of Ravenna, bounded to the north by the Comacchio Valleys and to the south by the city of Cervia, is characterized by a population of about 350,000 inhabitants, whose density more than triples during the summer. In this area, many unpermitted and poorly-constructed wells have been drilled by bathing establishments and farms, resulting in environmental damage [*Giambastiani et al.*, 2007].

Anthropogenic activities have modified the original ecosystem and now the once sandy coastline is characterized by river and canal mouths, lagoons, pine forests (e.g., San Vitale and Classe), heavily urbanized areas (e.g., the cities of Marina Romea and Cervia), industrial facilities, and reclaimed agricultural lands [*Antonellini et al.*, 2008]. The entire coast is threatened by salinization of the phreatic aquifer and seawater encroachment inland along the rivers (e.g., Reno, Lamone, Fiumi Uniti, and Bevano rivers), natural and anthropogenic land subsidence, direct contamination from water bodies open to the sea, destruction of coastal dunes with consequent reduction of their barrier effect, insufficient aquifer recharge and sea level rise. In particular, over the last few decades the land surface has dropped to 4 m below mean sea level in some areas. This in turn has modified the rivers and regular groundwater flow regimes. These inland areas require protection from river flooding and marine intrusion with dikes and levees. A partially artificial drainage network was built in the coastal area to lower

the phreatic level and keep the agricultural land dry. Unfortunately, this management process is complex and the presence of these modified drainage networks has not been able to mitigate saltwater intrusion.

The coastal phreatic aquifer of Ravenna is primarily located within the littoral sands, and locally in the shallow marine wedge deposits. The groundwater basin is unconfined in the east, but 3–4 km from the coast it becomes overlain and confined by the most recent alluvial fine-grained continental deposits. The basin thickness varies from a maximum of 30 m in the area of San Vitale Forest to a minimum of about 15 m near the city of Cervia [Antonellini *et al.*, 2008]. From east to west, the major sedimentary units consist of: (i) a wedge of fine-grained (fine sand to silty clays) sediments representative of a shallow marine environment; (ii) littoral sands representative of the foreshore, deep-shore, and the sand dune environments adjacent and inland of the beach. The westernmost portion of the area is characterized by the presence of clay back-shore lagoon deposits [Bondesan *et al.*, 1995; Amorosi *et al.*, 2002]. Some continental-type alluvial deposits (clay and silt) overlay the littoral sands and lagoon deposits in the west. Based on geologic data from slug tests and grain size analyses [Antonellini *et al.*, 2008; Ulazzi *et al.*, 2007], the hydraulic conductivity of the aquifer is relatively high near San Vitale Forest (1.1–24.8 m/day) and Cervia (11–21 m/day), and is generally lower in Classe Forest (0.2–7.7 m/day). Along the entire coast, the hydraulic head measured in wells is almost always above mean sea level, with values ranging from 0.5 to 4 m in winter, and from –0.5 to 3.5 m in summer. It is observed that water salinity (groundwater at the water table) varies seasonally. For instance, salinity values are higher (22–44 g/L) during the summer periods (e.g., near Comacchio Valleys) compared to winter months where values generally range between 3 and 22 g/L. Moreover,

encroachment of sea water along rivers and canals, combined with subsidence and drainage from agricultural lands, contributes to enhance the salinization process [Antonellini *et al.*, 2008].

Along the coast of Ravenna, pine forests are situated mostly on sandy dunes and were planted in the last century by farmers to protect their land from sea-salt spray. Plant ecologists have reported that the distribution of plant species in the coastal area varies depending on elevation, soil salinity, water salinity, and the duration of various stress periods by which the vegetation is affected [Maas, 1984]. Based on soil and water salinity, plants along the coast can be divided into categories including very tolerant to salt (halophyte plants), tolerant/fairly, and tolerant/not tolerant to water/soil/sea-spray salinity [Hutchinson, 1991]. Increases in salinity within a coastal habitat will have direct and indirect effects on vegetation [Giambastiani *et al.*, 2009]. Along Ravenna coast, new sand is added to the beaches every few years from dredging the offshore Adriatic Sea in order to counteract the continuous erosion along the coast. The pine forests (*i.e.*, 50–150 m from the coast) and the adjacent farmlands are drained in winter to keep the groundwater level low. However, this increases the extent of saltwater intrusion in the phreatic aquifer, which is further enhanced by the transpiration of the pine trees [Antonellini *et al.*, 2010]. Natural pine seedling germination does not occur and new small pine trees are planted each year to replace dead plants. The most dramatic decrease in the diversity of plant species occurs where water salinity exceeds the 3 g/L threshold, above which most trees species become stressed, with the exception of a few, *i.e.*, *Pinus pinaster* (William Aiton, 1789) and *Pinus pinea* (Carl von Linné, 1753) [Giambastiani *et al.*, 2009].

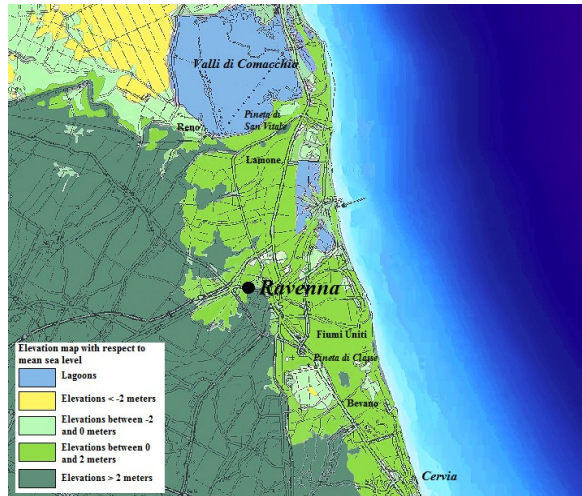


Figure 3.1 Map of the Adriatic coast around Ravenna [Felisa *et al.*, 2013].

3.2.1 GEOLOGICAL EVOLUTION

The geological evolution of the region has always been controlled by the alternation of continental and marine sedimentation. This large sedimentary basin (about 46000 km²) originates from the pit grown up between Oligocene and Miocene, due to the emergence of the Apennines and the presence of the Alps already almost fully emerged [Amorosi *et al.*, 2002]. The evolutionary history of the area continues alternating erosive and depositional phases. In Quaternary, sedimentation prevails on subsidence and alluvial continental deposits overlap marine ones. This phenomenon is relevant particularly in the eastern part of the Po Valley, where, because of glacial oscillations affecting also these latitudes during that period, they have pulsations of sea level that complicate the conditions of sediments deposition in areas near the coast. Considering about last 70000 years, i.e. starting from the last Würm glaciation (70000-18000

years ago), the sea level decreases progressively, up to about 100 m from the current level. This lowering contributes to turn Northern Adriatic into a wide floodplain, while the area between the actual isobaths of -60m and -100m, located between Ancona and Pescara, was characterized by lagoon and marine-coastal environments. The thickness of the sediments, that testifies Würm regression, is about 50m, consisting mostly of clayey silts with interbedding of sands and clays [Amorosi *et al.*, 1999].

3.2.2 STRATIGRAPHIC EVOLUTION

The Ravenna phreatic aquifer consists of sandy, silty and clayey sediments that alternate in the vertical sequence according to the various depositional cycles, which have characterized this area over time [Amorosi *et al.*, 2004]. The main depositional cycles, affecting the shallow part of Po Valley coastal plain, have been recognized as (i) regression system tract (FRST), (ii) lowstand system tract (LST), (iii) transgressive systems tract (TST), and (iv) highstand system tract (HST) [Amorosi *et al.*, 1999].

FRST is characterized by a high lowering of sea level, i.e. about 120 meters, in the period between 125 ka and 30 ka. The following stage, i.e. LST (30 ka - 16 ka), the north Adriatic area became a floodplain with wide and little carved valleys, where the sedimentation occurred only between 18 ka and 16 ka. TST (16 ka - 5.5 ka) is characterized by marine ingression, which contributed to move inland sedimentary barrier-lagoon environments. The sedimentation of this period consists of organic pelite, in marshland and/or lagoon facies, which many authors interpreted as corresponding initial stage of modern Po delta [Amorosi *et al.*, 1999; Bondesan *et al.*, 1995]. The last phase, i.e. HST, corresponds to a strong

progradation of Po delta, due to a greater contribution of river sediments and increase erosion combined with subsidence; in this phase, deltaic sands and sand bars, with alternation of mudstones and fine sands of prodelta, overlay organic pelite, representing the highest marine ingressions of the area.

In the last 2000 years, minor fluctuations of sea level caused the deposition of bars and sand dunes, locally intercalated with thin layers of silt and clay facies behind the dunes (Amorosi et al. 1999). Within the latest transgressive-regressive sequence, in the south eastern portion of the Po Valley, 8 minor cycles are detectable, with a duration of about 1000 years, and a thickness of 3-5 m (Figure 3.2) [Amorosi et al., 2005].

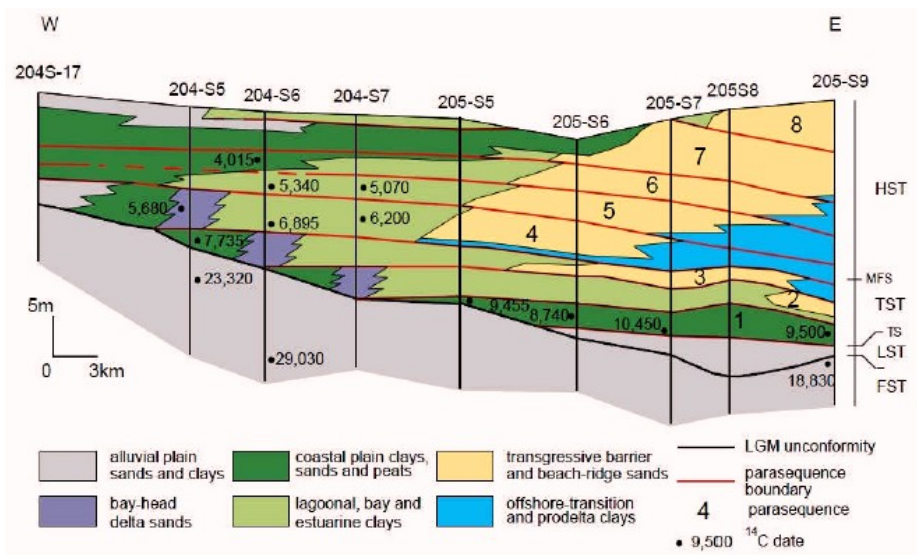


Figure 3.2 Southeast Po Valley section, with the transgressive-regressive sequence subdivided in 8 minor cycles [Amorosi et al., 2005].

3.2.3 SURFACE GEOLOGY AND PALEODUNES

Shallow geology consists of paleo cords (phreatic aquifer), outcropping or buried by silt-clay continental material, with a thickness varying from 1 to 4 m, brought on site by reclamation of the last century [Stefani and Vincenzi, 2005].

Figure 3.3 depicts a typical cross section of the coast, located in Lido di Dante, where sediments of beach and dune are outcropping near coastal dunes and below historic pinewoods, forming the shallow portion of the phreatic aquifer. Between the two bodies of paleodunes, there are marine deposits buried by fine continental sediments. Moving westwards, towards the quarry area, the same situation occur with greater thickness. This portion of the aquifer becomes confined (Figure 3.3). Figure 3.4 shows the location of outcropping sands, and consequently phreatic aquifer, where natural recharge results higher. It is evident that, in most cases, these areas coincide with historical and coastal pinewood, along with eastern areas of Ravenna city and southern ones of Classe forest.

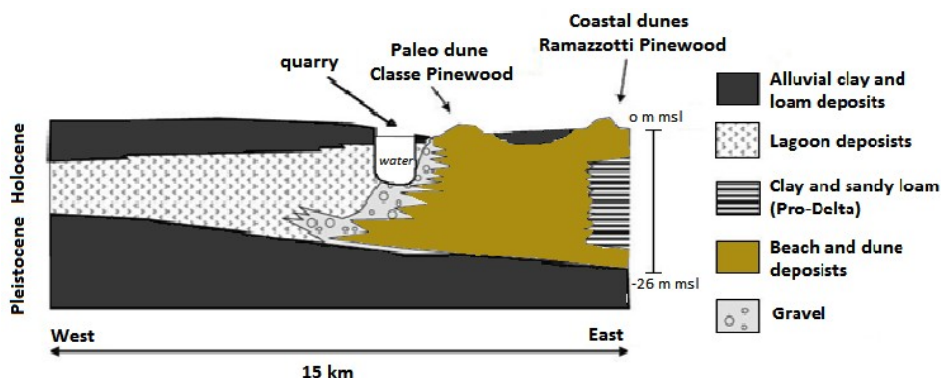


Figure 3.3 Southeast Po Valley section, with the transgressive-regressive sequence subdivided in 8 minor cycles [modified from *Amorosi et al.*, 2005].

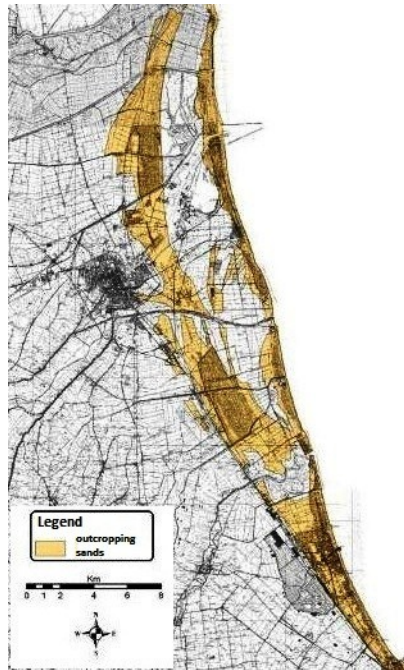


Figure 3.4 Map of outcropping sands [Greggio, 2013]

3.2.4 RECENT EVOLUTION OF COASTLINE

In the coastal Po region, environment gradually changed from marine, brackish and fresh, from the moment of maximum marine ingression to date. The maximum extension of freshwater marshes occurred about 2300 years ago in the area of Po delta, while in the southern area freshwater wetlands were present about 400 years ago. The evolution of the territory includes the presence of a narrow brackish lagoon along the coastline from Chioggia to Classe until 1600. In the coastal area of Ravenna, the progradation of the coastline was homogeneous between IV century A.C. and XVII century A.D. In the same period, an abundant progradation of Primaro mouth, i.e. the actual Reno river, occurred, which was then

dismantled in the following centuries. The transported sediments were re-deposited to form paleodunes, on which historical pinewoods settled.

The areas of Marina Romea and Lido di Dante, i.e. V Basin, have a recent origin. Sedimentation changed from lagoon (brackish environment) to continental only in recent historical times, during the last phase of progradation of the coastline (1851-1894 A.D), with a rate of advance of 20 m/year. In particular, in the area near Bevano river, the progradation was caused by erosion of sediments of deltaic cusps, which consequently were redistributed along the coast from sea currents, inducing a correction of the coastline [Stefani and Vincenzi, 2005].

Currently, the beaches and coastal dunes are eroded along the Adriatic coast. In 2003, the altitude of the dunes was reduced by about 1 m from a single storm event [Ciavola *et al.*, 2007].

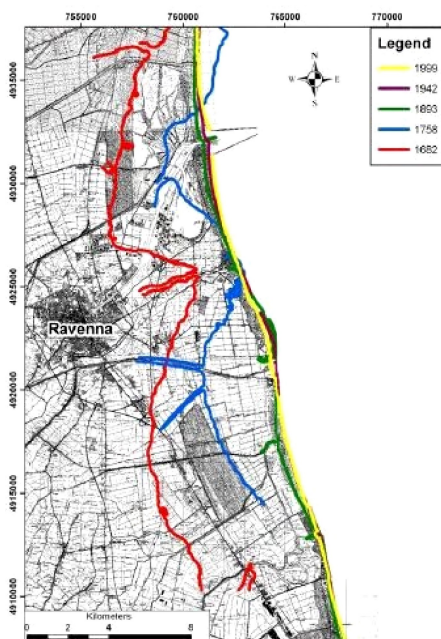


Figure 3.5 Evolution of coastline in Ravenna area, from 1682 to 1999. It is evident the progradation of the coast, due to reclamation activities.

3.2.5 TOPOGRAPHY AND SUBSIDENCE

Elevation of surface, combined with the problem of subsidence, represents a critical issue in the study area. Indeed, saltwater intrusion in coastal aquifer, from a theoretical point of view, provides that the depth of saltwater-freshwater interface is about 30 times the height of phreatic surface above sea level, according to Ghyben-Herzberg law (see Chapter 2) [Fetter, 2001]. Consequently, a variation of a few cm of piezometric level causes a large displacement of the interface.

From the analysis of the different isokinetics related to subsidence, it has been possible to reconstruct the topography of the study area [Greggio, 2013]. The reconstructed topography shows how the elevation varies mainly between 4 and -2m above sea level. The territory has an elevation between 0 and 1 m above sea level and shows no dominant gradients; the highest quotes are in correspondence of paleodunes and coastal dunes, reaching up to 4 m above sea level. The most depressed area is located west of Pineta di Classe, with elevation of -2m a.s.l. Other portions of the territory are below sea level, generally corresponding to the newly formed territories between Pineta di Classe and Pineta Ramazzotti, and the north area of Reno estuary (Figura 2.13). Superficial watersheds are often river banks and main roads, because of low gradients of the area.

The same topographic analysis was conducted at the scale of V Basin, south of Ravenna, which shows that altitudes here vary between -2.5 m near the quarry up to 4m a.s.l., in proximity of coastal dunes and in the western part of the basin. Excluding the two pinewoods in the area, whose elevation reaches also 4m a.s.l (Pineta Ramazzotti), the central agricultural areas, delimited by paleodunes, are at the same elevation of sea level, and

in the portion in direct contact with Bevano river, the altitudes are below sea level of few centimeters.

3.2.5.1 LAND SUBSIDENCE

Subsidence, due both to tectonic origins and differential compaction of Plio-Quaternary sediments, plays a key role in the evolution of these environments. The average speed of subsidence in Ravenna area, for the entire Quaternary, was approximately 1.8 to 3 mm/year [Sestini, 1992]. Recently, rates of natural subsidence were increased by anthropogenic factors, i.e. groundwater and hydrocarbons extraction [Gambolati *et al.*, 1991; Gambolati and Teatini, 1998; Carminati *et al.*, 2002]. Another anthropic contribution is represented by embankment interventions and control of watercourses, dramatically reducing sedimentary supply in the coastal area. Consequently, large areas were below sea level, with "basins" among the recent dunes and river banks.

Gradual increase in subsidence rates occurred during rapid industrialization in Ravenna area (1972-1977), reaching average values of 40-60 mm/year, in the municipal area, especially near industrial pole. In particular, between 1972 and 1973, highest value of subsidence were recorded, i.e. 110 mm/year [Teatini *et al.*, 2005].

Since the '80s, subsidence began to decrease until a lower rate of 5 mm/year for about 35% of the entire municipality. This process went forward, and currently the phenomenon appears to be reduced, with a lower rate of 3 mm/year, even if for some coastal areas, e.g. in correspondence of extraction wells "Dosso degli Angeli" and "Angela- Angelina", values of 10 mm/year are still recorded, very high if compared to natural threshold.

The general improvement of the situation is definitely correlated with the closure of many extraction wells, and replacement of water supply by groundwater with adduction of surface water from Reno river and Ridracoli dike, through the Romagna aqueduct [*Preti, 2000*].

Gas fields are not the only responsible for subsidence extended to the entire territory of Ravenna, although it should be noted that the effects, even if localized, can be severe if the oil fields are located near the coastline. However, there is a close correlation, already clearly demonstrated [*Carbognin et al., 1984*], between the depressurization of the aquifers and the magnitude of subsidence caused by groundwater exploitation. Therefore subsidence reached higher values in areas of greatest piezometric reduction, e.g. in industrial and pumping concentrated poles. Water withdrawal from a shallow soil layer causes a lowering of the interstitial pressure, that in turn causes an increase in the load supported by grains of the ground: this corresponds to an elastic deformation of the ground, followed by a compaction of the layers which corresponds to a permanent plastic deformation. Moreover, the strong depressurization involving both groundwater from phreatic and artesian aquifer, recalls laterally and vertically saline water that has settled in the same strata. A phenomenon that often follows the intensive pumping is the rise of saline waters fossils, often found immediately below the exploited aquifer system.

In summary, over the past 35 years, the elevation of areas most influenced by subsidence was reduced by 1.5 m [*Teatini et al., 2005*], increasing sea water ingression in coastal aquifers. Another consequence of subsidence induced by hydrocarbon extraction is the ascent of water level to the surface topography, requiring mechanical drainages in the overall coastal area of Ravenna.

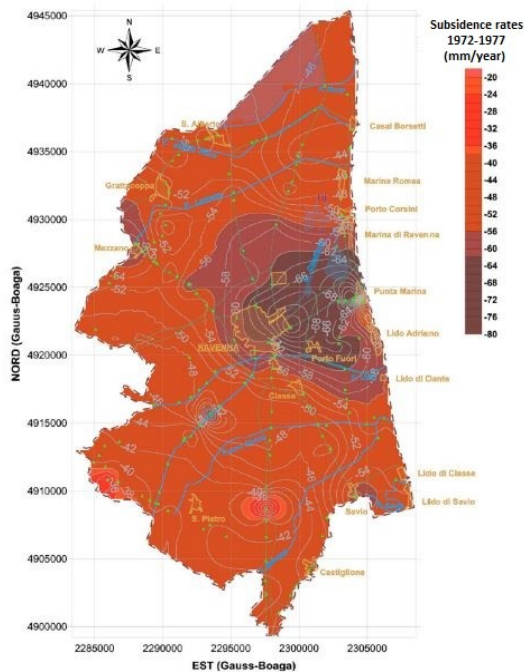


Figure 3.6 Subsidence rates in the period 1972-1977, in Ravenna area (Fonte Servizio Geologico –Comune di Ravenna, 2006)

3.2.5.2 LAND USE

All soils present in the coastal portion of Ravenna are potentially exposed to the risk of salinization, due to the depressed topography, drainage and the strong presence of salt water in the aquifer. The map of land use of Emilia-Romagna (Figure 2.17) (Corticelli, 2003) shows that the territory is mainly agricultural. The rest of the area is occupied by pinewoods, i.e. the historical Pineta di Classe and San Vitale, coastal pinewoods, wetlands, i.e. Punta Alberete and Valle Mandriole, brackish valleys, i.e. Piallassa Baiona, Piomboni, Ortazzo and Ortazzino.

Land use is very articulated in V Basin. Moving from the coast towards west, you find Pineta Ramazzotti, an agricultural field mainly cultivated for seed, then there is Pineta di Classe and the quarries. In the westernmost area, agricultural areas are located, in which, unlike the previous, higher percentages of orchards and vineyards are present.

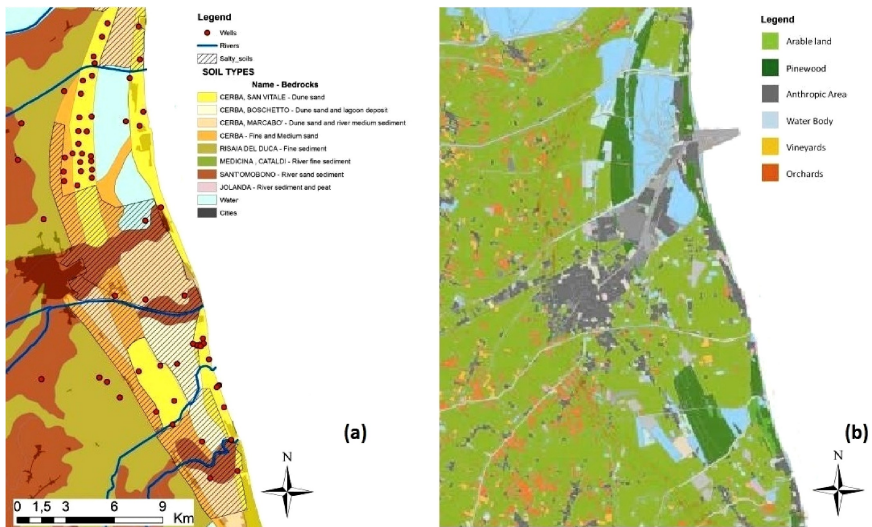


Figure 3.7 (a) Soil map of Ravenna [modified from *Corticelli*, 2003]. Dashed lines represent agricultural soils potentially exposed to salinization; (b) Land use map of Ravenna [from Emilia-Romagna Region].

3.2.6 HYDROLOGY OF THE AREA

The hydrological system of Ravenna area is extremely complex, because it comprises water bodies of different origin (natural or artificial) and with different destination of use. The elements more relevant of this area are definitely the brackish basins and Pialasse, river courses, channels forming the network of land reclamation, intake structures and distribution of river water and the Adriatic Sea.

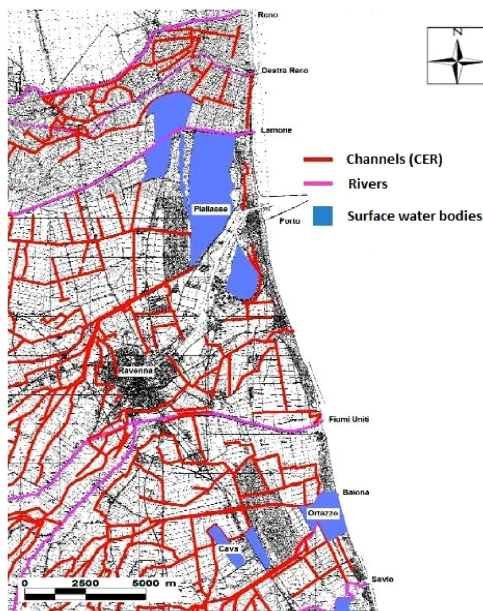


Figure 3.8 Map of surface water bodies. In blue, wetlands and lakes; in magenta, rivers; in red, channels [Greggio, 2013].

Many watercourses cross this territory and interact with the aquifer, i.e. Reno, Lamone, Fiumi Uniti, Bevano and Savio. Currently, the structure of river does not reflect the original natural one, due to the multiple actions of rectifications and embankment realized in the last century, to facilitate the flow of water towards the sea and prevent flooding. Exceptions are the mouths of Bevano and Savio, who maintain the original meandering conformation. The investigations, carried out by Emilia-Romagna Region in 2005, shows that most of the water flows are not derived from sources but from surface runoff. Discharges of rivers are variables and therefore reduced, maintaining average annual values really low. To deal the water problem in Romagna, since 1960 the Emiliano - Romagnolo Channel (Canale Emiliano-Romagnolo, CER) is active, representing one of the most

important hydraulic works of all Italy. By a derivation from Po river, it guarantees the water supply of a region characterized by intensive agricultural activities and many urban and industrial settlements. This infrastructure charges all rivers of Ravenna, ensuring 224 million m³ of water per year.

Pialasse, currently owned by the City of Ravenna, are now reduced to four, all located in the northern part of the study area, near Candiano channel. Pialassa della Baiona, which is the largest, stretches along the territory between Lamone river and Fossatone drain; Pialassa della Risega is located between Fossatone and Via Cerba drain, while Pontazzo occupies the southern part of the territory. Their total area covers about 1200 ha and they are connected to the sea through the Candiano channel. Pialassa del Piombone, south of Candiano channel, has an area slightly larger than 300 ha, since much of its surface has been filled and occupied by industrial facilities, and currently is reduced to a port structure without any naturalistic interest. Southernmost, at the mouth of Bevano, the wetland Ortazzo is located, an ancient valley of fresh water dammed and obtained from the conversion of previous rice fields, that nowadays is subject to the influence of brackish groundwater resulting in a wide coastal lake, partly controlled by the introduction of water from Bevanella channel and Fosso Ghiaia [Emilia Romagna, 2009].

In the southern part of the study area, there are lakes of different dimensions, arising from the extraction activities of active or disused quarries. From these areas, gravel is drawn (their location is not accidental, but represents the closing point of the aquifer), used in construction as conglomerate in reinforced concrete.

To complete the analysis of the hydrological framework, it is necessary to analyze the multiple constructions located in the area, i.e. reclamation

channels, drainage channels connected to pumping systems, that keep the territory dry to ensure the agricultural activities. In Ravenna area, there are channels of first order, managed by Consorzio di Bonifica della Romagna, and a vast series of secondary channels, which allow the fast runoff of rainfalls. Currently, the network covers the entire drainage area under study, including coastal dunes, albeit correspond to areas with greater elevation, in order to protect the pine forests. These channels are used in a different way according to the climate: in winter, and in general when the climate requires it, they collect rainwater and drain the area; in the summer season, however, some of them are kept filled with water, so as to ensure a water resource usable for irrigation to the surrounding agricultural areas. The large area, subjected to mechanical drainage, is divided into several sub-basins, which are governed by a series of dewatering pumps managed by Consorzio di Bonifica della Romagna. Almost all coastal territory requires mechanical drainage; only westernmost basins own natural gradient. There are two pumping stations, even if the only active is the one of V Basin: this pumping system drains all lands located west of the plant, but thanks to a dense network of channels, also collects all water coming even from Pineta Ramazzotti.

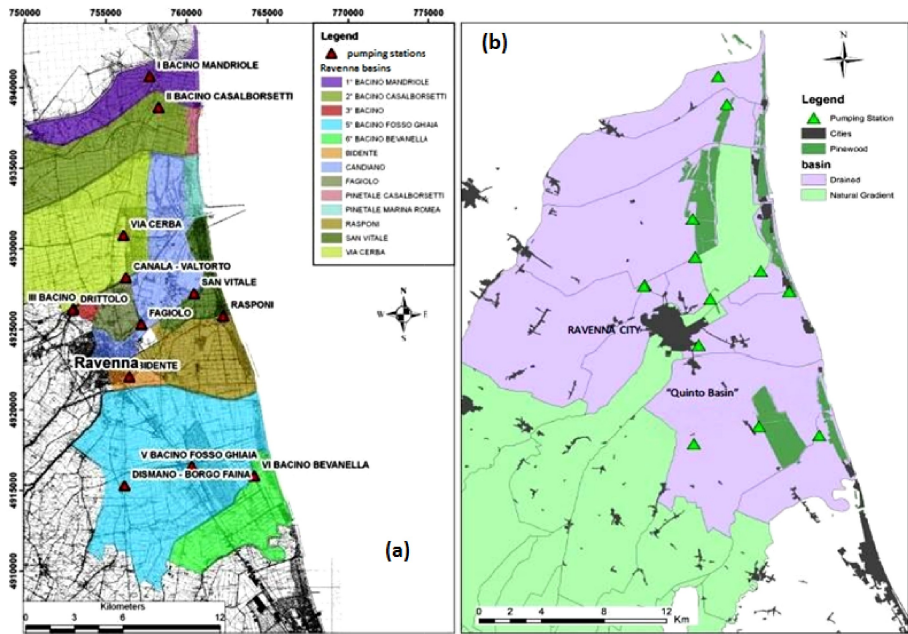


Figure 3.8 (a) Watersheds of Ravenna area, with pumping stations; (b) Watersheds with natural gradient towards the sea.

3.3 MONITORING OF THE AQUIFER

To understand the mechanisms beyond the different process of salinization involving the coastal phreatic aquifer of Ravenna, it has been necessary the realization of different networks of monitoring wells, managed by Regione Emilia-Romagna and University of Bologna. In the following, the two different surveys are presented.

3.3.1 EMILIA-ROMAGNA REGION SURVEY NETWORK

Since 2009, the Geological, Seismic and Soil Survey of Emilia - Romagna, i.e. Servizio Geologico, Sismico e dei Suoli (SGSS), has undertaken a study project on coastal phreatic aquifer [Bonzi *et al.*, 2010], in order to create an updated knowledge framework, outlining the physical characteristics, the dynamics and possible fragility of the subsurface environment. In the first phase of this study, a geological model of the aquifer was developed, while in the next step a quali-quantitative monitoring network of groundwater was planned and carried out.

The phreatic coastal aquifer is a geological body which has been the subject of extensive research at local scale, sometimes for hydrogeological modeling purposes [Ulazzi *et al.*, 2007], or as part of geognostic surveys related to engineering constructions [Esca *et al.*, 2006; Venturini, 2008]. At provincial scale, a study covering the northern coastal territory and focused mainly on the monitoring of hydrogeological and hydrochemical parameters of the water table, was conducted by the Province of Ferrara in 2001 [Gargini *et al.*, 2001]. At regional scale, instead, the aquifer is known indirectly through the geological reconstructions of Holocene transgressive - regressive sedimentary wedge from different studies in literature [Rizzini, 1974; Amorosi *et al.*, 2003; Stefani, Vincenzi, 2005].

In the first phase of the work, the geological model of the aquifer was reconstructed, relying on the informations derived from the regional Digital Terrain Model, i.e. DTM, and from a geological analysis which provided a new subsurface stratigraphic reconstruction of Emilia-Romagna coastal plain. The analyses were based on the large amount of data contained in the database of Emilia-Romagna SGSS, mainly well stratigraphies, penetration test and surveys. From these analyses, it has been possible to reconstruct the map of the surface of coastal aquifer roof, with its geometrical characteristics, including the tendency to widen towards west. Figure 3.9(a) depicts clearly that the phreatic aquifer is properly in the southern sector, where it is also very thin, while in the central and northern parts it is free near the coast and becomes, proceeding westward, semi-confined and then confined, with the roof gradually oldest and buried by low permeable deposits.

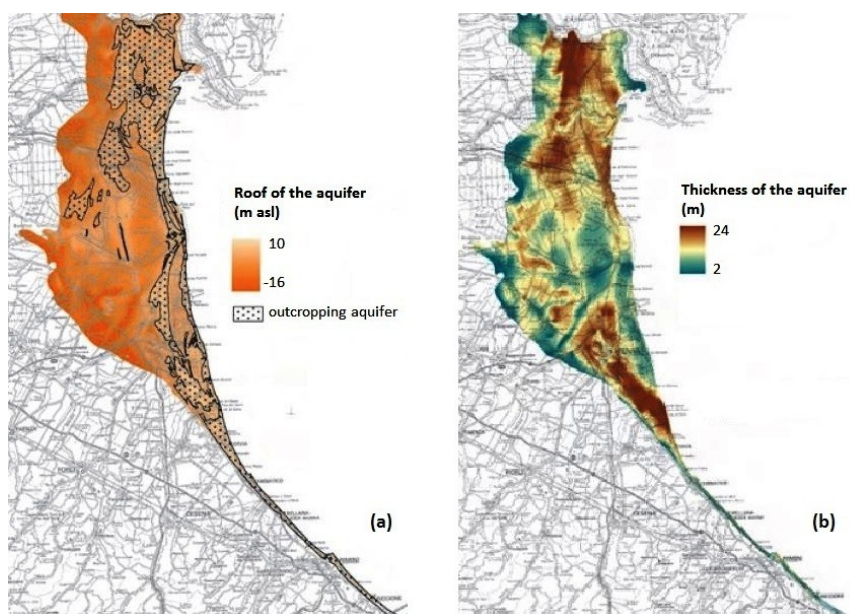


Figure 3.9 (a) Surface of aquifer roof, along Emilia-Romagna coast; (b) Thickness of the aquifer along the coast [modified from *Bonzi et al.*, 2010].

After the reconstruction of the geological model of the aquifer, a monitoring network was prepared, with 30 wells, of which 11 are located in the province of Ferrara, 12 in Ravenna, 2 in Forli-Cesena and Rimini (Figura 3.10). All piezometers were placed in public areas, or protected and closed by a manhole of 40x40 cm, to ensure the greatest possible duration in time. The location of the wells was chosen to obtain a homogeneous distribution of data on the portion of the aquifer, and to represent the phenomenon of salt wedge ingression in different portions of coastal aquifer. Generally, transects perpendicular to the shore line were privileged, but in some cases it was decided to locate a point of measurement that would allow to evaluate the relationships with the surface water or the possible different responses of the system in the presence of a confined or semi-confined aquifer. All wells were drilled where the coastal aquifer is phreatic, except in two cases in the province of Ravenna, where piezometers affect a portion of an aquifer confined by fine sediments overlying alluvial ones. Once the wells were installed, the precise dimensioning of piezometers was provided by GPS. For each piezometer was finally prepared a monography, summarizing all the technical characteristics and location [see Appendix B].

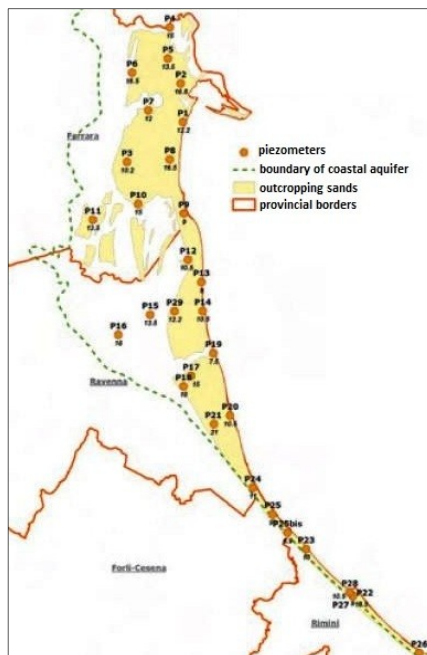


Figure 3.10 Location and depth of the wells of the monitoring network [modified from Bonzi *et al.*, 2010].

The hydrogeological monitoring, still in progress, has provided for the measurement of quali - quantitative parameters of groundwater, according to a schedule based on the evaluation of similar previous works [Carbognin *et al.*, 2005; Piccinini *et al.*, 2008]. Six measurement campaigns were made in a hydrological year (one every two months), from the month of June 2009, compatibly with the weather and logistics.

Each piezometer measures the depth of groundwater and the trend with depth of the specific electrical conductivity EC (mS/cm), the temperature T (°C), and Total Dissolved Solids TDS (g/l), where informations are recorded every meter with a multiparameter probe. From the measurements, the vertical profiles (log) of each parameter for all piezometers are obtained, in different seasonal conditions.

The reconstruction of the log conductivity of every piezometer for each measurement campaign and the comparison among them has been very useful to evaluate the characteristics of the groundwater and the dynamics of the phenomenon of marine ingression at local scale. The information of the individual piezometers were used to make a first summary of the distribution of the water quality of coastal phreatic aquifer at regional scale. In particular, evaluating the thickness of freshwater above the transition zone ($EC \leq 2.5$ mS/cm), it was possible to represent data at regional scale, identifying the areas in which this thickness is always present, is more or less accentuated or is always absent (Figure 3.11(a)). Within these areas, the shape of conductivity profile in each piezometer shows appreciable differences in some cases. This shape is directly proportional to the salinity and depends on hydrodynamic parameters characteristic of the site, distribution of piezometric heads in the system, and mass balance. The shape of the log is a peculiar element for each piezometer and, in most cases, has a regular behaviour in time. The thickness of fresh water above the transition zone and the absolute values of conductivity, especially at the points closest to the sea, result to be more variables. For example, piezometer P18 - Classe (Figure 3.11 (b)) records the same values of EC with depth and its profile is always repeated in an identical manner. It is possible to notice a thickening of the superficial portion of freshwater in spring months of 2010, as a result of the winter rainfalls. The increase of this thickness, which results in an increase in the hydraulic load, has not, however, effect on the transition zone, which remains stable over time [see Appendix B for the complete monography of P18].

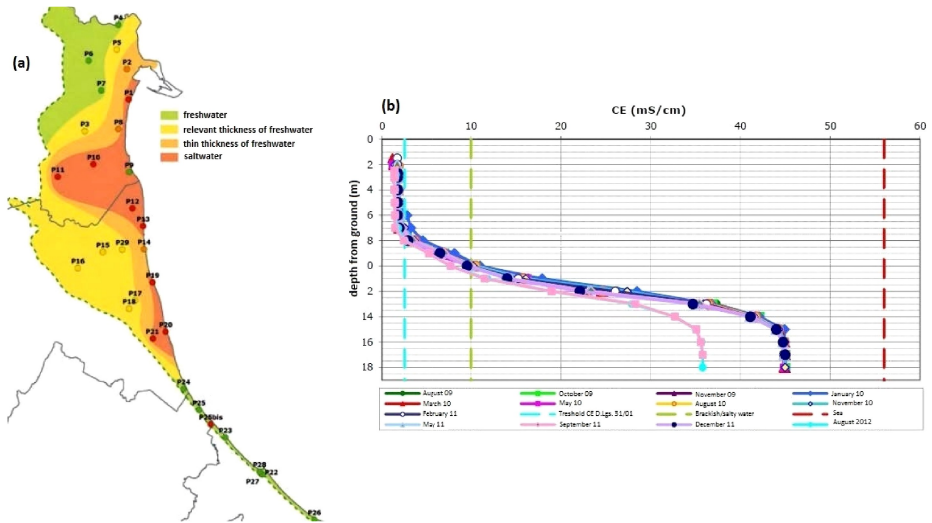


Figure 3.11 (a) Regional synthesis based on the presence and the thickness of freshwater above the transition zone; (b) Electrical conductivity (EC) compared to depth, for piezometer P18-Classe, in different months (2009-2012) [modified from *Bonzi et al.*, 2010].

3.3.2 UNIVERSITY OF BOLOGNA (RAVENNA) SURVEY NETWORK

To characterize from a lithological point of view the coastal phreatic aquifer of Ravenna, and to study in detail its geochemistry, a new piezometric network was planting at aquifer scale, within the *Coastal Salt Water Intrusion* project, result of an agreement between the University of Bologna, ENI and the Municipality of Ravenna. Unlike wells implanted in previous research projects, in most cases located within the pine forests, in this case the wells have been distributed as homogeneous as possible.

The choice of the type of well to be monitored is crucial in groundwater study [Hantush, 1964; Shalev et al., 2009]. Within the project, the selected piezometers are entirely fenestrated and completely penetrating the aquifer.

The emplacement of the gravel pack, external to the piezometer, has been avoided, in order to prevent the creation of preferential flow paths during the sampling phase.

In April 2010, the installation of 37 new wells began. The work was realized in two campaigns, respectively in the south (April 2010) and in the north (September 2010) of Ravenna (Figure 3.12). The drillings have different final depths, according to the need to install a deep piezometer or to arrive to the clay basement that delimits the aquifer. This base has a variable depth, varying between -30 m near the coast and, then, decreasing depth westward. Despite the large number of wells available, in February 2011 two other wells were excavated, with the same design characteristics. These wells are located near an irrigation canal, west of Pineta Ramazzotti in Lido di Dante [see Appendix B for more details]. After the installation of the piezometers, the elevation of the mouth well was detected, and consequently the topographic surface, through a GPS survey integrated by a leveling campaign. In June 2010, a first campaign was performed on new wells. During this phase, electrical conductivity and temperature profiles were performed in the well, and groundwater depth has been measured. The same data were recorded in a second campaign, performed in the overall aquifer, in December 2010, with the addition of chemical and isotopic analysis on samples. In parallel to data collection at the overall aquifer scale, monitoring seasonal campaigns have been conducted in the transect within V Basin, collecting, also in this case, electrical conductivity, temperature profiles, and samples for chemical analysis in the laboratory. The transect was monitored in December 2010, in February, April and June 2011. In July 2012, a monitoring campaign was performed, dedicated exclusively to the coastal portion V Basin, including, in addition to the previous analysis, even the field measurements of some elements as

compounds of nitrogen and iron, otherwise not measurable in the laboratory [Greggio, 2013].

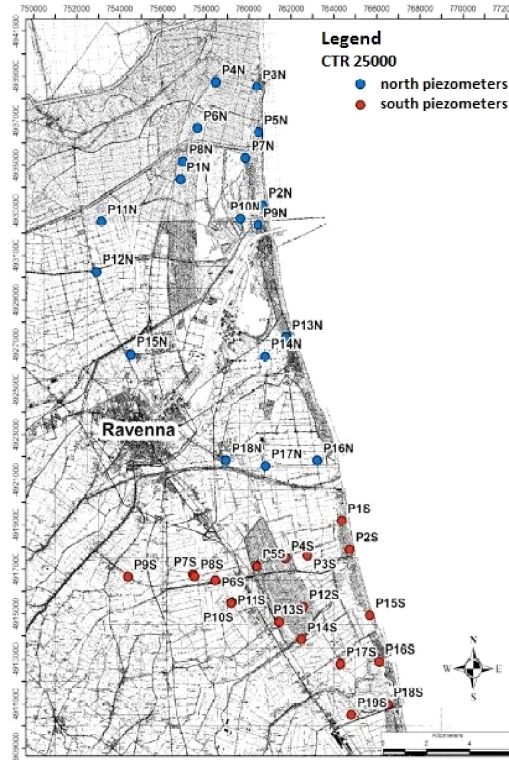


Figure 3.12 Localization of the 37 monitoring wells of *Coastal Salt Water Intrusion* project [Greggio, 2013].

In the following, elaborations realized from different studies are presented. Figure 3.13 shows groundwater depth maps, at overall aquifer scale. It is possible to notice, regardless of season, that the area where water table is deeper is west of Pineta di Classe, in correspondence of the territory more depressed morphologically; here elevations below sea level are reached, also of few meters. Similarly, it is clear that water table is constantly above the sea level in the area of well P9S, located about 10 km from the coastline. Other points, where water table is depressed, are in the

southern portion of Pineta di San Vitale and its northern summit, whose values are about -1m a.s.l. Comparing the maps for the months of June and December 2010, it is clear that groundwater depths tends to decrease from summer to winter, especially in correspondence of the phreatic aquifer (coastal dunes and historical pine forests), and adjacent to the main water bodies, i.e. Fiumi Uniti and Lamone. Even in the most depressed part of the analyzed area, groundwater depth varies from -3.7m in June to - 2.8m in December 2010. Similarly, behind the well P9S, it changes from 1.7m to 2.3m, respectively in June and December. This analysis is confirmed by Figure 3.14, which depicts the areas where the water table is higher or lower than sea level.

Since water table is almost always at sea level or below, also due to the low topography of the area, there is a dominant flow direct from the sea inland along the coastal plain, as shown in Figure 3.15. Pialasse, open to the sea, and the Adriatic itself serve as a constant load for the coastal area, directing most flow vectors inland. Considering water pumps, in most cases the portions of the aquifer that are depressed coincide with the area interested by their presence. Similarly, also the flow vectors converge towards these lifting systems. Among the main watersheds of these underground reservoirs, Fiumi Uniti in the south and the course of Lamone in the north are included. Also Punta Alberete, as in general the entire western portion of the Pineta San Vitale, turns out to be a point of origin of the flow vectors, that shows the presence of a hydraulic head above sea level.

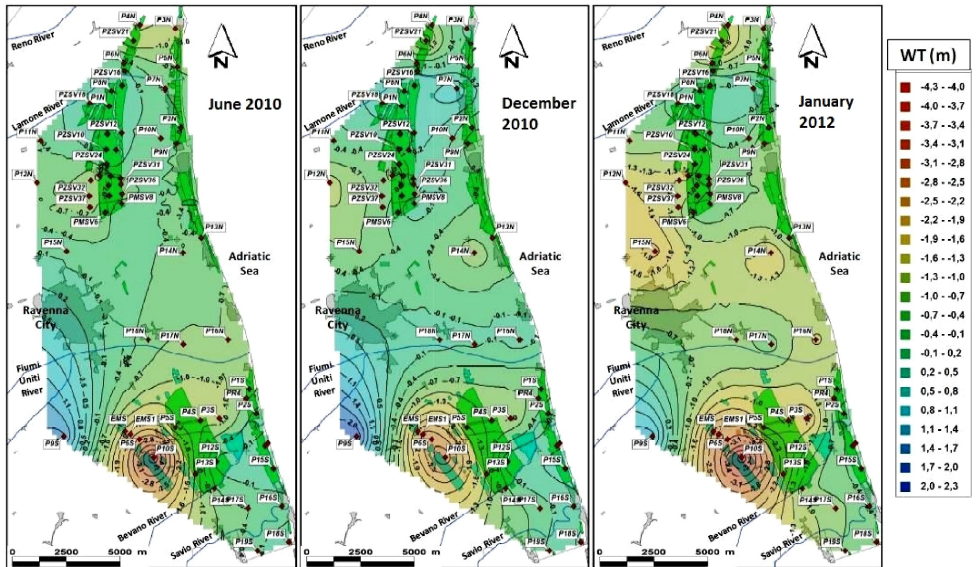


Figure 3.13 Map of groundwater depth, for June 2010, December 2010, and January 2012 [modified from Greggio, 2013].

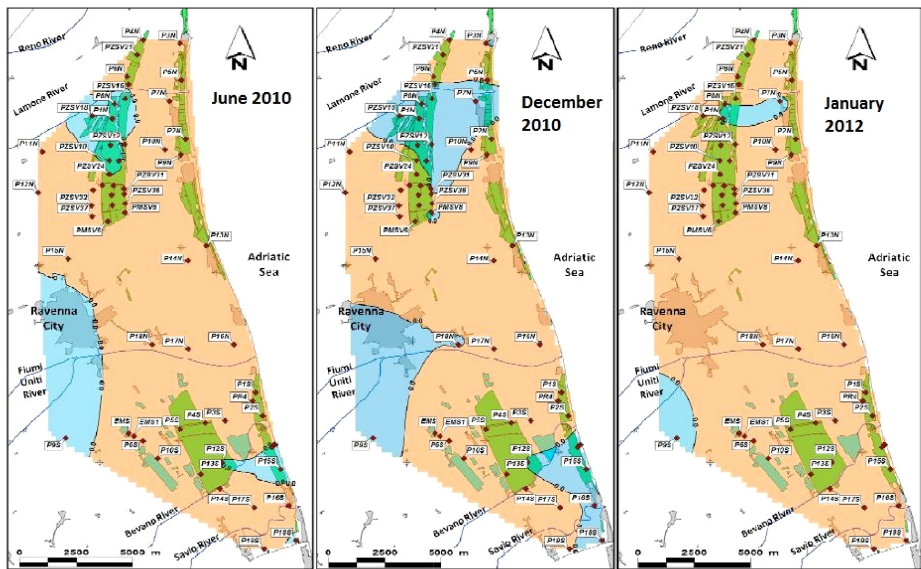


Figure 3.14 Maps of portions of territory where groundwater is above sea level (blue) or below sea level (orange) [Greggio, 2013].

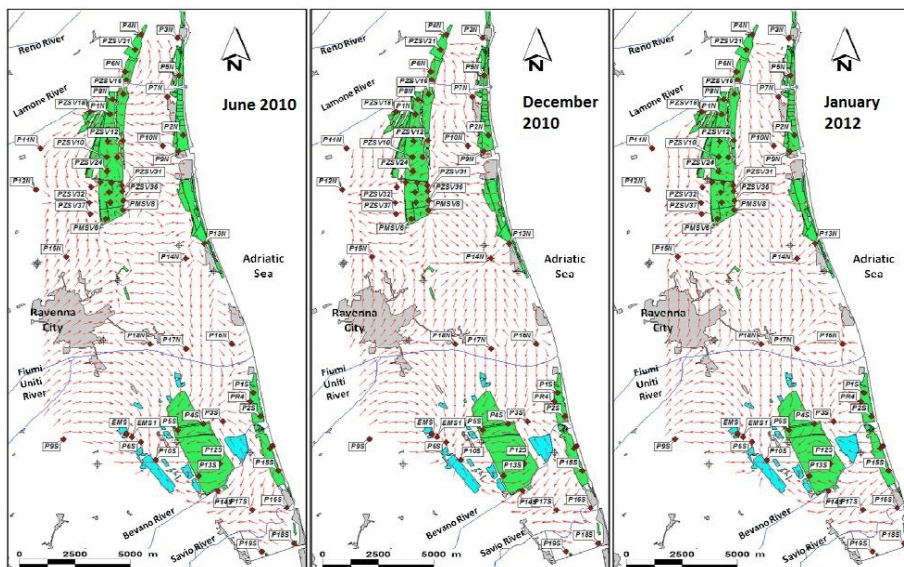


Figure 3.15 Maps of flow vectors [Greggio, 2013]

3.4 FOCUS ON SOUTH RAVENNA

The present dissertation focuses in particular on the southern part of Ravenna littoral, from Lido di Dante in the north to Lido di Classe in the south (Figure 3.16). This area, as discussed in detail previously, is affected by many issues, i.e. low water table level, insufficient aquifer recharge, sea water encroachment along rivers and canals, land reclamation drainage, water pumping from wells, up-welling of connate water from the bottom of the aquifer, evapotranspiration, natural and anthropogenic land subsidence. All these factors need to be appropriately described in order to understand the dynamics occurring in this low coastal plain.



Figure 3.16 Location of the study area.

In particular, this area is strongly affected by groundwater salinization, due to (i) salt-water intrusion from the sea boundary, because of the strong hydraulic gradients landwards, and (ii) upwelling of Holocene brackish and salty water from the bottom of the aquifer, where the water table is below

sea level [Mollema *et al.*, 2013]. Moreover, the site owns a high natural and environmental value, entirely located within the Regional Park of the Po Delta - Station "Pineta di Classe and Saline di Cervia", and protected as "natural beauty", Special Protection Area, Site of Community Importance, Ramsar, and Oasis of wildlife protection.

The area object of study is characterized by a row of active dunes in the east, covered by halophilic bushy and grass vegetation, adjacent to multiple rows of paleo-dunes inland covered by pine trees (*Pinus pinaster*) [Antonellini, Mollema, 2010]. The paleo-dunes, on which the coastal pine forest grows, is drained by two ditches parallel to the coast, while farmland extends to the east past the last row of paleo-dunes. As discussed in Section 3.2.4, this territory is relatively young and affected by natural, i.e. differential compaction of sediments, and anthropogenic, i.e. water and gas withdrawal, land subsidence. The first is 2-3 mm/year, while the latter presents order of 3 mm/year today, with peaks in south Ravenna up to 15 mm/year.

The low topography requires a land reclamation drainage system to keep the Ravenna territory dry, and this purpose is achieved thanks to a dense network of canals, organized in mechanical drainage basins [Stefani, Vincenzi, 2005]. Coastline progradation and land reclamation have allowed for freshening of the ground water in the upper permeable sedimentary sequence below the study area during the past 150-200 years, although recently this trend has been reversed in some parts of the aquifer.

The shallow coastal aquifer, with a depth of 20-30 meters, is formed by a sequence of sand and silty-clay bodies [Amorosi *et.*, 2004], whose sediments were deposited in the last sea level high stand (Figure 3.17) [Marchesini *et al.*, 2000]. Most of the shallow aquifer is made up by beach bar sands. North of the Bevano River, some silty-clay deposits, belonging

to a distal delta sedimentary environment, are found at an average depth of 10 m and have a thickness up to 15 m. These fine-grained deposits disappear in a southward direction. The sands of the aquifer are often covered, at the surface, by thin levels of continental clay [Amorosi *et al.*, 2005]. The coastal phreatic aquifer of this area contains scattered freshwater lenses floating on top of brackish and saline water, and is recharged only via rainfall infiltration and excess irrigation [Antonellini *et al.* 2008; Mollema *et al.* 2013; Vandenbohede *et al.*, 2014].

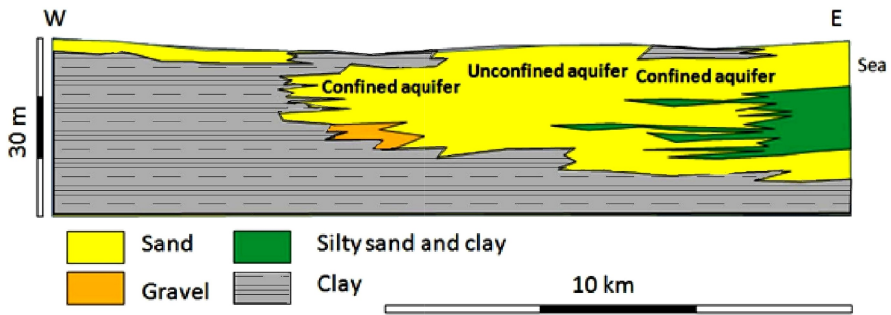


Figure 3.17 Schematic East-West cross sections showing the structure of the shallow coastal aquifer south of Ravenna.

4. Methodology

4.1 TIME SERIES ANALYSIS

A time series is a sequence of values collected over time on a particular variable, that can be observed at discrete times, averaged over a given time interval, or recorded continuously with time [Haan, 1977]. If the time series is characterized by observations of a single phenomenon, it is called univariate time series, otherwise it is multivariate. It can be distinguished into deterministic or stochastic, depending on the events that are observed, or a combination of both.

A deterministic time series $\{x_t, t \in T\}$ is defined by a function $\Psi_t = \Psi(t, x_{t-1}, x_{t-2}, \dots)$ such that $E(y_t - \Psi_t)^2 = 0, t \in T$, hence the series can be predicted starting from the past values, without committing any errors. A stochastic time series, indeed, represents a phenomenon whose temporal evolution is aleatory, hence, given the uncertainty of the process, every prediction is affected by errors.

Following a classical approach, also known as Components Analysis, a time series is a combination (additive/multiplicative) of three deterministic components (trend, seasonality, cycle) and a stochastic term (white noise). In this way, all the components are defined through classical statistical inference, e.g. mean, variance. Alternatively, the modern approach aims to determine a theoretical reference model, where the parameters are estimated through past observations: this approach is able to generate a time series as similar as possible to that one under analysis. Once

demonstrated the reliability of the model, it can be used to make statistical predictions, i.e. study the future events of a certain phenomenon by continued stability in the general structural properties that have occurred in the past [*Battaglia, 2007*].

In this work the focus is on the stochastic approach to study time series, whereby a time series can be considered as a realization of a random process.

4.2 TIME SERIES AS A STOCHASTIC PROCESS

Each observation x_t can be considered as a realization of a random variable X_t , hence a time series $\{x_t, t \in T\}$ is a realization of a family of random variables $(X_t)_{t \in T}$, i.e. a finite realization of a stochastic process [Battaglia, 2007].

A probability space (W, F, P) is considered, where W is the set of elementary elements, F is the algebra of events on W , and P is the probability measure defined on F , and a parametric space T , defined as a set of times. A real stochastic process $(X_t)_{t \in T}$ is a function $x(\omega, t)$, finite with real values, that associates a number to every couple (ω, t) , consisting of a random variable ω and a temporal instant t [Yaglom, 1962].

A first classification of stochastic processes is based on set T and on the type of variables involved in the process. It is possible to define:

- discrete processes with discrete parameters;
- discrete processes with continuous parameters;
- continuous processes with discrete parameters;
- continuous processes with continuous parameters.

In particular, a process with discrete parameters is characterized by a discrete set T , e.g. set N or Z , while one with continuous parameters is defined on a interval of R . Usually hydrologic time series are considered as continuous processes with discrete parameters: t assumes integer values and indexes the observations realized with constant time step, e.g. measurements every hour, day and so on. Observed values, i.e. realizations of individual process variables, have a continuous distribution and can be referred either to instantaneous or cumulative measurements, e.g. average daily flow [Battaglia, 2007].

A state of process at instant t is defined as x_t at fixed $t \in T$. The trajectory of process associated with ω is the application $t \rightarrow x_t(\omega)$, for every fixed $\omega \in W$ [Yaglom, 1962].

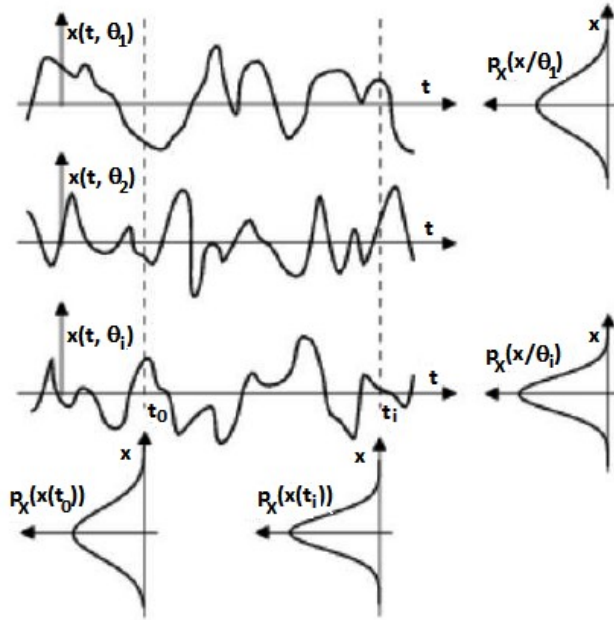


Figure 4.1 Status and trajectory of a stochastic process.

A stochastic process is completely described by the joint distribution of (x_1, \dots, x_n) for every time instant, so we need to know all possible distribution functions:

$$F(x_1, \dots, x_n) = \Pr(X_{t_1} < x_1, \dots, X_{t_k} < x_k) \tag{4.1}$$

The features of a stochastic process are hence linked to its probability distribution, which involves an infinite number of components, consequently it is impossible to estimate them. A stochastic time series is a finite part of a realization of a stochastic process, so only one trajectory can

be considered among the infinite ones that the process could generate. For this reason, it is possible to describe the process on the basis of the first two moments of the variable X_t , i.e. mean, variance and covariance:

$$\mu_t = E[X_t] \tag{4.2}$$

$$\sigma^2 = Var[X_t] = E[X_t - \mu_t]^2 \tag{4.3}$$

$$\gamma_{t_1,t_2} = E\{[X_{t_1} - \mu_{t_1}][X_{t_2} - \mu_{t_2}]\} \tag{4.4}$$

If $t_1 = t_2 = t$, autocovariance and variance coincide, because autocovariance is defined as the variance among random variables of the same stochastic process, spaced apart by a time lag equal to l :

$$l = |t_2 - t_1| \tag{4.5}$$

Alternatively, the autocovariance is defined as the covariance when $l = 0$. Another useful feature to describe the process is the autocorrelation function (ACF), which allows to determine the correlation among X_{t_1} and X_{t_2} , and assumes values between -1 and 1:

$$\rho_{t_1,t_2} = \frac{\gamma_{t_1,t_2}}{\sigma_{t_1,t_2}} \tag{4.6}$$

4.3 STATIONARY STOCHASTIC PROCESSES

In order to further simplify the discussion of the problem, the class of stochastic processes is narrowed and hereinafter the ones able to satisfy two conditions are considered. First, the behaviour of the process does not degenerate as parameter t increases, and it is sufficient to verify that moments of finite order has finite value. Secondly, the statistical properties of the process are constant for all values of t . A process responding to these conditions is stationary [Battaglia, 2007].

The hypothesis of stationarity is crucial for statistical forecasting. Indeed, stationary stochastic processes have special properties that make them suitable for the probabilistic modeling of many time series. There are two types of stationarity.

A stochastic process $\{x_t, t \in T\}$ is strictly stationary if, for every $n \in \mathbb{N}$, $(t_1, \dots, t_n) \in T^n$, and for every h such that $t_i + h \in T^n$:

$$P(X_{t_1} = x_1, \dots, X_{t_n} = x_n) = P(X_{t_1+h} = x_1, \dots, X_{t_n+h} = x_n) \quad (4.7)$$

where P is the probability density function if the distribution is absolutely continuous. If $n = 1$, it follows that distribution of X_t is the same for each t , while the mean and the variance are constant and time - independent:

$$\mu_t = \mu \quad (4.8)$$

$$\sigma_t^2 = \sigma \quad (4.9)$$

In this case, the autocovariance function depends only on time lag among the two variables and not on instants t_1 and t_2 . Hence, imposing $t_1 = t$ and $t_2 = t + h$, it is possible to obtain:

$$\gamma_{t,t+h} = E\{[X_t - \mu][X_{t+h} - \mu]\}, \quad \forall h \quad (4.10)$$

In stationary stochastic processes, autocovariance represents the linear relationship among pairs of random variables composing the process, which are temporally out of phase by an amount equal to h . It is characterized by the following properties:

$$\gamma(0) = Var(X_t) \quad (4.11)$$

$$\gamma(h) = \gamma(-h) \quad (4.12)$$

Since autocovariance function is strictly linked to autocorrelation function (ACF), it follows that ACF has similar properties:

$$\rho(0) = 1 \quad (4.13)$$

$$\rho_h = \rho_{-h} \quad (4.14)$$

$$|\rho_h| \leq 1 \quad (4.15)$$

The graphical display of the relationship between the correlation coefficient and the parameter h is called the correlogram. The points are generally joint with the x-axis by vertical segments, whose length represents the degree of linear correlation of process variables. A process with uncorrelated variables is characterized by the absence of vertical segments:

$$\rho(h) = \begin{cases} 1 & \text{per } h = 0 \\ 0 & \text{per } h \neq 0 \end{cases} \quad (4.16)$$

If correlation is strong, there will be rather long vertical segments, and the value of h indicates the time lag between the two variables considered [Battaglia, 2007].

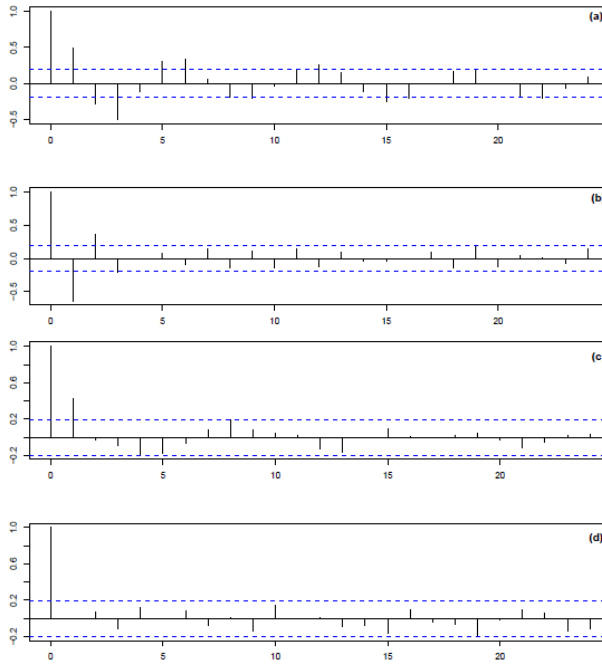


Figure 4.2 Examples of correlograms. **(a)** Seasonal component of 6 lags; **(b)** Fast oscillations; **(c)** Positive autocorrelation at lag 1; **(d)** White noise.

In time series, correlation among variables X_t and X_{t+h} can be influenced by linear intermediate relationships $X_{t+1}, X_{t+2}, \dots, X_{t+h-1}$, hence it is useful to define partial autocorrelation function (PACF):

$$P(h) = \text{Corr}[X_t - E(X_t | X_{t+1}, \dots, X_{t+h-1}), X_{t+h} - E(X_{t+h} | X_{t+1}, \dots, X_{t+h-1})] \quad (4.17)$$

The hypothesis of strictly stationarity is an ideal condition, unattainable in practice because it imposes constraints on the entire distribution and the moments of any order. For most of the applications, it is possible to rely on the assumption of weak stationarity or covariance stationarity.

A stochastic process $\{x_t, t \in T\}$ is weak stationary of order s if, for

every $n \leq s$, $(t_1, \dots, t_n) \in T^n$, and for h such that $t_1 + h \in T^n, \forall i$:

$$E\{X_{t_1} X_{t_2} \dots X_{t_n}\} = E\{X_{t_1+h} X_{t_2+h} \dots X_{t_n+h}\} \quad (4.18)$$

It follows that strictly stationarity implies weak stationarity of order s [Battaglia, 2007]. Usually, a stationarity of order 2, involving the first two moments, is sufficient. In this case, mean, variance, and covariance of any pair of observations depend only on h and not on t :

$$E[X_t] = \mu \quad \forall t \quad (4.19)$$

$$\gamma[X_t, X_{t+h}] = \gamma_h \quad \forall t, h \quad (4.20)$$

From (4.20), if $h = 0$, the variance γ_0 of a stochastic process is constant. Since stationarity of the second order is satisfactory, in the following we will refer to this form of stationarity.

4.3.1 INVERTIBILITY ASSUMPTION

Considering a stationary stochastic process $(X_t)_{t \in T}$, it is possible to determine univocally autocovariance and autocorrelation function, but not vice versa. These function do not describe completely a process, and it is demonstrable that there are more processes characterized by the same autocovariance function. The hypothesis of invertibility is introduced to avoid model multiplicity problem, whereby only one process, among different ones with the same autocovariance function, is invertible. Furthermore, this assumption allows to express a stochastic process as a function of past random variables and a random error.

In conclusion, a stochastic process $(X_t)_{t \in T}$ is invertible if there is a

linear function h and a white noise process such that for every t :

$$X_t = h(X_{t-1}, X_{t-2}, \dots) + \varepsilon_t \quad (4.21)$$

4.3.2 ERGODICITY AND ESTIMATION OF THE MOMENTS OF A STATIONARY PROCESS

A stationary process is ergodic if all statistical properties can be determined starting from a single realization of the process. This property is really fundamental for time series analysis. Being the generating process of the series unknown, the only way to go back to the characteristics of the process is to make inference on the data of the observed series. For a stationary ergodic process, it is possible to estimate the mean value:

$$\hat{\mu} = \frac{1}{n} \sum_{t=1}^n x_t \quad (4.22)$$

The estimator of autocovariance function is defined as:

$$\hat{\gamma}_h = \frac{1}{n} \sum_{t=1}^{n-h} (x_t - \hat{\mu})(x_{t+h} - \hat{\mu}) \quad (4.23)$$

If $h = 0$ in (4.23), we obtain the estimator of variance:

$$\hat{\sigma}^2 = \gamma_0 = \frac{1}{n} \sum_{t=1}^n (x_t - \hat{\mu})^2 \quad (4.24)$$

From (4.23) and (4.24), the estimator of autocorrelation is:

$$\rho_h = \frac{\hat{\gamma}_h}{\hat{\gamma}_0} \quad (4.25)$$

4.4 FROM NON-STATIONARY TO STATIONARY TIME SERIES

Most of real processes are not stationary, especially those representing weather or hydrologic time series [Coulibaly and Baldwin, 2005; Wang *et al.*, 2014]. In these situations, the original time series is transformed into a stationary one in order to maintain the advantages described previously. To achieve this goal, first time series is analyzed, then non-stationary part of the observed series is estimated and finally appropriate transformations are used to remove it and make the series stationary. The presence of non-stationary part is due to three factors, i.e. trend, seasonality, and cycle. One of the easiest way to understand the meaning of these three elements is to report time series data on a chart with time on x-axis, as shown in Figure 4.3.

A trend exists when there is a long-term increase or decrease in the data, and represents the underlying direction of the phenomenon. The presence of this factor means that the time series is not perfectly aligned with respect to the horizontal axis, but it follows an increasing or decreasing trajectory. The trend is a relevant component if considering economic time series, while is less evident for hydrological or climate data. Seasonality consists of changes that may occur with similar intensity in the same periods every year, but with different intensity during the same year. Finally, cycle component represents fluctuations sign around the trend. It is easily confused with the trend, and for this reason it is usually associated with the first factor.

According to classical additive, or multiplicative, decomposition model, time series data can be represented as the realization of a process which is function of the three factors described above, i.e. deterministic

components of the process, to which a factor is added, or multiplied. This latter is the white noise, which is the probabilistic component of the process. The noise has an erratic nature that determines the number of short-term fluctuations. Normally it is treated as a stationary stochastic process.

In the following, some methods for estimation and subsequent removal of trend and seasonal component from time series are discussed.

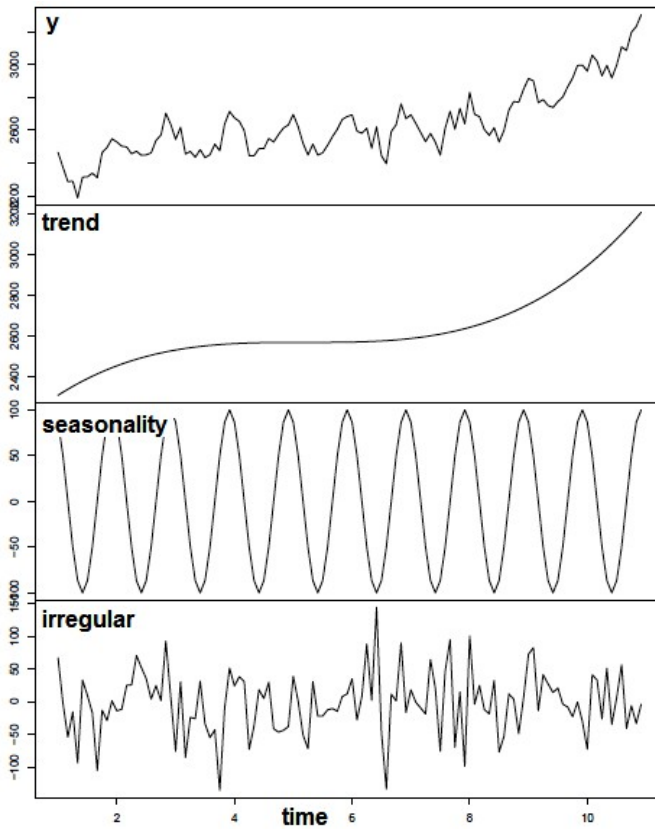


Figure 4.3 Components of a non-stationary time series y_t . It is possible to notice that the amplitude of seasonal oscillations and irregular component are equal, regardless the level of the original time series.

4.4.1 ESTIMATING AND REMOVING TREND COMPONENT

First step to make a stationary series is trying to build a new series that is only a function of the component you want to remove, in this case the trend. Two different approaches are usually followed, relying on parametric or non-parametric interpolation.

Analytical or parametric interpolation supposes that trend effect is a mathematical function of time. Graphically, this corresponds to fit the data with a straight line or a parabola indicating the underlying trend. Ordinary least squared method are then adopted to estimate the parameters of the function, that corresponds substantially to perform a regression analysis on the data.

Mechanical or non-parametric interpolation replaces each data with the average of the data relating to a range that includes it, i.e. moving average. The final effect is known as smoothing of the series, since the oscillations disappear and only the underlying trend remains.

Once interpolation has been estimated, it is necessary to purge the data from the estimated trend, i.e. detrending the series. To achieve this goal, the estimated component can be subtracted from data, or splitted if the model is multiplicative, but this method is related to the procedure used for the representation of the trend, hence it can be affected by all possible errors made in the first estimation phase. Alternatively, a technique of differentiation of the observed series can be adopted to avoid this problem, which consists in calculating the differences between each data and the previous one for a number of times necessary to remove the underlying trend. Following the latter approach, the detrended series retains a direct relationship with data from original series, but dynamic properties are totally different [*Battaglia, 2007*].

4.4.2 ESTIMATING AND REMOVING SEASONAL COMPONENT

The removal of seasonal component is usually subsequent detrending operations. Generally this component is associated to a periodic function, whose period depends on the seasonality that you want to remove, e.g. 12 months if a yearly seasonality is detected.

The parameters of the periodic function can be estimated on collected data in a similar way as discussed in 4.4.1, i.e. analytical interpolation. An easier approach consists in assuming the seasonal effect of each month equal to the average of all the data for that month in different years, reducing the estimation of seasonality to the calculation of monthly average.

Regarding the removal of seasonal component, there are two possibilities, i.e. (i) either to subtract/divide computed monthly average from data, or (ii) use differentiation technique. In this case, the latter procedure is different from the one discussed in 4.4.1; indeed, rather than previous observation, data of previous year in the same season is subtracted from original data.

Once seasonality has been removed, the initial time series can be considered only a function of the random component treated as a stationary stochastic process.

4.5 MAIN STATIONARY STOCHASTIC PROCESSES

In the following, the main features of stochastic processes commonly adopted in time series analysis are discussed. All processes satisfy the assumptions of reversibility and ergodicity.

4.5.1 AUTOREGRESSIVE PROCESSES AR(p)

The general form of an autoregressive (AR) process of order p [Box and Jenkins, 1976; Piccolo, 1990] is given by:

$$X_t = \phi_0 + \phi_1 X_{t-1} + \dots + \phi_p X_{t-p} + \varepsilon_t \quad (4.26)$$

where ϕ_i , $i = 0, \dots, p$, are constant model parameters, while $\{\varepsilon_t\}$ is a white noise process, with each element characterized by an identical, independent, mean-zero distribution. In this process, variable X_t consists in weighted sum of past values of the variable, to which a white noise, evaluated on actual time, is added.

It is convenient to use a time-series “operator”, called the lag operator when writing equations such as (4.26). This operator is defined as:

$$L^h X_t = X_{t-h} \quad (4.27)$$

The parameters of (4.26) can be written as $\phi(L) = (1 - \phi_1 L - \dots - \phi_p L^p)$, hence polynomial process AR(p) can be written in the following compact form:

$$\phi(L)X_t = \varepsilon_t \quad (4.28)$$

4.5.2 MOVING AVERAGE PROCESSES MA(q)

The general form of a moving average (MA) process of order q [Enders, 2004] is defined as:

$$X_t = \varepsilon_t + \varphi_1 \varepsilon_{t-1} + \dots + \varphi_q \varepsilon_{t-q} \quad (4.29)$$

where φ_j , $j=0, \dots, q$, are constant model parameters, and $\{\varepsilon_t\}$ is still a white noise process. In this process, variable X_t consists in weighted sum of a sequence of random variables, with zero-mean and constant variance.

It is usual to express the parameters of (4.29) as $\varphi_i = -\theta_i$, hence it becomes:

$$X_t = \varepsilon_t - \theta_1 \varepsilon_{t-1} - \dots - \theta_q \varepsilon_{t-q} \quad (4.30)$$

Introducing then the lag operator defined in (4.27), model parameters can be written as $\theta(L) = (1 - \theta_1 L - \dots - \theta_q L^q)$, and polynomial process MA(q) can be written as:

$$X_t = \theta(L)\varepsilon_t \quad (4.31)$$

4.5.3 AUTOREGRESSIVE MOVING AVERAGE PROCESSES ARMA(p,q)

Linear stochastic processes, described by (4.26) and (4.30), can be combined in a single model, i.e. ARMA (p,q) [Box and Jenkins, 1976; Hamilton, 1994]:

$$X_t - \sum_{i=1}^p \phi_i X_{t-i} = \phi_0 + \varepsilon_t - \sum_{j=1}^q \theta_j \varepsilon_{t-j} \quad (4.32)$$

The process defined by (4.32) consists of p autoregressive terms, involving p lagged values of the variable, and q moving-average terms, with q lagged values of the innovation ε . If $q = 0$, hence there are no moving-average terms, then the process is a pure autoregressive process, i.e. AR(p). Similarly, if $p = 0$ and there are no autoregressive terms, the process is a pure moving-average, i.e. MA(q).

Using lag operator notation defined in (4.27), we can rewrite the ARMA(p, q) process compactly as:

$$\phi(L)X_t = \phi_0 + \theta(L)\varepsilon_t \tag{4.33}$$

It is possible to demonstrate that the stationarity of ARMA (p, q) process described in (4.33) depends only on the parameters of the autoregressive part. In particular, the process results stationary if and only if the roots of the order- p polynomial $\phi(L)$ all lie outside the unit circle.

4.6 BOX-JENKINS PROCEDURE

A commonly procedure for the construction of a model to generate a time series is the one provided by Box and Jenkins [Box and Jenkins, 1976]. Here, statistical analysis of time series is divided in three steps, explained in detail hereinafter:

- 1) model identification and model selection;
- 2) parameter estimation;
- 3) model checking by testing whether the estimated model conforms to the specifications of a stationary univariate process.

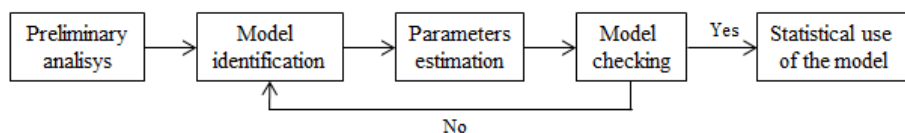


Figure 4.4 Box-Jenkins procedure.

4.6.1 MODEL IDENTIFICATION AND PARAMETERS ESTIMATION

First step to perform a statistical time series analysis is the choice of the correct autoregressive and moving average order, i.e. p and q . Since the ARMA model deals with stationary processes, previously this condition must be verified, and eventually transformations as described in 4.4.1 and 4.4.2 should be adopted.

Once time series is stationary, autocorrelation function (ACF) and partial autocorrelation function (PACF) of the stationary process are

estimated, and the corresponding correlogram is realized. From ordinary or partial correlogram plots, it is possible to determine the length of autoregressive and moving average process. Considering an AR(p) model, ACF plot tends to zero with a behaviour that depends on the values of the parameters ϕ_i , while PACF plot is different from zero for $h \leq p$ and becomes zero if $h \geq p+1$. A MA(q) process, on the other side, is characterized by an ACF different from zero for $h \leq q$, and becomes zero if $h \geq q+1$, while the PACF tends to zero with a behaviour depending on the values of the parameters θ_i .

However, it may happen that one of the two conditions is not verified clearly, and indeed the analysis of ACF and PACF leads to identify more possible models. Since the values of ACF and PACF are estimated from a sample and not exact, it is difficult to identify uniquely the pair (p,q) , because each analyzed series suggests a range of possible pairs able to ensure a good fitting to the data [Battaglia, 2007]. For this reason, additional model selection criteria are adopted to describe an ARMA process, based on parsimony principle, that suggests to prefer among various models the one characterized by less coefficients and a lower computational burden for parameters estimation. One of the most commonly used criteria is the Akaike information criteria (AIC) [Konishi and Kitagawa, 2008; Kadane and Lazar, 2004], defined as:

$$AIC = -\frac{2}{n}(\log L(\hat{\delta}) - k) \tag{4.34}$$

where k is the number of model parameter, i.e. $k=p+q+2$, $\hat{\delta} = (\hat{\phi}_0, \hat{\phi}_1, \dots, \hat{\phi}_p, \hat{\theta}_1, \dots, \hat{\theta}_q, \sigma_\varepsilon^2)$ is the vector of estimated parameters, $L(\hat{\delta})$ is the function of maximum likelihood of data, and $-2k/n$ is a "penalty" term, that depends positively on the number of estimated parameters.

AIC function increases when the goodness of fit of the model decreases, otherwise it decreases. Moreover, considering equal values of $\log L$, AIC is greater for the model with more parameters.

The procedure for identification of the model is recursive, i.e. the selected values of p and q are those able to minimize AIC function.

4.6.2 TESTING GOODNESS-OF-FIT OF THE MODEL

The final stage of the procedure provides for control of adequacy of the model. Residuals are defined as differences between observed values of the dependent variable and the ones generated by the model:

$$e_t = y_t - \hat{y}_t \quad (4.35)$$

If the model has been correctly identified, residuals satisfy the initial assumptions on white noise, i.e. ε_t : zero-mean, with constant variance and normal distribution. A first check can be done graphically, analyzing the scatter plot of residuals versus time. If all assumptions are met, the points of scatter plot tend to arrange themselves randomly, producing a cloud of points without any structure. Alternatively, it is possible to test for normality, i.e. checking if residuals are distributed normally.

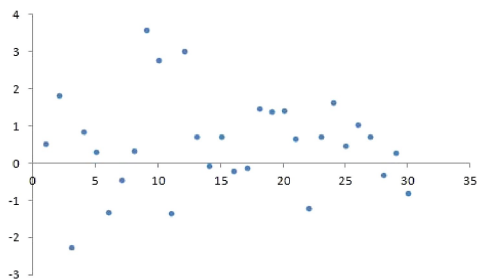


Figure 4.5 Example of scatter plot of residuals.

4.7 TIME SERIES ANALYSIS WITH LINEAR MODELS

In the context of time series, a model consists of one or more equations that link actual or lagged values of one or more processes, in order to describe the time course of observed phenomena [Battaglia, 2007].

Considering now the object of study of this work, i.e. the salinization process of the aquifer, we expect that theoretical model, built from the observed time series, will be able to fit the data in the best possible way, and to correlate the hydrological variables involved in the phenomenon.

In the remainder of this section, the focus is on the analysis of multiple stationary stochastic processes, i.e. multivariate series, defined on the same parametric set [Beck and Katz, 2011]. Only linear dependencies between processes will be considered, in order to assess the compliance that simpler linear models have with observations, although probably the relationships among hydrological variables are non-linear [Sivakumar, 2009; Amorocho and Orlob, 1961].

4.7.1 STATIC LINEAR MODELS

Linear models are defined static when the relationship that characterizes them consists only of current variables, i.e. variables associated at the same time.

4.7.1.1 SIMPLE LINEAR REGRESSION MODEL

In simple linear regression model, there is only an independent variable or regressor, i.e. x_t , linked to the dependent variable y_t :

$$y_t = \beta_0 + \beta_1 x_t + \varepsilon_t \quad (4.36)$$

where y_t is the model response, β_0 is the regression constant, i.e. the intercept of the line, β_1 is the linear regression coefficient, i.e. the slope of the line, and ε_t is the error.

Considering a data set of observed values, Equation (4.36) can be written in matrix form:

$$\mathbf{y} = \mathbf{x}\boldsymbol{\beta} + \boldsymbol{\varepsilon} \quad (4.37)$$

$$\begin{bmatrix} y_{t_1} \\ \dots \\ y_{t_N} \end{bmatrix} = \begin{bmatrix} 1 & x_{t_1} \\ \dots & \dots \\ 1 & x_{t_N} \end{bmatrix} \begin{bmatrix} \beta_0 \\ \beta_1 \end{bmatrix} + \begin{bmatrix} \varepsilon_{t_1} \\ \dots \\ \varepsilon_{t_N} \end{bmatrix} \quad (4.38)$$

where \mathbf{y} is the vector $N \times 1$ of model responses, i.e. observed data, \mathbf{x} is the matrix $N \times 2$ of independent variables, with the first column of unit value in correspondence of the intercept of the model, $\boldsymbol{\beta}$ is the vector 2×1 of the model parameters, and $\boldsymbol{\varepsilon}$ is the vector $N \times 1$ of errors.

The model is represented graphically by a straight line in xy space, hence building a simple linear regression model basically means to determine the regression line.

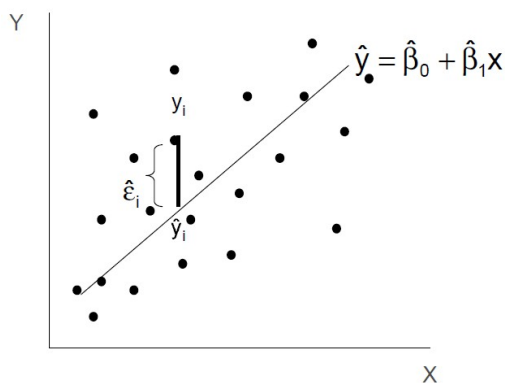


Figure 4.8 Regression line.

4.7.1.2 MULTIPLE LINEAR REGRESSION MODEL

Multiple linear regression models are adopted when the number of dependent variables at time t increases. If the problem becomes multidimensional, e.g. two dimensions, graphically there will be a plane instead of a straight line. In this case, comparing with Equation (4.36), it is possible to obtain:

$$y_t = \beta_0 + \beta_1 x_{1,t} + \dots + \beta_m x_{m,t} + \varepsilon_t \quad (4.39)$$

where y_t is the model response, β_0 is the regression constant, β_1, \dots, β_m are the linear regression coefficients, $x_{1,t}, \dots, x_{m,t}$ are the independent variables, and ε_t is the error.

The error in Equations (4.36) - (4.39) has the following features:

$$E(\varepsilon | x_1, \dots, x_m) = 0 \quad (4.40)$$

$$Var(\varepsilon | x_1, \dots, x_m) = \sigma^2, \text{ hence } Var(y | x_1, \dots, x_m) = \sigma^2 \quad (4.41)$$

$$Cov(\varepsilon_i, \varepsilon_j) = 0, \quad \forall i \neq j \quad (4.42)$$

$$\varepsilon \sim N(0, \sigma^2) \quad (4.43)$$

Equation (4.39) can be expressed in matrix form:

$$\mathbf{y} = \mathbf{x}\boldsymbol{\beta} + \boldsymbol{\varepsilon} \quad (4.44)$$

$$\begin{bmatrix} y_{t1} \\ \dots \\ y_{tN} \end{bmatrix} = \begin{bmatrix} 1 & x_{t1}^1 & \dots & x_{t1}^m \\ \dots & x_{t2}^1 & \dots & x_{t2}^m \\ \dots & \dots & \dots & \dots \\ 1 & x_{tN}^1 & \dots & x_{tN}^m \end{bmatrix} \begin{bmatrix} \beta_0 \\ \dots \\ \beta_m \end{bmatrix} + \begin{bmatrix} \varepsilon_{t1} \\ \dots \\ \varepsilon_{tN} \end{bmatrix} \quad (4.45)$$

where \mathbf{y} is the vector $N \times 1$ of model responses, \mathbf{x} is the matrix $N \times (m+1)$ of independent variables, $\boldsymbol{\beta}$ is the vector $(m+1) \times 1$ of model parameters, and $\boldsymbol{\varepsilon}$ is the vector $N \times 1$ of errors.

The matrix systems, represented in (4.37) and (4.44), can be solved in order to estimate the coefficients by minimizing the sum of errors of linear regression, hence the average error becomes equal to zero.

This procedure, i.e. the Ordinary Least Square (OLS) method, works as follow. Considering a vector of estimates \mathbf{b} evaluated from a sample of n units, the vector of theoretical values \mathbf{y}^* of the dependant variable is determined, with the assumption of a perfect linear dependence, and consequently it is possible to estimate the vector of residuals:

$$\mathbf{y}^* = \mathbf{X}\mathbf{b} \quad (4.46)$$

$$\mathbf{e} = \mathbf{y} - \mathbf{y}^* \quad (4.47)$$

OLS procedure allows to find the coefficient vector \mathbf{b} able to minimize the sum of squared deviations among empirical an theoretical values:

$$\Phi(\mathbf{b}) = \sum_{i=1}^n (y_i - y_i^*)^2 = (\mathbf{y} - \mathbf{X}\mathbf{b})^T (\mathbf{y} - \mathbf{X}\mathbf{b}) = \mathbf{y}^T \mathbf{y} - 2\mathbf{b}^T \mathbf{X}^T \mathbf{y} + \mathbf{b}^T \mathbf{X}^T \mathbf{b} \mathbf{X} \quad (4.48)$$

$$\frac{\partial \Phi(\mathbf{b})}{\partial \mathbf{b}} = \mathbf{0} \quad (4.49)$$

$$\mathbf{X}^T \mathbf{X} \mathbf{b} = \mathbf{X}^T \mathbf{y} \quad (4.50)$$

Finally we are able to assess the value of \mathbf{b} :

$$\mathbf{b} = (\mathbf{X}^T \mathbf{X})^{-1} \mathbf{X}^T \mathbf{y} \quad (4.51)$$

It is possible to demonstrate that \mathbf{b} is BLUE (best linear unbiased estimator) for $\boldsymbol{\beta}$.

4.7.2 DYNAMIC MODELS

Dynamic linear models are described by equations with lagged variables of one or more units of time, in addition to the current variables [Beck and Katz, 2011]. The model is very similar to an ARMA process, except that moving-average is applied to the explanatory variable x instead of the white-noise process.

4.7.2.1 DISTRIBUTED LAG MODEL

A distributed lag model is a dynamic model in which the effect of a regressor x on y occurs over time rather than all at once. In the simple case of one explanatory variable and a linear relationship, we can write the model as:

$$y_t = \alpha + \beta(L)x_t + u_t = \alpha + \sum_{s=0}^{\infty} \beta_s x_{t-s} + u_t \quad (4.52)$$

where y_t is the model response, i.e. the dependent variable, α is the regression constant, β_s are the model parameters to estimate, i.e. the lag weights that define the pattern of how x affects y over time, x_t are the independent variables, and u_t is the stationary error term.

As previously mentioned, Equation (4.52) is very similar to the infinite-moving-average representation of an ARMA process, except that the lag polynomial representing the moving-average is applied to the explanatory variable x rather than to a white-noise process. Of course it is not possible to assess an infinite number of coefficients, hence one approach can be to truncate the lag in a finite length q , which is appropriate if the lag distribution is effectively zero beyond q periods, or to use a functional form that allows the lag distribution in (4.52) to decay gradually to zero.

For a distributed lag model with a finite moving-average representation of length q , Equation (4.52) can be written as:

$$y_t = \alpha + \beta(L)x_t + u_t = \alpha + \sum_{s=0}^q \beta_s x_{t-s} + u_t \quad (4.53)$$

Also in this case, the main focus is to determine the model parameters β_s , which depend on the order of the process q , i.e. the delay effect of x on y . In general, the lag weights β_s are a smooth function of s . If the unrestricted finite distributed lag estimates contradict this smoothness, one can choose to restrict the model to impose smooth lag weights. Restricting the lag coefficients can not only impose smoothness, but also reduces the number of parameters that must be estimated. There are many patterns of smoothness that can be selected to impose a restrictive structure on the weights. One simple restriction on the lag weights is that they decline linearly from an initial positive or negative impact effect to zero at a lag of length $q + 1$:

$$\beta_s = \frac{q+1-s}{q+1} \beta_0, \quad s = 1, \dots, q \quad (4.54)$$

A more common application of restricted distributed lags is the polynomial distributed lag, first explored by *Shirley Almon* [1965]. The most common application of the polynomial distributed lag is restricting the lag coefficients to lie on a quadratic function:

$$\beta_s = \tau_0 + \tau_1 s + \tau_2 s^2 \quad s = 0, \dots, q \quad (4.55)$$

Substituting (4.55) in (4.53), we obtain:

$$\begin{aligned}
 y_t &= \alpha + \beta(L)x_t + u_t = \alpha + \sum_{s=0}^q \beta_s x_{t-s} + u_t = \\
 &= \alpha + \tau_0 \sum_{s=0}^q x_{t-s} + \tau_1 \sum_{s=0}^q s x_{t-s} + \tau_2 \sum_{s=0}^q s^2 x_{t-s} + u_t = \\
 &= \alpha + \tau_0 z_t^0 + \tau_1 z_t^1 + \tau_2 z_t^2 + u_t
 \end{aligned} \tag{4.56}$$

where $z_t^0 = \sum_{s=0}^q x_{t-s}$, $z_t^1 = \sum_{s=0}^q s x_{t-s}$, $z_t^2 = \sum_{s=0}^q s^2 x_{t-s}$.

Parameters estimation problem becomes now a coefficients estimation issue. The determination of order q of the process and coefficients relies on an iterative procedure. First, a range of variation of the order q is established a priori. At each iterative step, for a fixed value of q , a multiple linear regression problem is solved and τ coefficients are evaluated. Consequently β_s are computed from (4.56) and substituted in Equation (4.54) in order to obtain the predict values $y_{pred,t}$ which allow to determine the squared errors:

$$\hat{u}_t^2 = (y_{pred,t} - y_{obs})^2 \tag{4.57}$$

The residual represents the simplest form that likelihood function can assume. Last step of the iterative procedure is the computation of AIC (4.34), in this case expressed by:

$$AIC = \ln \left[\sum_{t=1}^T \frac{\hat{u}_t^2}{T} \right] + \frac{2k}{T} \tag{4.58}$$

where T is the dimension of our observation set, and $k = q+1$. The optimal order of the model is the value of q able to minimize the deviation between estimated series and observed series, hence the value able to minimize AIC function.

4.7.2.2 AUTOREGRESSIVE DISTRIBUTED LAG MODEL (ARDL)

An autoregressive distributed lag (ARDL) model is an ARMA process, with a set of lagged dependent variables, where the moving-average polynomial is applied to the independent variables instead of the white noise. The general form represents an extension of ARMA process to distributed lag model previously discussed:

$$\phi(L)y_t = \delta + \beta(L)x_t + u_t \quad (4.59)$$

where δ is a constant, $\phi(L)$ is a p - order polynomial and $\beta(L)$ is a q - order polynomial.

Expanding the lag polynomials, Equation (4.59) can be written as:

$$y_t = \delta + \phi_1 y_{t-1} + \dots + \phi_p y_{t-p} + \beta_0 x_t + \beta_1 x_{t-1} + \dots + \beta_q x_{t-q} + u_t \quad (4.60)$$

With a sample of T observations, this model can be estimated for $T - \max\{p, q\}$ observations.

As in ARMA models, the coefficients of p - order polynomial $\theta(L)$ affect only the first q lags of the dynamic lag distribution of the effect of x on y . The behaviour of the “tail” of the lag distribution beyond q depends entirely on the autoregressive polynomial $\phi(L)$. The estimation of p and q follows the same considerations for ARMA process, discussed in Section 4.6.1. The property that the dynamic effect is stable is verified only if the roots of $\phi(L)$ lie outside the unite circle.

5. Results and discussion

5.1 APPLICATION OF TIME SERIES ANALYSIS

In this Section, the influence of natural recharge and pumping rate on groundwater levels is evaluated. Consequently the relationship between groundwater levels and the salinity at the top of the phreatic surface is determined. In particular, an approach based on Time Series Analysis is applied to analyze the dynamics among these factors in the shallow phreatic aquifer south of Ravenna (Figure 5.1, discussed in Section 3.4).



Figure 5.1 Location of the piezometers (red dot from *Greggio* [2013], yellow from *Bonzi et al.* [2010]) and pluviometers (blue dot, from ARPA Emilia-Romagna) in the study area.

5.2 TIME DELAY AMONG NATURAL RECHARGE AND PHREATIC LEVEL

In the study area, several piezometers have been installed to monitor the aquifer in the context of the analysis developed by *Bonzi et al.* [2010], and *Antonellini et al.* [2008]. In Appendix B, the main features of these piezometers are presented.

It is interesting to observe that the minimum values of water table are usually detected in autumn (September-December), while the maximum values are registered in the period January-May, as depicted in Figure 5.2. An exception is EMS1, located near a quarry, for which two minima are recorded in June and December 2011, while higher levels are observed in August-October, in correspondence of the minimum records in the other piezometers. Groundwater levels recorded in the piezometers near the coast are below sea level, as a confirmation of the inverse flow of freshwater, from sea to inland, described in Section 3.4. Piezometer MAR2 shows a different behaviour compared to the others, since groundwater level reaches its highest values during the months June - July.

Measurements of water table are affected by natural recharge, in this study considered as the contribution provided by rainfalls, daily registered in the area of interest by two pluviometers (ARPA Emilia-Romagna): PL1 - "Classe" and PL2 - "Idrovora Fosso Ghiaia" (see Figure 5.1). The trend recorded by the pluviometers is similar, with higher values of rainfall during autumn, in particular in the months of September-November, and smaller in summer, usually in May-July. Since the trend depicted for both the pluviometers is similar, in the following only the rainfall data registered at PL1 - "Classe" are considered, to assess the relationship with groundwater levels.

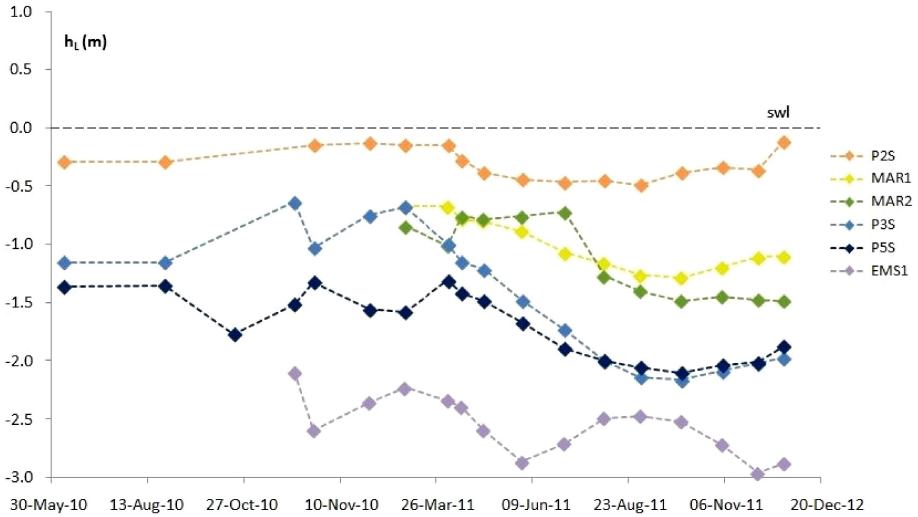


Figure 5.2 Groundwater levels h_L (m asl) versus time, recorded from 06/08/10 till 12/22/2011, for the piezometers of the University network [Greggio, 2013].

Time series of rainfall and water table can be considered as realizations of stochastic processes [Law, 1974; Bárdossy, 1998; Davison, Ramesh, 1996; Rodriguez *et al.*, 1987]. Even in presence of few piezometric data, it is possible to observe a correlation among them. By means of time series analysis, in order to better describe this correlation, the time delay, T_D , between the two time series is identified, as depicted in Figure 5.3. Specifically, the following function is minimized:

$$\min_{T_D} \sum_{i=1}^{t_{max}} [a(t_i) - b(t_i + T_D)]^2 \tag{5.1}$$

where t_i represents a generic day from 1 to t_{max} , days correspondent to the first and last piezometric measurements (see Figure 5.2), $a(t_i)$ is the rainfall measured at time t_i (in mm) and $b(t_i + T_D)$ is the groundwater level measured at time $t_i + T_D$ (in mm).

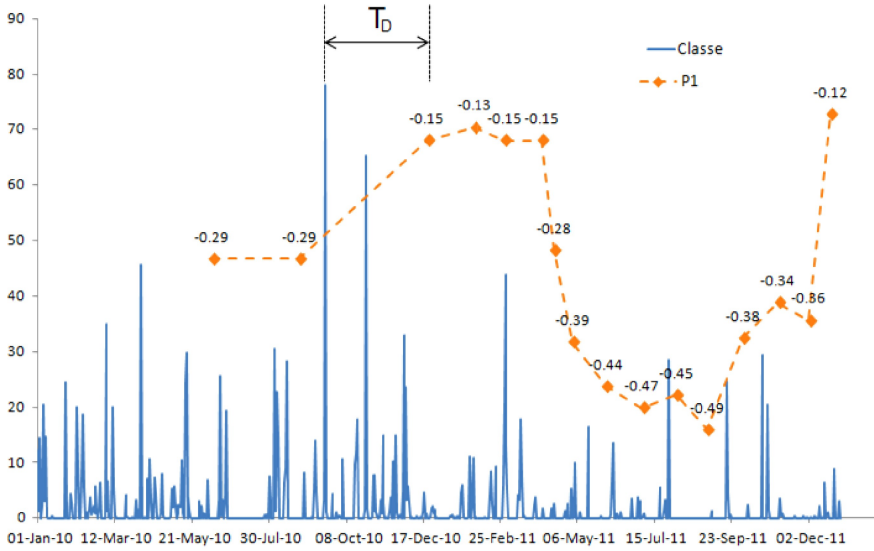


Figure 5.3 Comparison of rainfall time series (mm), recorded at PL1-"Classe", and groundwater level (m a.s.l.) observed at piezometer P2S. Time delay T_d is displayed among the measurements.

From this first analysis, the time delay T_D has been derived. It is possible to observe that each measurement of water table is mainly affected by rainfall events occurred 3-4 months before, depending on peculiar features of areas, as land use and permeability of soil. Once T_D is computed, the two time series are overlapped, in order to identify the correlation between correspondent values. Figures 5.4 and 5.5. depict these results by means of normalized scatter plot, considering correlations among daily rainfall events - phreatic level and cumulative rainfall events - phreatic level respectively. In Figure 5.4, the scatter plots show a very good correlation among the two processes, with a coefficient of determination, R^2 , ranging between 0.75 and 0.96, while the time delay of each single couple of correspondent values varies in the range 80-100 days, with an average value of about 90 days. The higher correlation is found in

the piezometers installed in sandy soils, e.g. MAR1, MAR2, P5S. The piezometers in silty soils are usually associated to smaller value of R^2 . Regarding to P2S, it is shown a trend that reflects its proximity to the coast, hence the coefficient of determination results smaller than the others even if it is located in a pinewood, in sandy soil. In Figure 5.5, similar results are presented by considering cumulative precipitation events, i.e. $h_{R,cum}$, occurred in consecutive days, with values of $h_{R,cum}$ higher than 0.5 mm. Correlations exhibit high values also with this assumption, with R^2 ranging from 0.7 to 0.88. With respect to the previous analysis, it is observed that the correlation coefficient seems to decrease, except for piezometers MAR1 and P3S, for which the values are higher.

These first analyses show that a delayed effect exists when the relationship among natural recharge and groundwater level in phreatic coastal aquifer is investigated. This delay is variable according to the characteristics of soils, but quite relevant in terms of correlation.

In the following, dynamic models are applied to examine in detail the link among different variables included in the complex dynamics of the recharge process.

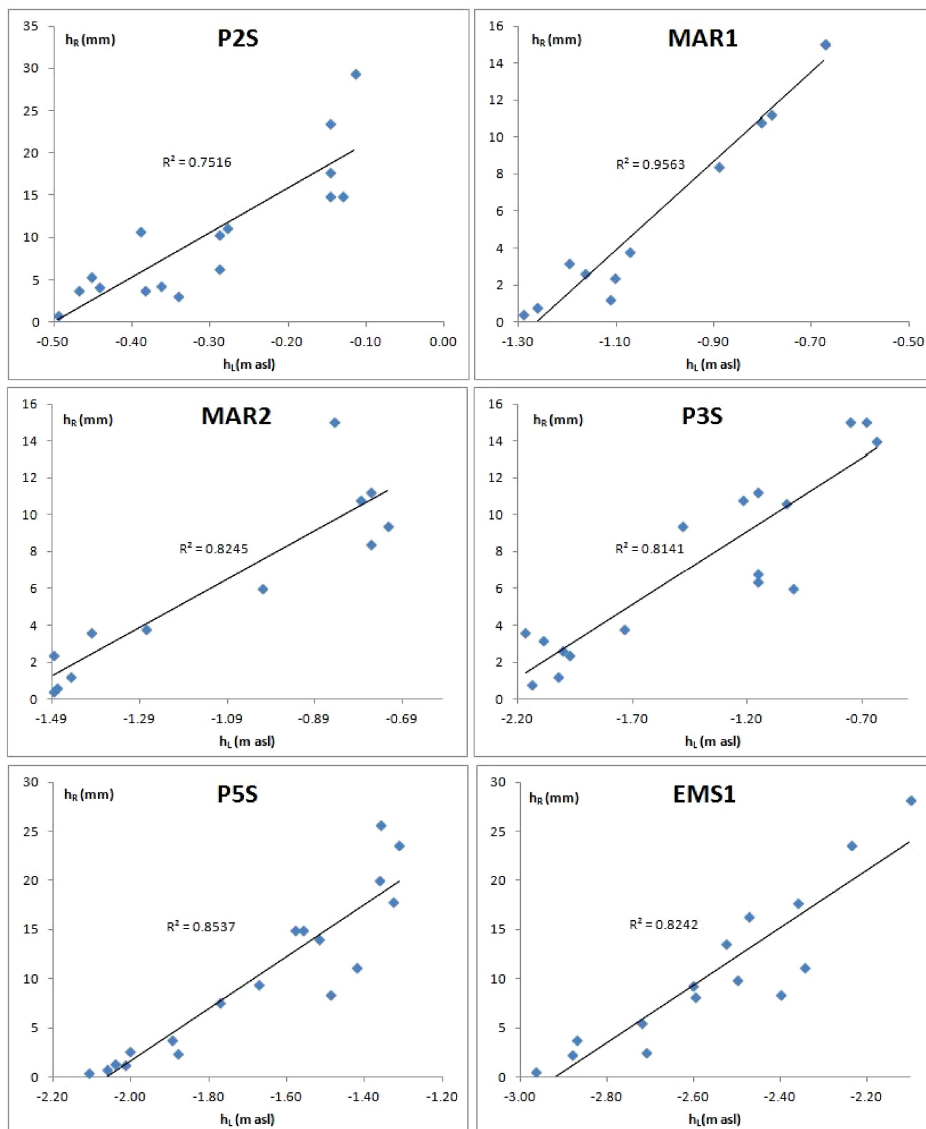


Figure 5.4 Single rainfall events h_R (mm) measured at PL1-"Classe", versus groundwater level h_L (mm asl), registered in the piezometers of Figure 5.1.

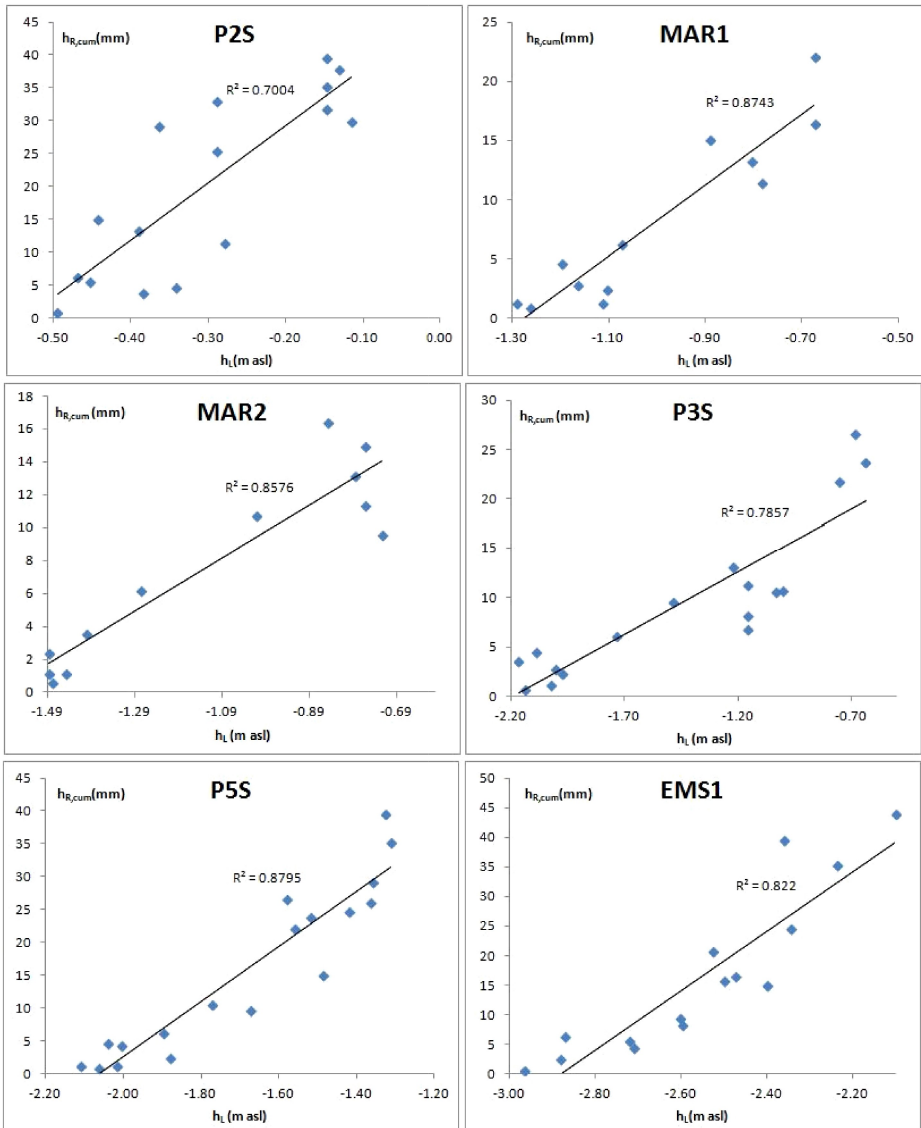


Figure 5.5 Cumulative rainfall events $h_{R,cum}$ (mm) measured at PL1-"Classe", versus groundwater level h_L (mm asl), registered in the piezometers of Figure 5.1

5.3 CHARACTERISTICS OF THE AREA

Before proceeding with any further analysis, it is necessary to identify more consistently the features of the piezometers on which we intend to calibrate the models. Figure 5.6 shows a partition of the area of interest, realized considering homogeneous properties for each zone, i.e. land use, permeability of soils, and the presence of driving forces as pumping machines or channels. In this context, the work is focused on area 1, along the coastline, where the Pineta Ramazzotti is located. The characteristics of the piezometers are collected in Appendix B.



Figure 5.6 Subdivision of the area, according to homogeneous properties of monitoring wells.

5.4 STATIONARITY OF TIME SERIES

In order to apply the dynamic models discussed in Chapter 4, a primary analysis on stationarity of time series of the variables of interest is necessary. In particular, the goal is to achieve a weak stationarity, i.e. variance and covariance of any pair of observations (y_t, y_{t-s}) depending only on s and not on t .

Considering monthly rainfall time series recorded at PL1 - "Classe" (Figure 5.6), the dataset from 2000 to 2012 is reported in Table 5.1. The time plot in Figure 5.7 (a) shows a series with no trend, but that seems to include a seasonal component to be considered. This idea is confirmed by Figure 5.7 (b), where the seasonal component is repeated every year.

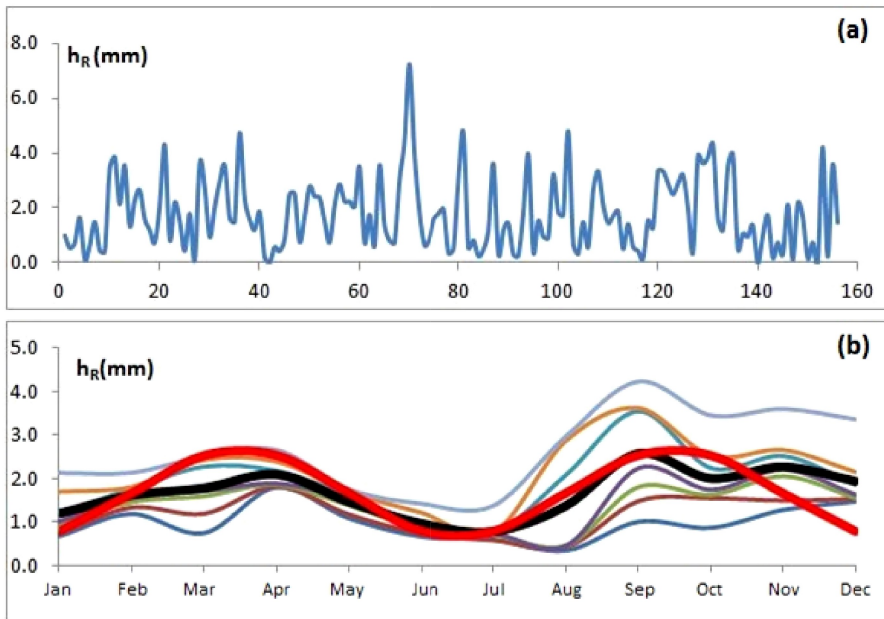


Figure 5.7 (a) Time series of monthly average rainfall from 2000 to 2012, recorded at PL1-"Classe"; (b) Average rainfall for each month versus year: the thick red line represents a spline to detect the presence of seasonal component.

		2000	2001	2002	2003	2004	2005	2006	2007	2008	2009	2010	2011	2012
Jan	Med	1.0	3.6	0.5	2.3	1.7	0.7	0.7	0.5	1.0	2.1	3.4	1.2	0.3
	Std	5.2	8.5	1.6	5.7	4.6	2.2	2.2	1.3	2.0	5.9	6.6	2.9	1.0
Feb	Med	0.5	1.3	1.8	1.6	2.8	1.8	0.9	1.2	0.9	1.5	2.9	3.5	2.1
	Std	1.6	2.9	5.2	5.5	5.4	4.8	2.6	3.0	2.8	3.4	5.0	8.9	11.7
Mar	Med	0.7	2.3	0.1	1.2	2.4	0.6	1.6	3.6	3.2	1.7	2.5	4.0	0.1
	Std	2.5	5.8	0.3	4.9	5.7	2.1	4.7	7.9	7.2	3.6	7.2	9.1	0.6
Apr	Med	1.7	2.7	3.6	1.9	2.4	3.6	1.8	0.3	1.8	1.9	2.9	0.5	2.2
	Std	3.7	7.0	8.1	3.6	5.0	10.9	3.3	1.3	4.5	3.4	8.4	1.2	4.1
May	Med	0.1	1.6	2.8	0.2	1.5	1.4	2.0	1.2	1.8	0.5	3.2	1.1	1.7
	Std	0.5	3.7	5.6	1.0	5.4	5.2	4.8	3.2	4.3	1.5	6.8	3.5	4.8
Jun	Med	0.7	1.2	1.0	0.0	0.7	0.8	0.4	1.5	4.8	1.4	2.0	1.0	0.2
	Std	2.4	3.2	2.9	0.1	2.5	3.8	1.3	4.2	21.3	3.5	5.7	2.7	0.6
Jul	Med	1.5	0.7	2.0	0.6	2.1	0.7	0.5	0.3	0.7	0.6	0.4	1.4	0.8
	Std	3.8	3.5	6.3	3.3	7.6	2.0	2.1	1.0	3.0	2.3	1.4	5.2	3.9
Aug	Med	0.5	2.1	3.0	0.4	2.9	3.0	3.1	0.3	0.3	0.4	3.9	0.0	0.0
	Std	2.4	6.8	7.6	1.6	13.1	12.0	7.1	0.9	1.4	2.3	8.5	0.0	0.1
Sep	Med	0.4	4.3	3.6	0.9	2.2	4.4	4.8	1.8	1.5	0.2	3.6	1.0	4.2
	Std	1.4	9.7	9.0	3.1	7.3	13.9	14.1	4.9	3.7	0.6	14.1	4.5	9.4
Oct	Med	3.4	0.9	1.6	2.5	2.3	7.2	0.6	4.0	0.6	1.6	3.9	1.7	0.2
	Std	7.8	2.5	4.2	6.1	7.8	18.8	2.0	9.1	2.2	5.7	12.2	6.3	1.2
Nov	Med	3.9	2.2	1.5	2.5	2.1	4.0	0.8	0.4	2.7	1.3	4.3	0.2	3.6
	Std	9.5	3.9	3.4	7.2	4.3	6.7	2.9	1.2	4.5	2.9	7.7	0.7	8.0
Dec	Med	2.1	1.5	4.7	0.8	3.5	1.9	0.3	1.5	3.4	3.4	1.6	0.8	1.5
	Std	7.5	4.5	8.8	1.9	8.2	3.7	0.5	5.0	5.0	7.1	4.3	2.0	2.8

Table 5.1 Monthly average values (mm/month) and standard deviations recorded at PL1-"Classe", from 2000 to 2012.

To make the time series stationary, a parametric approach is adopted in this work, relying on seasonal "dummy" variables. Since the amplitude of oscillations does not change in time, the time series can be seen as an additive model:

$$y_t = T_t + S_t + I_t = S_t + I_t \quad (5.2)$$

where T_t represents the trend component, varying slowly in time and determining the level of the series (in this case, it is assumed that $T_t = 0$), S_t is the periodic component, and I_t is the erratic term that can be assimilated to a stationary stochastic process. Assuming that the seasonal component is expressed as follow by means of the coefficients φ_i , Equation (5.2) becomes:

$$y_t = \varphi_1 d_{1,t} + \dots + \varphi_{12} d_{12,t} + I_t \tag{5.3}$$

where $d_{1,t}$ is a variable equal to 1 if the month of January is considered and 0 elsewhere, $d_{2,t}$ is equal to 1 in February, and so on. These kind of variables are usually called "dummy" [Almon, 1965; Thomas, Wallis, 1971]. Equation (5.3) can be re-written in matrix form as:

$$\begin{bmatrix} y_{t_1} \\ y_{t_2} \\ \dots \\ y_{t_N} \end{bmatrix} = \begin{bmatrix} 1 & 0 & 0 & 0 & 0 & 0 & 0 & 0 & 0 & 0 & 0 & 0 \\ 0 & 1 & 0 & 0 & 0 & 0 & 0 & 0 & 0 & 0 & 0 & 0 \\ 0 & 0 & 1 & 0 & 0 & \dots & \dots & \dots & \dots & \dots & \dots & \dots \\ \dots & \dots & \dots & \dots & \dots & \dots & \dots & \dots & \dots & \dots & \dots & \dots \\ 0 & 0 & 0 & 0 & 0 & 0 & 0 & 0 & 0 & 0 & 0 & 1 \\ 1 & 0 & 0 & 0 & 0 & 0 & 0 & 0 & 0 & 0 & 0 & 0 \\ 0 & 1 & 0 & 0 & 0 & 0 & 0 & 0 & 0 & 0 & 0 & 0 \\ \dots & \dots & \dots & \dots & \dots & \dots & \dots & \dots & \dots & \dots & \dots & \dots \\ 0 & 0 & 0 & 0 & 0 & 0 & 0 & 0 & 0 & 0 & 0 & 1 \\ \dots & \dots & \dots & \dots & \dots & \dots & \dots & \dots & \dots & \dots & \dots & \dots \end{bmatrix} \cdot \begin{bmatrix} \varphi_1 \\ \varphi_2 \\ \dots \\ \varphi_{12} \end{bmatrix} + \begin{bmatrix} I_{t_1} \\ I_{t_2} \\ \dots \\ I_{t_N} \end{bmatrix} \tag{5.4}$$

where y_{t_1}, \dots, y_{t_N} are the observed values, and I_{t_1}, \dots, I_{t_N} is the vector of erratic components. To remove the seasonal component, Multiple Linear Regression (MLR) is employed to solve the problem and determine the unknown coefficients φ_i .

Dealing with monthly data, it is reasonable to require that $\sum \varphi_i = 0$, i.e. during a year the sum of the seasonal component is equal to 0. Hence, the previous MLR problem is solved assuming the following

constraint:

$$\mathbf{a}_{12 \times 1} = \begin{bmatrix} 1 \\ 1 \\ \dots \\ 1 \end{bmatrix} \rightarrow \mathbf{a}^T \cdot \boldsymbol{\varphi} = 0 \rightarrow \hat{\boldsymbol{\varphi}}_{\mathbf{a}} = \hat{\boldsymbol{\varphi}} - \frac{\mathbf{a}^T \hat{\boldsymbol{\varphi}}}{\mathbf{a}^T \mathbf{a}} \mathbf{a} \quad (5.5)$$

In this way, the seasonal component S_t results a time series with mean equal to zero, while I_t , i.e the stationary component, conserves the mean of the original time series y_t , since we imposed $T_t = 0$. Figures 5.8 shows the resulting time series if (a) the constraint (5.5) is imposed, and if (b) it is not considered.

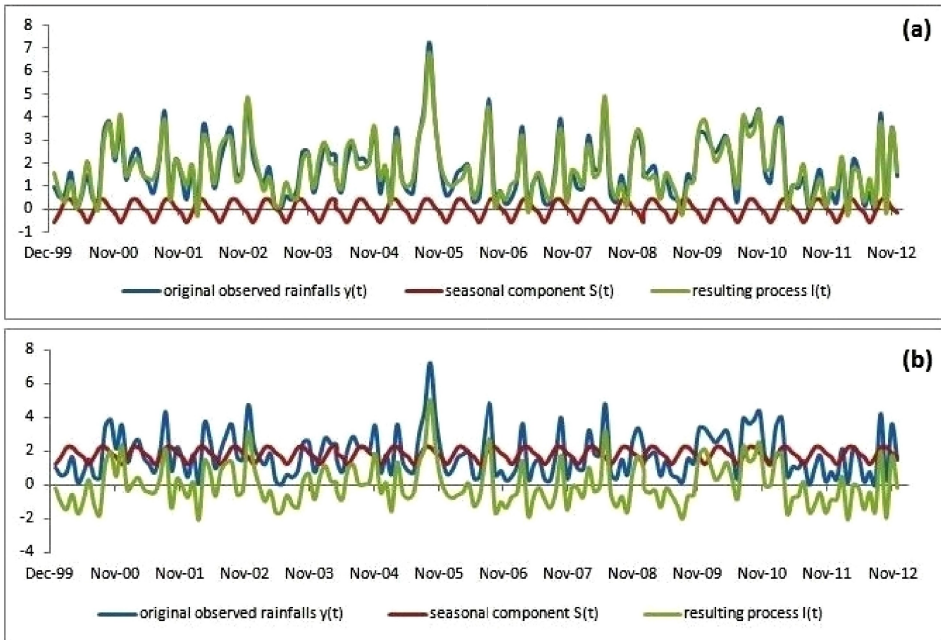


Figure 5.8 (a) Time series deseasonalized imposing the constraint on seasonal component (5.5); (b) Time series deseasonalized without the constraint.

It is possible to notice, in Figure 5.8 (a), that S_t , i.e. the seasonal component, is a zero-mean process, while I_t conserves the same mean of the original time series y_t . In Figure 5.8 (b), this behaviour is the opposite, since I_t becomes a zero-mean process. In both cases, the magnitude of the seasonal component does not change: the series is just shifted by a quantity equal to the average of the entire process y_t , i.e. 1.79.

The same procedure is applied to groundwater level time series. For the analyses, the monitoring well P20 (Emilia-Romagna Region) has been selected among the piezometers of area 1 (Figure 5.6), since it presents the highest number of measurements in the period 2009 - 2012, both of phreatic level and salinity concentration at the top of the aquifer [for details, refer to Appendix B]. Since in some months measurements are not present, first available data have been interpolated, and consequently extrapolated at monthly scale. The resulting values of this operation are presented in Table 5.2, while in Tables 5.3 and 5.4 the values derived from MLR regression with and without constraint are reported.

Aug-09	0.27	Aug-10	0.5	Aug-11	0.33
Sep-09	0.27	Sep-10	0.57	Sep-11	0.28
Oct-09	0.35	Oct-10	0.64	Oct-11	0.30
Nov-09	0.56	Nov-10	0.66	Nov-11	0.34
Dec-09	0.8	Dec-10	0.66	Dec-11	0.38
Jan-10	1.01	Jan-11	0.65	Jan-12	0.41
Feb-10	1.14	Feb-11	0.64	Feb-12	0.45
Mar-10	1.22	Mar-11	0.63	Mar-12	0.48
Apr-10	1.21	Apr-11	0.61	Apr-12	0.47
May-10	1.12	May-11	0.59	May-12	0.12
Jun-10	0.89	Jun-11	0.55	Jun-12	0.35
Jul-10	0.55	Jul-11	0.45	Jul-12	0.25

Table 5.2 Monthly average values of groundwater levels (m a.s.l.) registered at P20.

I(t) - constraint on seasonal component					
Aug-09	0.29	Aug-10	0.52	Aug-11	0.35
Sep-09	0.27	Sep-10	0.57	Sep-11	0.28
Oct-09	0.33	Oct-10	0.62	Oct-11	0.28
Nov-09	0.57	Nov-10	0.67	Nov-11	0.35
Dec-09	0.77	Dec-10	0.63	Dec-11	0.35
Jan-10	1.03	Jan-11	0.67	Jan-12	0.43
Feb-10	1.16	Feb-11	0.66	Feb-12	0.47
Mar-10	1.22	Mar-11	0.63	Mar-12	0.48
Apr-10	1.19	Apr-11	0.59	Apr-12	0.45
May-10	1.13	May-11	0.60	May-12	0.13
Jun-10	0.86	Jun-11	0.52	Jun-12	0.32
Jul-10	0.57	Jul-11	0.47	Jul-12	0.27

Table 5.3 Erratic components I_t (mm) obtained from monthly values of Table 5.3, considering the constraint (5.5) on seasonal component.

I(t) - without constraint on seasonal component					
Aug-09	-0.34	Aug-10	-0.19	Aug-11	-0.18
Sep-09	-0.39	Sep-10	-0.15	Sep-11	-0.23
Oct-09	-0.36	Oct-10	-0.10	Oct-11	-0.21
Nov-09	-0.14	Nov-10	-0.06	Nov-11	-0.13
Dec-09	0.03	Dec-10	-0.10	Dec-11	-0.11
Jan-10	0.26	Jan-11	-0.07	Jan-12	-0.01
Feb-10	0.46	Feb-11	0.01	Feb-12	0.14
Mar-10	0.50	Mar-11	-0.02	Mar-12	0.17
Apr-10	0.45	Apr-11	-0.05	Apr-12	0.17
May-10	0.38	May-11	-0.04	May-12	-0.12
Jun-10	0.09	Jun-11	-0.11	Jun-12	0.10
Jul-10	-0.21	Jul-11	-0.15	Jul-12	0.08

Table 5.4 Erratic components I_t (mm) obtained from monthly values of Table 5.3, without considering the constraint (5.5) on seasonal component.

Again, I_t from Table 5.3 shows the same mean of the original process, while I_t from Table 5.4 is a zero-mean process.

Aiming to apply dynamic models, the stationarity of the resulting process I_t is assessed, both for rainfall and groundwater level time series, in the case of a zero-mean process. It is possible to demonstrate that the results exhibit the same behaviour in both two cases.

5.5 APPLICATION OF THE ARDL MODEL ON TIME SERIES: RAINFALLS - PHREATIC LEVEL

As discussed previously in Section 4.7.2.2, Equation (4.60) represents an Auto-Regressive Distributed Lag (ARDL) model, obtained combining an autoregressive (AR) part, with p lagged values of the dependent variable, and a moving-average (MA) part, with q lagged values of the independent variable. In Section 4.6.1, the procedure to obtain the order p and q of the two parts is described. For simplicity, the equation of the model is recalled:

$$y_t = \delta + \phi_1 y_{t-1} + \dots + \phi_p y_{t-p} + \beta_0 x_t + \beta_1 x_{t-1} + \dots + \beta_q x_{t-q} + u_t$$

and in matrix form:

$$\begin{bmatrix} y_{t_1} \\ y_{t_2} \\ \dots \\ y_{t_N} \end{bmatrix} = \begin{bmatrix} 1 & z_{t_1}^0 & z_{t_1}^1 & z_{t_1}^2 & y_{t_1-1} & \dots & \dots & y_{t_1-p} \\ 1 & z_{t_2}^0 & z_{t_2}^1 & z_{t_2}^2 & y_{t_2-1} & \dots & \dots & y_{t_2-p} \\ \dots & \dots & \dots & \dots & \dots & \dots & \dots & \dots \\ 1 & z_{t_N}^0 & z_{t_N}^1 & z_{t_N}^2 & y_{t_N-1} & \dots & \dots & y_{t_N-p} \end{bmatrix} \cdot \begin{bmatrix} \delta \\ \xi_0 \\ \xi_1 \\ \xi_2 \\ \phi_1 \\ \dots \\ \phi_p \end{bmatrix} + \begin{bmatrix} u_{t_1} \\ u_{t_2} \\ \dots \\ u_{t_N} \end{bmatrix} \quad (5.6)$$

To determine coefficients ζ_0 , ζ_1 , ζ_2 , and consequently β_i , refer to Section 4.7.2.1.

Assuming as dependent variables the groundwater level time series, and as regressors the rainfall time series, both stationarized as previously described, first the autocorrelation function (ACF) of the dependent variable is evaluated, in order to define the autoregressive order of the process. Figure 5.9 shows the ACF for groundwater levels measured at P20. It is evident that, after 3 lags, the correlogram depicts values lower than the 95%-confidence bounds, hence it seems that it is relevant to consider $p = 4$, i.e. retain terms till y_{t-4} for the autoregressive part.

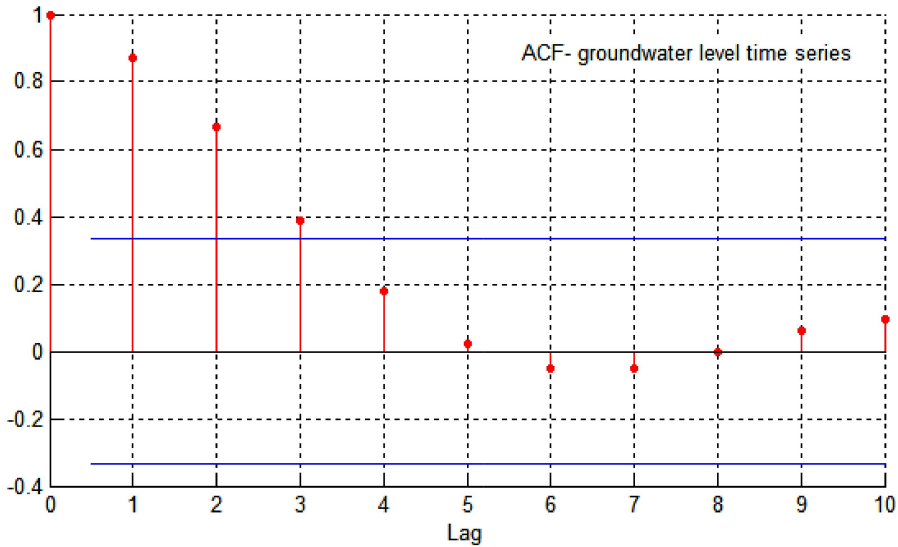


Figure 5.9 Autocorrelation function for groundwater levels. At lag 0, $\rho(0)=1$.

Consequently, the ARDL model describing the process results:

$$y_t = \delta + \phi_1 y_{t-1} + \phi_2 y_{t-2} + \phi_3 y_{t-3} + \phi_4 y_{t-4} + \sum_{s=0}^q \beta_s x_{t-s} + u_t \quad (5.7)$$

Relying on model selection criteria, AIC is used to evaluate the order q of the moving average part. For this case, a value equal to 4 is detected, meaning that the actual observed value seems to be affected by rainfall events occurred till 4 months before; this result is in good agreement with the one obtained in Section 5.2.

By solving a MLR regression problem, the coefficients of (5.7) are obtained, reported in Table 5.5. Finally, Figure 5.10 depicts the comparison among model predictions and observations, showing a very high correlation, i.e. R^2 , with a slope of the regression line almost equal to 1, representing a good approximation of the model to the data.

δ	-0.0049
β_0	0.0344
β_1	0.0175
β_2	0.0056
β_3	-0.0013
β_4	-0.0031
ϕ_1	0.8911
ϕ_2	0.1842
ϕ_3	-0.3341
ϕ_4	-0.0682

Table 5.5 Coefficients of (5.7), obtained by solving the MLR problem.

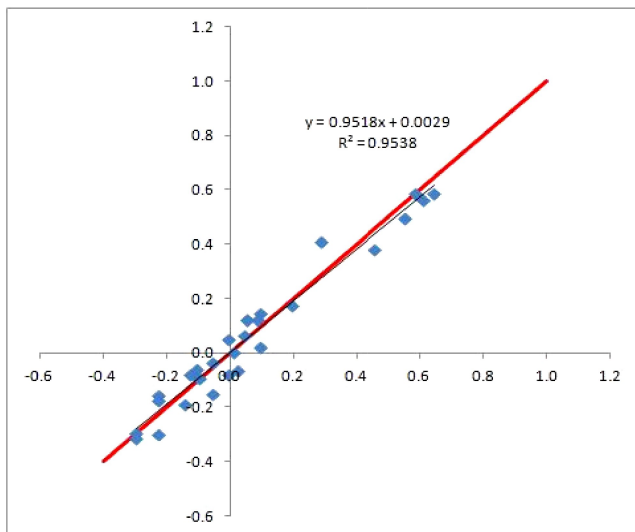


Figure 5.10 Comparison among model predictions and observations.

The validation of the model preserves good correlations, as depicted in Figures 5.11 (a) and (b). Here, the comparisons among model predictions and observations are presented in the case of 10% and 25% of data employed for validation.

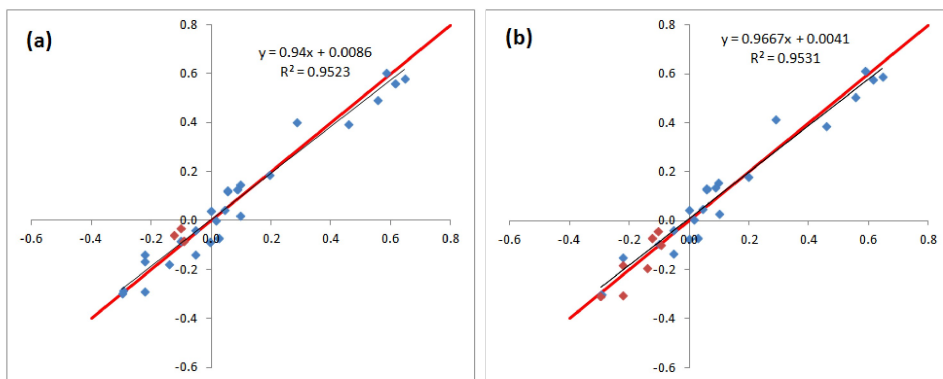


Figure 5.11 (a) Comparison among model predictions and observations, with 10% data used for validation; **(b)** Comparison among model predictions and observations, with 25% data used for validation.

5.5.1 Testing residuals and stability of the process

If the model has been correctly identified, residuals satisfy the assumption of behaving as a white noise, i.e. a zero-mean process, with constant variance and normal distribution. Furthermore, the erratic component should be uncorrelated. Figure 5.12 (a) shows the comparison among the estimated CDF of the residuals and the correspondent normal distribution. Residuals are computed as $e_t = y_t - \hat{y}_t$, where y_t is the observed values, and \hat{y}_t is the model predictions. In Figure 5.12 (b), the ACF of the residuals is obtained, showing a pattern with no correlations among each steps outside the confidence bounds. It is possible to observe that the only autocorrelation value outside the 95%-confidence interval, i.e. ± 0.3465 , occurs at lag 0, as expected for a white noise process. Based on these results, the erratic terms can be considered as a realization of a white-noise process. Figures 5.13 (a)-(d) present the same analyses for the cases of 10% and 25% of available data employed for validation.

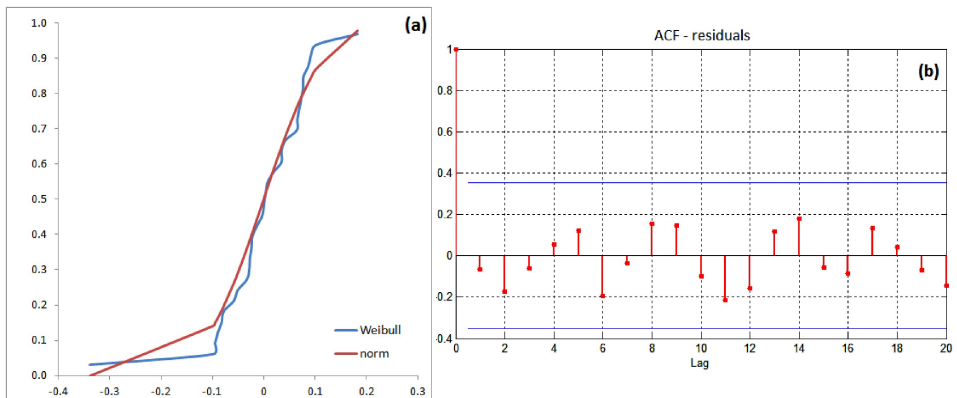


Figure 5.12 (a) Comparison among Weibull and normal distribution of residuals; (b) Autocorrelation function (ACF) of residuals.

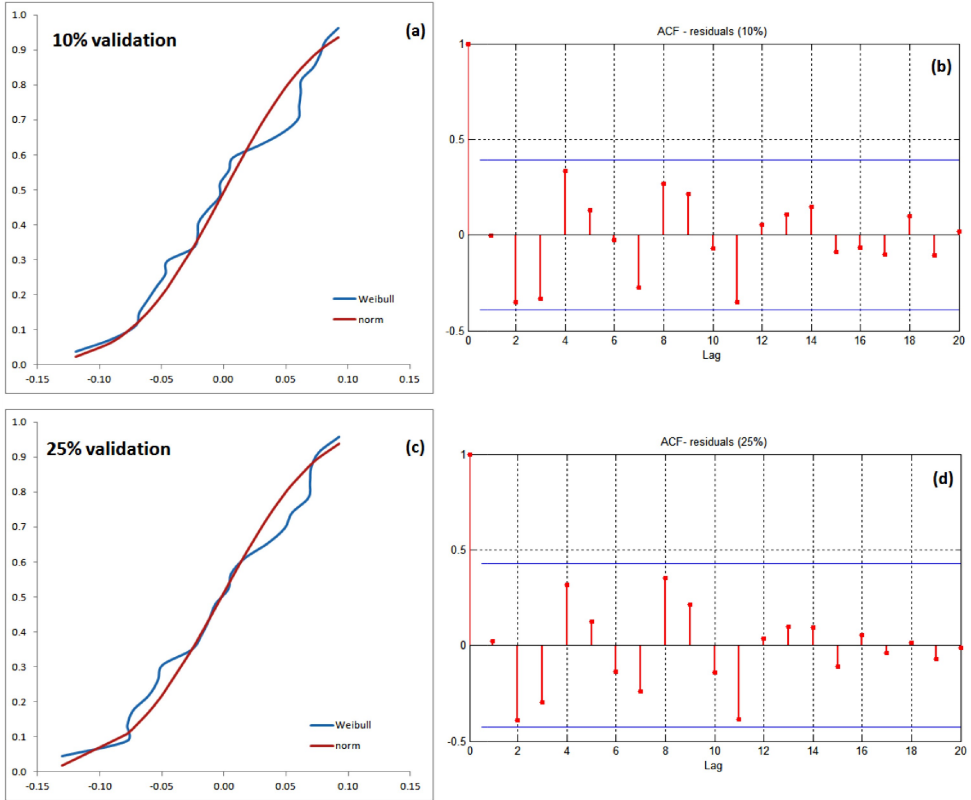


Figure 5.13 (a), (c) Comparison among Weibull and normal distribution of residuals, for 10% and 25% of available data employed for validation ; (b), (d) Autocorrelation function (ACF) of residuals, for 10% and 25% of available data employed for validation.

To check the stability of the model, another test to perform relies on the computation of the roots of polynomial $\phi(L)$ of order p , i.e. the polynomial of the autoregressive part of the process. These roots should all lie outside the unit circle, hence the roots $|r_j| > 1$. Evaluating the roots of the polynomial, as reported in Table 5.6, it is possible to notice that this assumption is satisfied, for all the cases discussed above. In case of complex roots, written as $a+bi$, the modulus must be higher than one to satisfy the condition.

Calibration of the model	
$\phi(L) = 1 - 0.8911L - 0.1842L^2 + 0.3341L^3 + 0.0682L^4$	
r_1	-4.7696
r_2	-2.250
$r_{3,4}$	$1.0557 \pm 0.5028i$
10% validation	
$\phi(L) = 1 - 1.202L + 0.316L^2 + 0.008L^3 + 0.152L^4$	
$r_{1,2}$	$-1.2239 \pm 2.0277i$
$r_{3,4}$	$0.9607 \pm 0.4998i$
25% validation	
$\phi(L) = 1 - 1.2322L + 0.3686L^2 - 0.0353L^3 + 0.1566L^4$	
$r_{1,2}$	$-0.9296 \pm 2.0197i$
$r_{3,4}$	$1.0427 \pm 0.4576i$

Table 5.6 Evaluation of the roots of the autoregressive polynomial, to assess the stationarity.

5.5.2 Comparison between other rainfall/water table time series

In the following analysis, rainfalls measured at PL1-"Classe" and groundwater level time series from piezometer P2S [Greggio, 2013], are considered. After deseasonalization of both time series [see Section 5.4, and refer to Appendix B], the p -order associated with the water table time series, i.e. the autoregressive part, is identified with the same methodology discussed previously. In this case, p is set equal to 3, while model selection criterion AIC returns a value of $q = 5$. Hence, the ARDL model describing the process becomes:

$$y_t = \delta + \phi_1 y_{t-1} + \phi_2 y_{t-2} + \phi_3 y_{t-3} + \sum_{s=0}^5 \beta_s x_{t-s} + u_t \quad (5.8)$$

The coefficients, obtained by solving a MLR problem, are displayed in Table 5.7, where again the roots of the autoregressive polynomial satisfy the assumption of lying outside the unit circle. Comparison among model predictions and observations are shown in Figure 5.14, and residuals depict a white-noise behaviour, considering a 95%-confidence interval (Figure 5.15).

δ	-0.0434
β_0	0.0116
β_1	0.0183
β_2	0.0215
β_3	0.0213
β_4	0.0177
β_5	0.0106
ϕ_1	1.116
ϕ_2	-0.9348
ϕ_3	0.0465

$\phi(L) = 1 - 1.116L + 0.9348L^2 - 0.0465L^3$	
r_1	18.89
$r_{2,3}$	$0.605 \pm 0.8788i$

Table 5.7 Upper: coefficients of (5.8) estimated by solving the MLR problem; Lower: evaluation of the roots of the autoregressive polynomial.

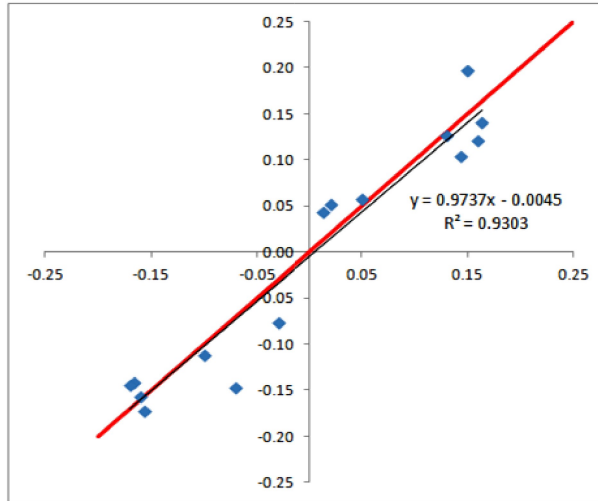


Figure 5.14 Comparison among model predictions and observed values.

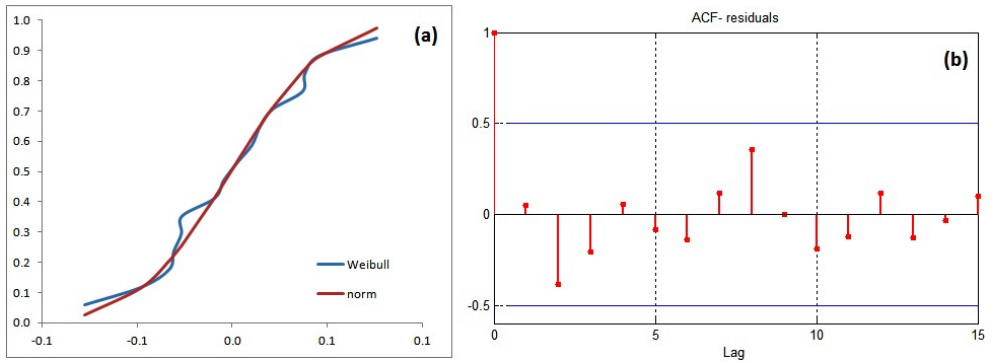


Figure 5.15 (a) Comparison among Weibull and normal distribution of residuals; (b) Autocorrelation function (ACF) of residuals.

5.6 APPLICATION OF THE ARDL MODEL ON TIME SERIES: PUMPING - PHREATIC LEVEL AND RAINFALLS - PUMPING

In the following, the influence of pumping rate on the phreatic level measured at P20, and the relationship between rainfalls at PL1-"Classe" and pumping time series are analyzed. Time series of rainfalls and groundwater levels are the same discussed in the previous sections. The pumping data have been recorded in the period 2009-2010 at Fosso Ghiaia (see Figure 5.6), located at 12°15'54.80"E, 44°21'11.88"N, and are referred to a drained basin with an area of 9200 km².

Before proceeding with the application of the ARDL model, pumping time series has been stationarized with the same methodology applied in the previous analysis, obtaining the results presented in Table 5.8, where the seasonal component is evaluated without considering the constraint.

Average montly pumping level (mm)				I(t) -without constraint on seasonal component			
Jan-09	0.52	Jan-10	1.54	Jan-09	-0.2850	Jan-10	0.7350
Feb-09	0.79	Feb-10	1.79	Feb-09	-0.1650	Feb-10	0.8350
Mar-09	0.56	Mar-10	2.56	Mar-09	-0.4775	Mar-10	1.5225
Apr-09	0.81	Apr-10	1.69	Apr-09	-0.1050	Apr-10	0.7750
May-09	0.45	May-10	1.67	May-09	-0.5275	May-10	0.6925
Jun-09	0.49	Jun-10	0.94	Jun-09	-0.4475	Jun-10	0.0025
Jul-09	0.54	Jul-10	0.62	Jul-09	-0.2650	Jul-10	-0.1850
Aug-09	0.43	Aug-10	0.81	Aug-09	-0.5250	Aug-10	-0.1450
Sep-09	0.31	Sep-10	0.72	Sep-09	-0.7275	Sep-10	-0.3175
Oct-09	0.40	Oct-10	0.76	Oct-09	-0.5150	Oct-10	-0.1550
Nov-09	0.26	Nov-10	1.53	Nov-09	-0.7175	Nov-10	0.5525
Dec-09	0.52	Dec-10	1.80	Dec-09	-0.4175	Dec-10	0.8625

Table 5.8 Left: average monthly pumping levels (mm), determined from pumping discharge in the period 2009-2010; Right: erratic components I_t (mm) obtained from monthly values, without considering the constraint (5.5) on seasonal component.

5.6.1 ARDL between phreatic level and pumping time series

Considering as dependent variable the phreatic level at P20, and the pumping rate as independent variable, the p -order of the autoregressive part is set $p = 5$, relying on the ACF plot. From AIC, $q = 3$ is obtained. The resulting model is:

$$y_t = \delta + \phi_1 y_{t-1} + \phi_2 y_{t-2} + \phi_3 y_{t-3} + \phi_4 y_{t-4} + \phi_5 y_{t-5} + \sum_{s=0}^3 \beta_s x_{t-s} + u_t \quad (5.9)$$

Table 5.9 displays the coefficients, obtained by solving the MLR problem, and the test on the roots of the autoregressive polynomial. Comparison among model predictions and observations is depicted in Figure 5.16, and the test on the residuals is presented in Figure 5.17. Again, it is possible to assume that the series of residuals is a white-noise process.

δ	0.0209	ϕ_1	1.4863
β_0	0.1045	ϕ_2	-0.8286
β_1	-0.0758	ϕ_3	0.0413
β_2	-0.1533	ϕ_4	0.5392
β_3	-0.128	ϕ_5	-0.3938

$\phi(L) = 1 - 1.4863L + 0.8286L^2 - 0.0413L^3 - 0.5392L^4 + 0.3938L^5$	
r_1	-1.4602
$r_{2,3}$	$0.3160 \pm 1.1167i$
$r_{4,5}$	$1.0988 \pm 0.2896i$

Table 5.9 Upper: coefficients of (5.9) estimated by solving MLR problem; lower: evaluation of the roots of the autoregressive polynomial.

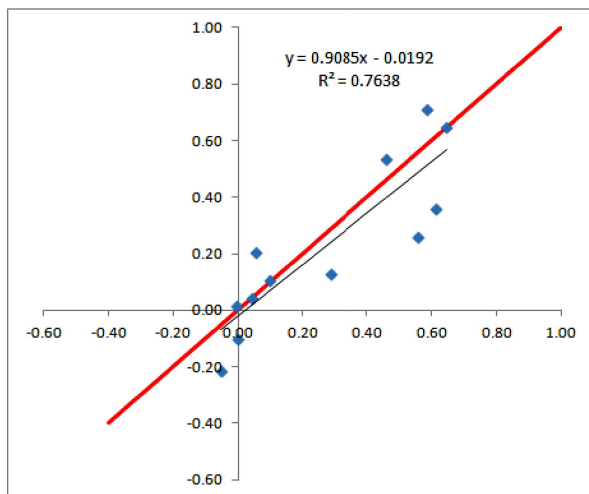


Figure 5.16 Comparison among model predictions and observed values.

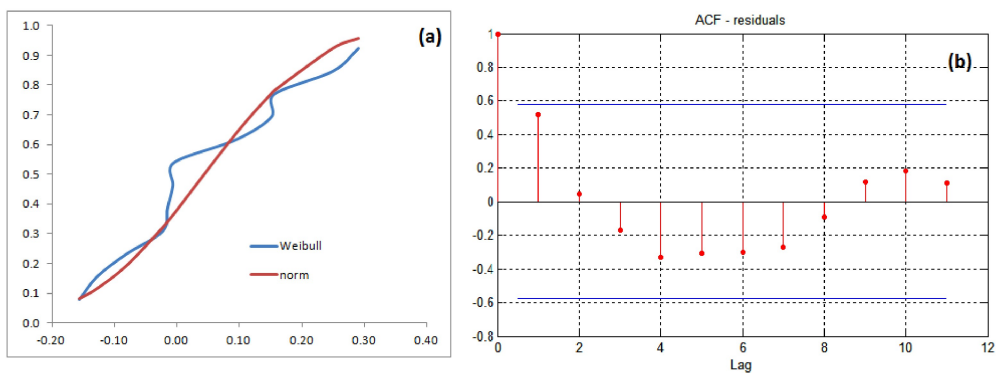


Figure 5.17 (a) Comparison among Weibull and normal distribution of residuals; (b) Auto Correlation Function (ACF) of residuals.

5.6.2 ARDL between rainfall and pumping time series

Considering as dependent variable the pumping rate time series at Fosso Ghiaia, and the rainfall time series as independent variable, the p -order of the autoregressive part results $p = 3$ from the ACF plot, and consequently $q = 2$ from the AIC criterion. The resulting model is:

$$y_t = \delta + \phi_1 y_{t-1} + \phi_2 y_{t-2} + \phi_3 y_{t-3} + \sum_{s=0}^2 \beta_s x_{t-s} + u_t \quad (5.10)$$

Table 5.10 displays the coefficients of (5.10) from solving the MLR problem, with the test on the roots of the autoregressive polynomial. Model predictions and observations are compared in Figure 5.18, while Figure 5.19 shows the test on the residuals.

δ	-0.0484
β_0	0.1366
β_1	0.0794
β_2	0.0339
ϕ_1	0.5804
ϕ_2	0.3134
ϕ_3	-0.4988

$\phi(L) = 1 - 0.5804L - 0.3134L^2 + 0.4988L^3$	
r_1	-1.345
$r_{2,3}$	$0.9867 \pm 0.7191i$

Table 5.10 Upper: coefficients of (5.10) estimated by solving MLR problem; Lower: evaluation of the roots of the autoregressive polynomial.

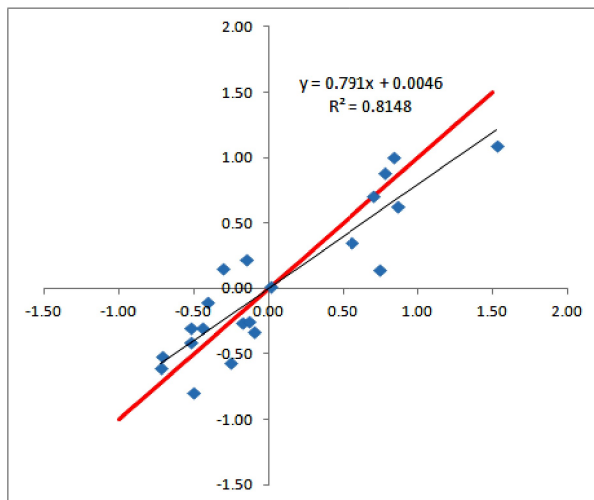


Figure 5.18 Comparison among model predictions and observed values.

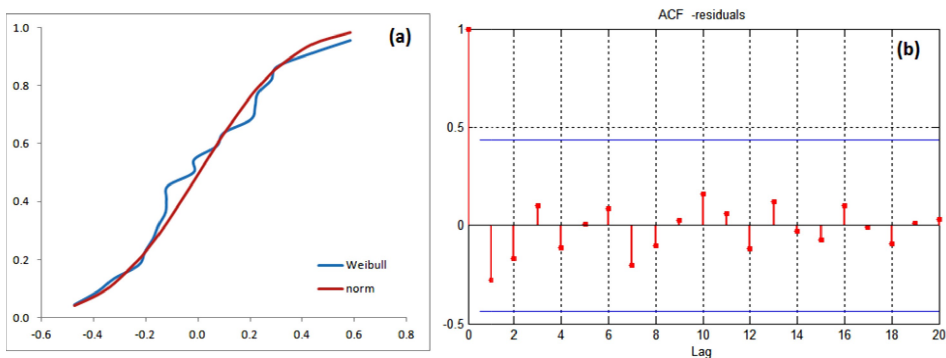


Figure 5.19 (a) Comparison among Weibull and normal distribution of residuals; **(b)** Autocorrelation function (ACF) of residuals.

5.7 APPLICATION OF THE GENERIC STATIC MODEL ON TIME SERIES: PHREATIC LEVEL - TOP SALINITY

Relying on classical analytical models, when groundwater level decreases, usually in autumn, it follows that saltwater wedge moves inland. The phreatic level, indeed, acts like a barrier, able to counteract saltwater intrusion. In the area of study, however, groundwater level is almost always below sea level, except where dunes are present, but even in the zones where the level is above the sea, the values of salinity are relatively high. This is probably caused by the origin of the area, since in the past this portion of territory was covered by the sea, and then reclamation activities turned this area into agricultural fields and pine forests (see Section 3 and references therein).

Here, the analysis is completed to understand the dynamics of the process, considering the relationship between water table and salinity time series. In particular, it is interesting to consider the salinity at the top of the aquifer, i.e. the top salinity. For both time series, data from P20 recorded from 2009 to 2012, are employed [Appendix B]. Evaluating the salinity on top of the aquifer allows to investigate consequently the effects on vegetation and soils.

The analyses above are based on the idea that a time delay exists among the parameters involved in the process. For example, the contribution of natural recharge in terms of rainfalls on groundwater levels is not instantaneous, due to different factors, e.g. soil properties, land use, presence of pumping machines or drainage channels. Observing the relationship between the phreatic level and top salinity, a delay effect is negligible. For this reason, the model of reference is the static model, discussed in Section 4.7.1.2.

Considering the top salinity time series as the dependent variable, and the groundwater level time series as the independent variable, the simple linear regression model (4.36) is recalled:

$$y_t = \beta_0 + \beta_1 x_t + \varepsilon_t$$

By applying an ordinary least square (OLS) method, the coefficients β_0 and β_1 are computed, with values of $\beta_0 = 21.94$ and $\beta_1 = -16.85$ respectively. Figure 5.20 depicts the regression line between the computed values of salinity and the observed salinity time series.

Studying this relationship, a question that has arisen was if including or not any other possible regressors to investigate their influence on top salinity, but as provided by different studies [*Graham, 2003; Jones, 1972*], if the regressors are correlated, and in particular rainfalls and groundwater levels are highly correlated, this could lead to spurious regression, with the least-squares estimates of the regression coefficients differing unpredictably from the true coefficients.

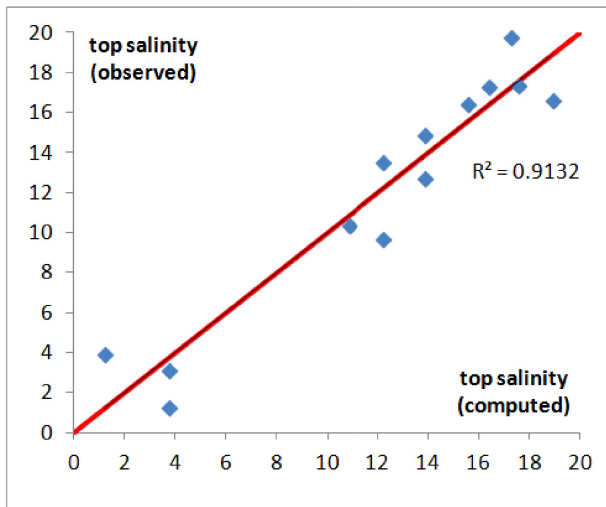


Figure 5.20 Comparison among model predictions and observed values.

5.8 FORECASTING TIME SERIES

The analysis discussed in the previous Sections emphasizes the discovery and understanding of the underlying mechanisms in the salinization process and provide a basis for building predictive models. In order to use the previous results to predict top salinity in the area of interest, it is necessary to start from rainfall forecasting. To this purpose, one may resort to ARIMA models, controlled by a series of shocks and relaxations [Engle and Granger, 1992].

The structure of an ARIMA (p,d,q) model is similar to the one of an ARMA (p,q) (4.33), but it is adopted when the original time series is not stationary. In particular, if $\{y_t, t = 1, 2, \dots, n\}$ is a non-stationary time series, the stationarized sequence z_t is obtained by:

$$z_t = (1 - L)^d y_t \tag{5.11}$$

where L is the lag operator (4.27), and d is the number of regular differencing necessary to turn the original time series into a stationary one.

Hence, the ARIMA (p,d,q) model is:

$$\phi(L)z_t = \phi_0 + \theta(L)\varepsilon_t \tag{5.12}$$

The focus is on predicting a rainfall time series, the main contribution on groundwater levels, and consequently on top salinity. Once the synthetic time series is created, the previous models, with their high correlations, can consequently be adopted to provide a forecast of the state variables depending on rainfalls. The adoption of an ARIMA model to forecast rainfall time series, and in general hydrologic parameters, is largely diffused as highlighted by many literature findings [Wang et al., 2014; Montanari et al., 1997; Box, 1967].

Considering available monthly rainfall data, recorded at PL1-"Classe" from 1990-2012, the ACF and PACF are first evaluated, as reported in Figure 5.21, for the original time series. From their analysis, it is possible to notice that, for the time interval considered, the seasonal component is not relevant, since at lag = 12 the correlation coefficient falls within the 95%-confidence bounds. Hence it seems possible to assume that the original model is stationary; in this case one could resort directly to an ARMA (p,q) model. Results of MLR problem are presented in Figure 5.22, while Figure 5.23 depicts the test on the residuals.

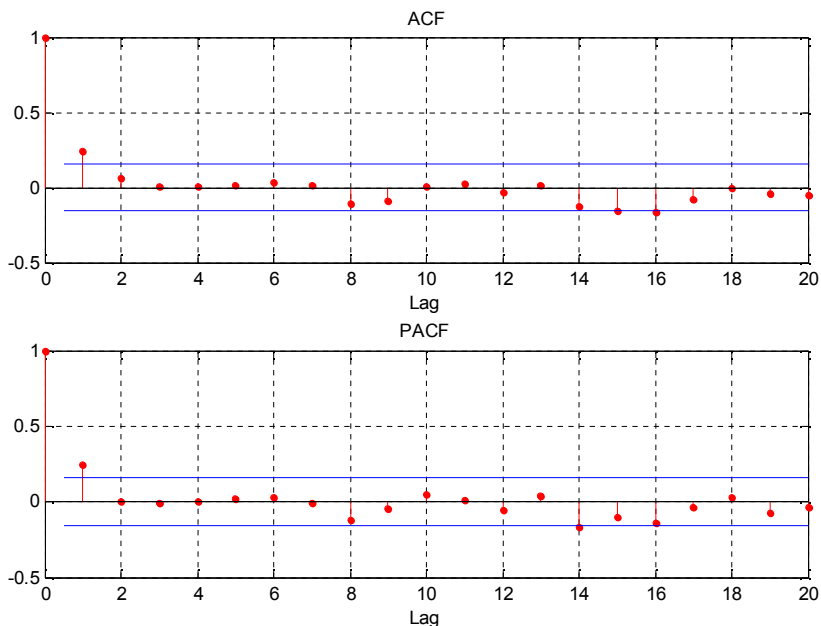


Figure 5.21 ACF and PACF of the original rainfall time series.

ARIMA(1,0,0) Model:

 Conditional Probability Distribution: Gaussian

Parameter	Value	Standard Error	t Statistic
Constant	1.35408	0.184857	7.32501
AR{1}	0.244147	0.0693238	3.52184
Variance	1.6143	0.194716	8.29055

Figure 5.22 Coefficients of the ARMA (1,0,0). It is possible to show that the roots of the autoregressive polynomial fall outside the unit circle.

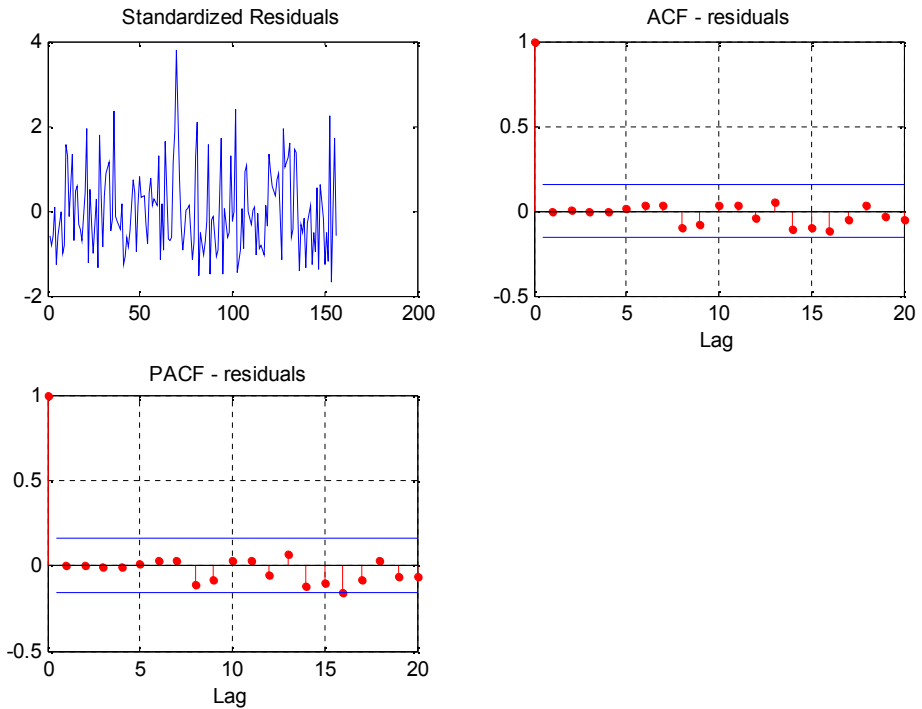


Figure 5.23 Test on residuals of ARIMA (1,0,0). It is possible to notice that they show a white-noise behaviour.

Considering an order of differencing $d = 1$, the ACF and PACF are shown in Figure 5.24. In this case, the ACF cuts off sharply after the first lag, while PACF dies out more gradually, and probably the time series has a MA signature, with three terms of moving average to consider. In particular, trying different combinations of models, the one that returns a smaller variance results an ARIMA (1,1,3), where the coefficients are reported in Figure 5.25. To complete the calibration, the test on residual is depicted in Figure 5.26.

Finally, after obtaining the model that describes the data more appropriately, it is possible to validate and make forecast analysis. In this case, 35% of data are employed for validation. The resulting forecast is shown in Figure 5.27 for the ARIMA(1,1,3).

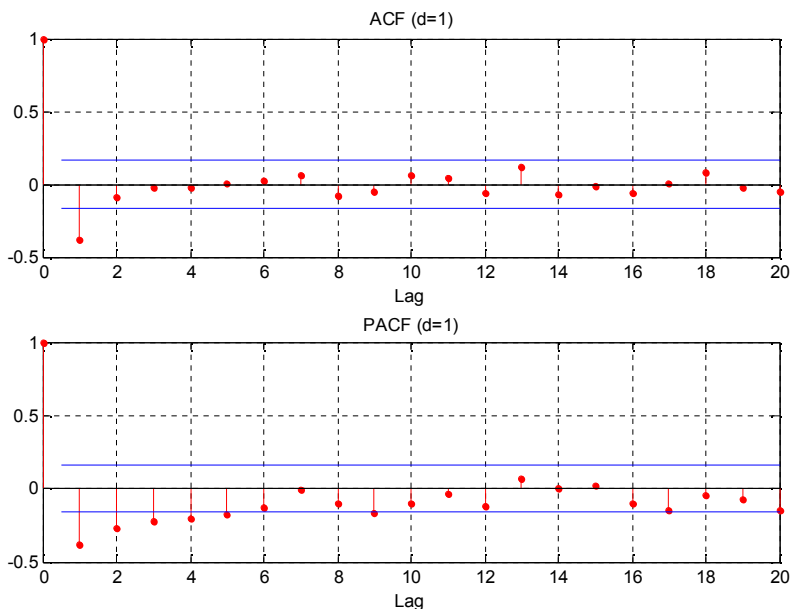


Figure 5.24 ACF and PACF of rainfall time series after non-seasonal differencing $d=1$.

ARIMA(1,1,3) Model:

 Conditional Probability Distribution: Gaussian

Parameter	Value	Standard Error	t Statistic
Constant	0.00123671	0.00158141	0.782029
AR{1}	-0.839263	0.175958	-4.76968
MA{1}	-0.860687	0.153885	-5.59306
MA{2}	-0.825279	0.227772	-3.62327
MA{3}	0.692481	0.101657	6.81194
Variance	1.87735	0.219206	8.5643

Figure 5.25 Coefficients of the ARIMA (1,1,3). Here, the stability of the polynomial depends on the roots of the autoregressive part, and again it is possible to show that they fall outside the unit circle.

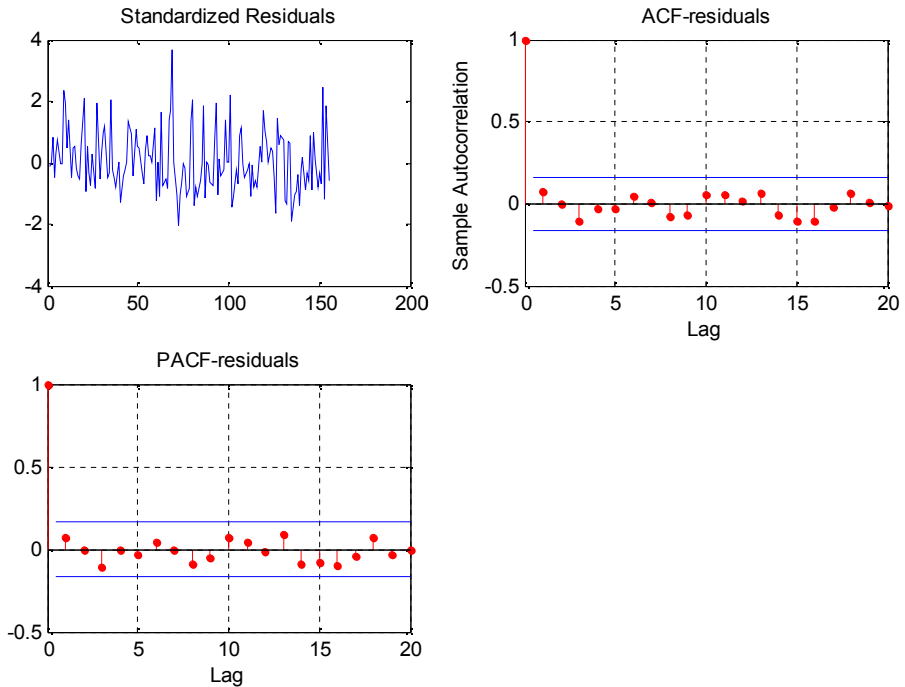


Figure 5.26 Test on residuals of ARIMA (1,1,3). Again, it is possible to notice that they show a white-noise behaviour.

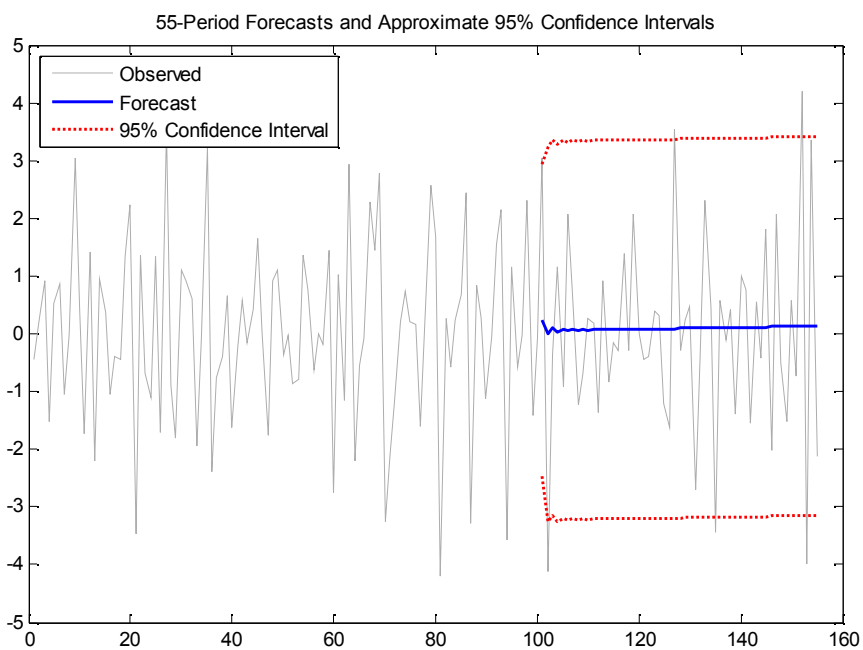


Figure 5.27 Forecast of rainfall time series, on 55 period.

6. Conclusions

The focus of the present work consists in understanding the processes linked to saltwater intrusion. Physically based approaches are useful to describe the mechanism of the phenomenon. High spatial variability of geological properties of subsurface environment, together with the scarcity of available measurements and uncertainty associated with the model itself, makes it impossible for a correct characterization of hydraulic - hydrologic parameters, that should be modeled as random variables or fields. Considering the uncertainties of the variables involved in the saltwater intrusion problem, these propagate through the model, hence the response, i.e. the position of saltwater interface, is affected by these uncertainties.

However, analytical and numerical modeling work well if the factors controlling groundwater salinization are few and constrained, or the amount of available data is extensive. If this does not occur, as in the case of study of this dissertation, data driven techniques can be adopted in order to understand the complex dynamics involving multiple drivers. In particular, these techniques allow to define a framework able to show the relationships among the parameters, starting from their time series analysis, and finally to evaluate the risk associated to the salinity of groundwater that can affect coastal vegetation and ecosystems.

Appendix A

MODEL REDUCTION TECHNIQUES: POLYNOMIAL CHAOS EXPANSION

In order to perform stochastic analysis, time intensive simulation methods based on Monte Carlo (MC) approach are typically applied. However, the computational demand associated with MC analyses is generally a limiting factor in case of complex numerical models and in the presence of a large number of uncertain parameters [Sudret, 2008]. An alternative to overcome these limitations relies on model reduction techniques, able to define surrogate models with negligible computational burden. The basic idea of model reduction methods consists in modifying the form of the selected model without introducing any simplifying assumptions in the description of the physical processes involved.

Among the possible families of surrogate models, those based on the Polynomial Chaos Expansion (PCE) theory introduced by Wiener [1938] have received particular attention in the recent years [Rajabi *et al.*, 2015; Najm, 2009]. For the PCE approach, a surrogate model is derived in a simple polynomial form depending only on the uncertain input parameters. The computation of the PCE approximation requires a very limited number of MC simulations performed on the original model.

Consider a selected model $y = f(\mathbf{p}, \mathbf{x}, t)$, that can be described as a relationship between M input parameters, collected in vector $\mathbf{p} = \{p_1, p_2, \dots, p_M\}$, and the model response, y , evaluated at spatial location \mathbf{x} and time t . If values of input parameters are uncertain, they can be modeled as

random variables with assigned distributions, and consequently the model response results random in turn. The PCE technique is based on the projection of the model response y , assuming it belongs to the Hilbert space of second-order random variables, in a probabilistic space, i.e. *Polynomial Chaos*, generated from a basis of multivariate orthogonal polynomials Ψ_j , where j is the order of the polynomial [Ghanem, Spanos, 1991; Soize, Ghanem, 2004]. The latter depends on vector ζ of independent random variables, whose distribution is linked to the choice of the polynomial basis [Xiu, Karniadakis, 2002]. The resulting metamodel, \tilde{y} of y , is a simple polynomial function, which is expressed in terms of a set of independent random variables, collected in vector ζ , as:

$$\tilde{y} = \tilde{f}(\mathbf{x}, t, \zeta(\mathbf{p})) = \sum_{j=0}^{P-1} a_j(\mathbf{x}, t) \Psi_j(\zeta(\mathbf{p})) \quad (\text{A.1})$$

Here, $P = (M+q)!/(M!q!)$ is the number of terms of the expansion, and q is the maximum degree considered; a_j represent unknown deterministic coefficients, while Ψ_j denote the suitable multivariate polynomial basis in the Hilbert space containing the response, i.e. the basis that generates the probabilistic space.

The probability distribution of input parameters affects the choice of the polynomial basis in (A.1), as presented in Table A.1. [Xiu, Karniadakis, 2002; Wiener, 1938]. Once the appropriate kind of polynomials is identified, the set of independent random variables ζ automatically stems from orthogonality condition, as the multivariate polynomial basis has to be orthonormal with respect to the joint PDF of ζ . The variables collected in ζ are then related to the input parameters in p via a simple isoprobabilistic transform [Sudret, 2008].

Distribution of random inputs		Polynomial basis	Support
Continuous	Gaussian	Hermite polynomials	$(-\infty, \infty)$
	Gamma	Laguerre polynomials	$[0, \infty)$
	Beta	Jacobi polynomials	$[a, b]$
	Uniform	Legendre polynomials	$[a, b]$
Discrete	Poisson	Charlier polynomials	$\{0, 1, 2, \dots\}$
	Binomial	Krawtchouk	$\{0, 1, \dots, N\}$
	Negative binomial	Meixner polynomials	$\{0, 1, 2, \dots\}$
	Hypergeometric	Hahn polynomials	$\{0, 1, \dots, N\}$

Table A.1. Distributions of random input and respective polynomial basis in the Wiener-Askey scheme.

In order to compute the expansion coefficients a_j in stochastic finite element analysis, the traditional approach consists in the minimization, in the Galerkin sense, of the residual present in the balance equation [Sudret, 2008; Ghanem, Spanos, 1991]. This solving method is identified as intrusive, requiring onerous and specific implementation in the finite element code [Sudret, 2008; Webster et al., 1996]. A non-intrusive regression-based approach can be employed to calculate the coefficients a_j [Sudret, 2008], upon minimization of the variance of a suitable residual ε , defined as the difference between the surrogate model response, \tilde{y} , and the solution given by the original model, y , with respect to the vector of the unknown coefficients \mathbf{a} :

$$ArgMin \left\{ E[\varepsilon^2], \mathbf{a} \right\} = ArgMin \left\{ E \left[\left(f(\mathbf{p}) - \tilde{f}(\zeta(\mathbf{p})) \right)^2 \right], \mathbf{a} \right\} \quad (A.2)$$

with $E[\cdot]$ denoting expected value.

Finally, the numerical strategy applied in order to obtain the PCE approximation of y can be summarized in the following steps, in which the original model is considered as a black box:

- (i) identification of the suitable polynomial basis with respect to the parameter distributions;
- (ii) definition of the PCE of minimum order ($q = 2$);
- (iii) generation of the optimum set of regression points (i.e. set of parameter values);
- (iv) runs of the original model for the set generate in (iii);
- (v) solution of the regression problem through eq. (A.2);
- (vi) evaluation of the quality associated with the PCE approximation to understand if the order chosen in (ii) is sufficient or not; if not $q = q+1$ and points (iii)-(vi) are repeated.

Once the PCE is available, simple analytical post-processing allows derivation of (i) the first two moments of the approximated response, and (ii) the global sensitivity indices of Sobol, that represent dimensionless ratios among the partial variance of the response, due to a generic subset of uncertain model parameters, and the total variance of the response [Sudret, 2008]. Specifically the mean of the model response coincides with the coefficient of the zero-order term, a_0 in the Equation (A.1), and the total variance of the response and the generic Sobol index are given, respectively, by:

$$V^{(\tilde{y})} = Var \left[\sum_{j=0}^{P-1} a_j \Psi_j(\zeta) \right] = \sum_{j=1}^{P-1} a_j^2 E[\Psi_j^2(\zeta)] \quad (\text{A.3})$$

$$S_{i_1, \dots, i_s}^{(\tilde{y})} = \frac{\sum_{\alpha \in \mathcal{O}_{i_1, \dots, i_s}} a_\alpha^2 E[\Psi_\alpha^2]}{V^{(\tilde{y})}} \quad (\text{A.4})$$

for the computation of $E[\Psi_\alpha^2]$ see e.g. Abramowitz, Stegun (1970).

Furthermore, the PCE metamodel represents a suitable basis to perform Monte Carlo simulations, allowing for a more efficient means to perform risk analysis or to solve inverse problems with reduced computational time/cost. This methodology has demonstrated excellent promise for use in many other applications related to flow and transport processes in porous media [Ciriello *et al.*, 2013; Ciriello, Di Federico, 2013].

Appendix B


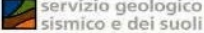

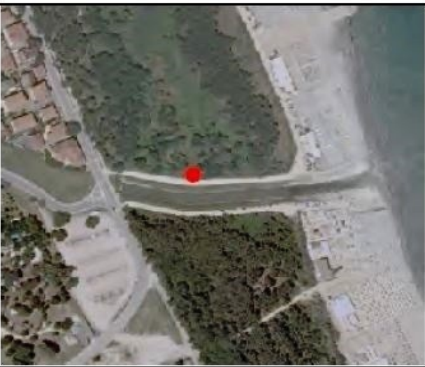

MONITORING NETWORK OF RAVENNA COASTAL PHREATIC AQUIFER

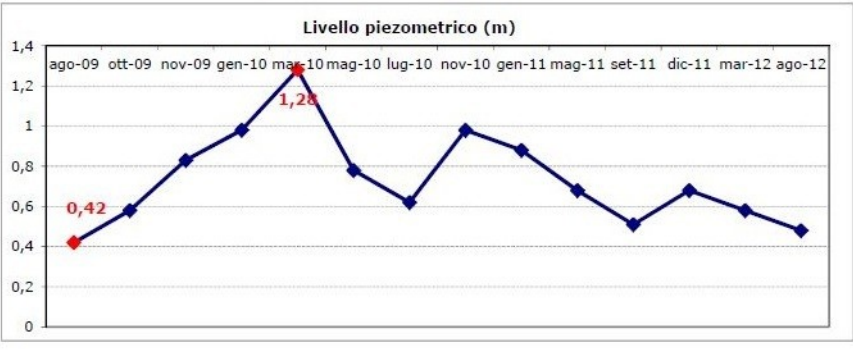
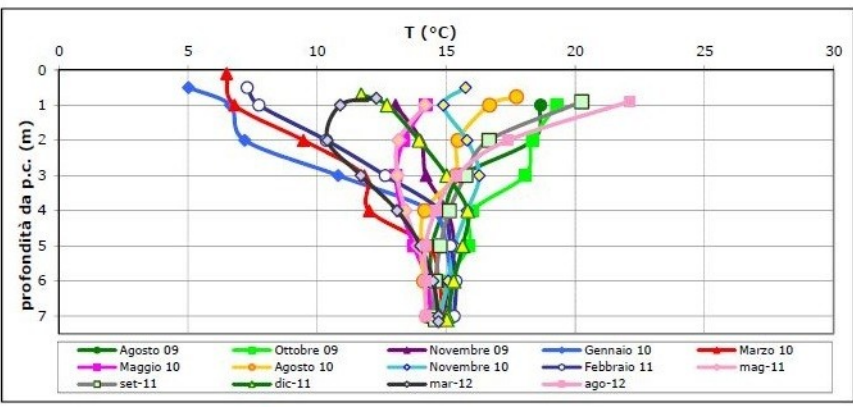
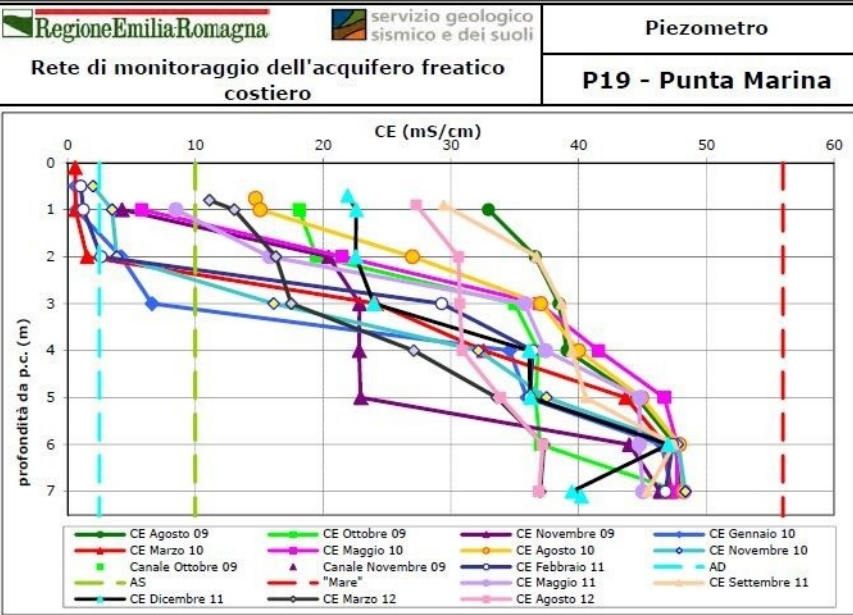
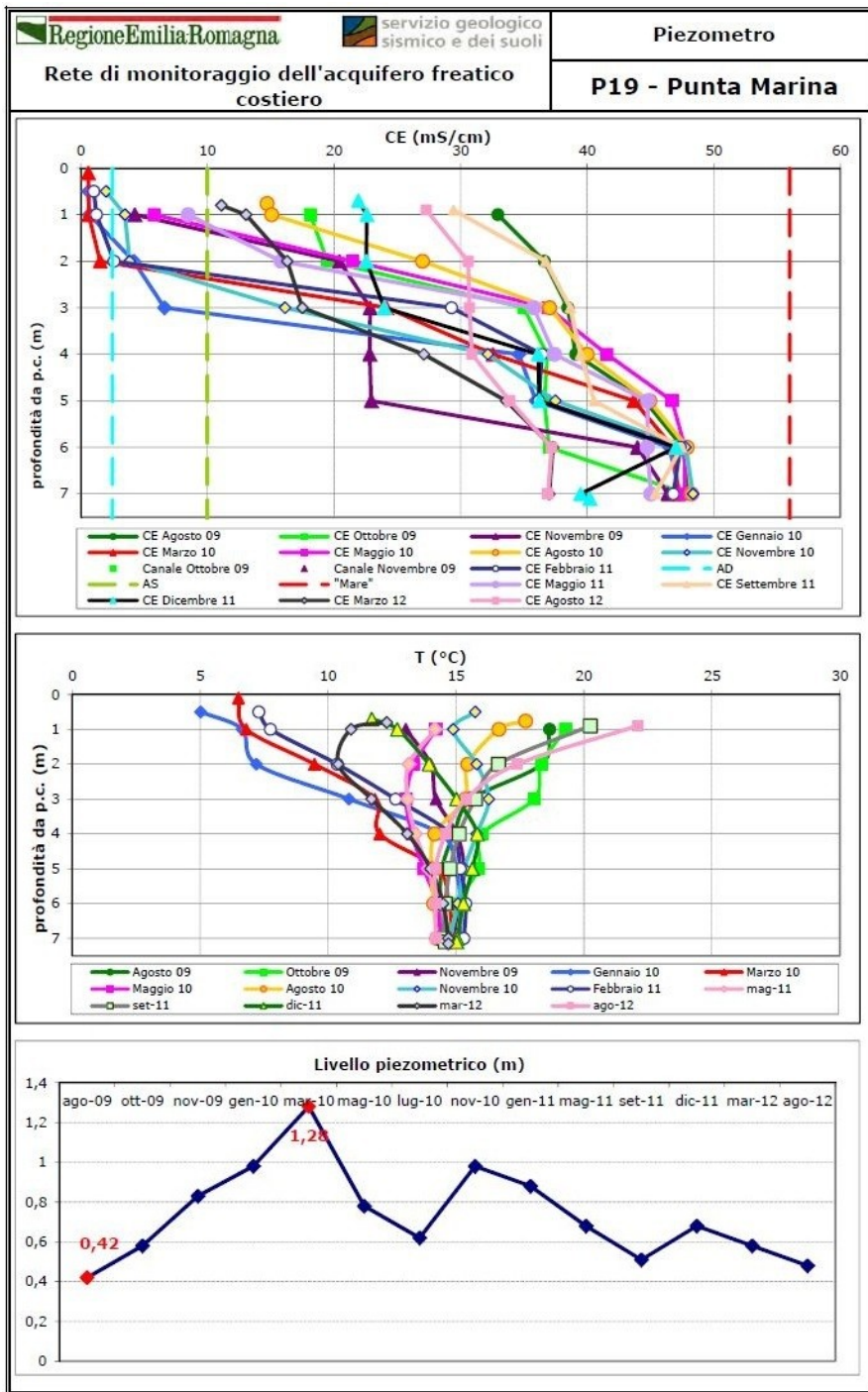







Figure B.1 Locations of monitoring wells along Ravenna coastline. In red, piezometers from University network; in yellow, piezometers from Emilia-Romagna Region; in dark blue, pluviometers from ARPA Emilia-Romagna.

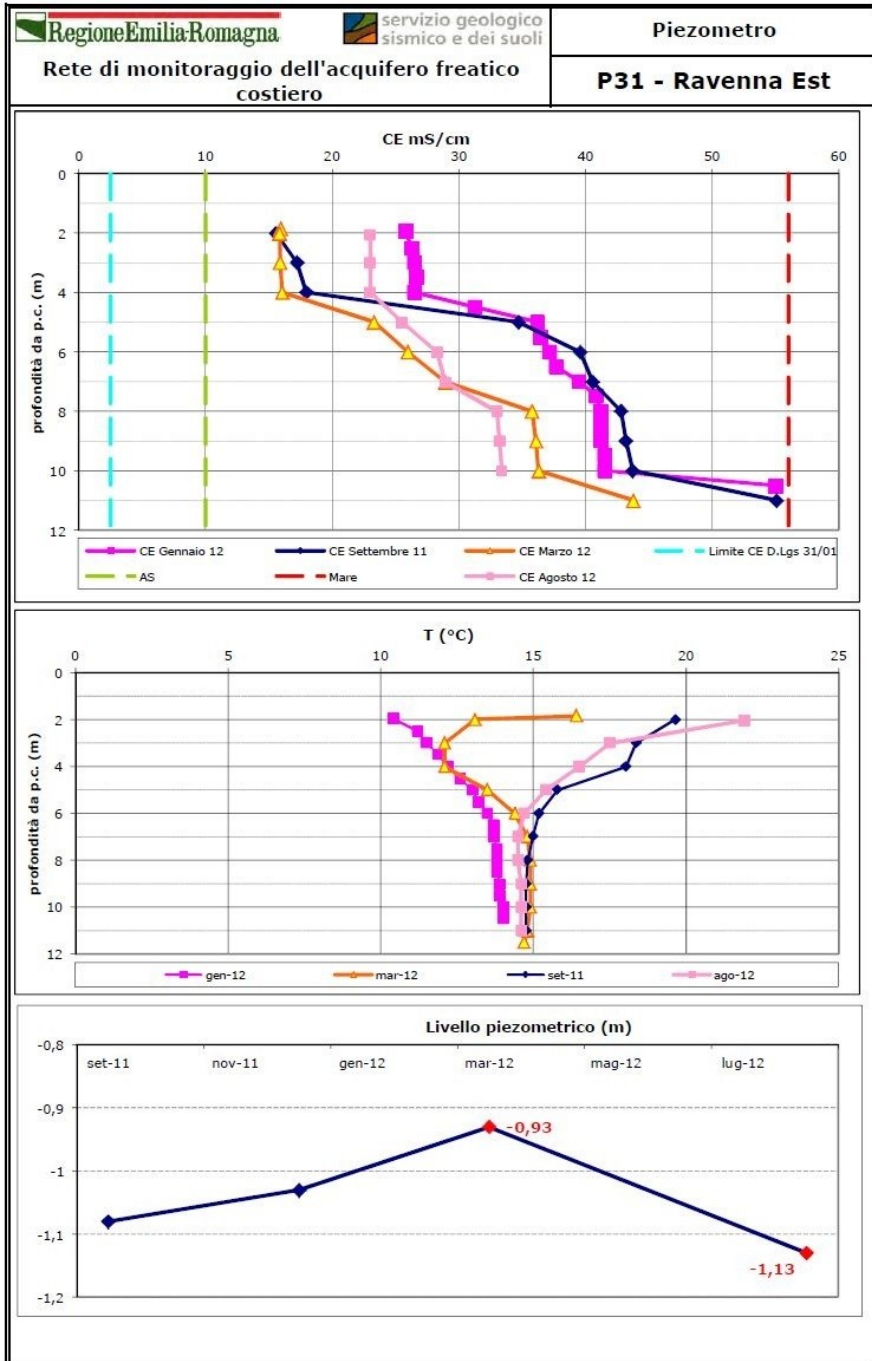
In the following, the main features of the monitoring wells from Emilia-Romagna Region and University of Bologna are presented.





EMILIA-ROMAGNA REGION NETWORK

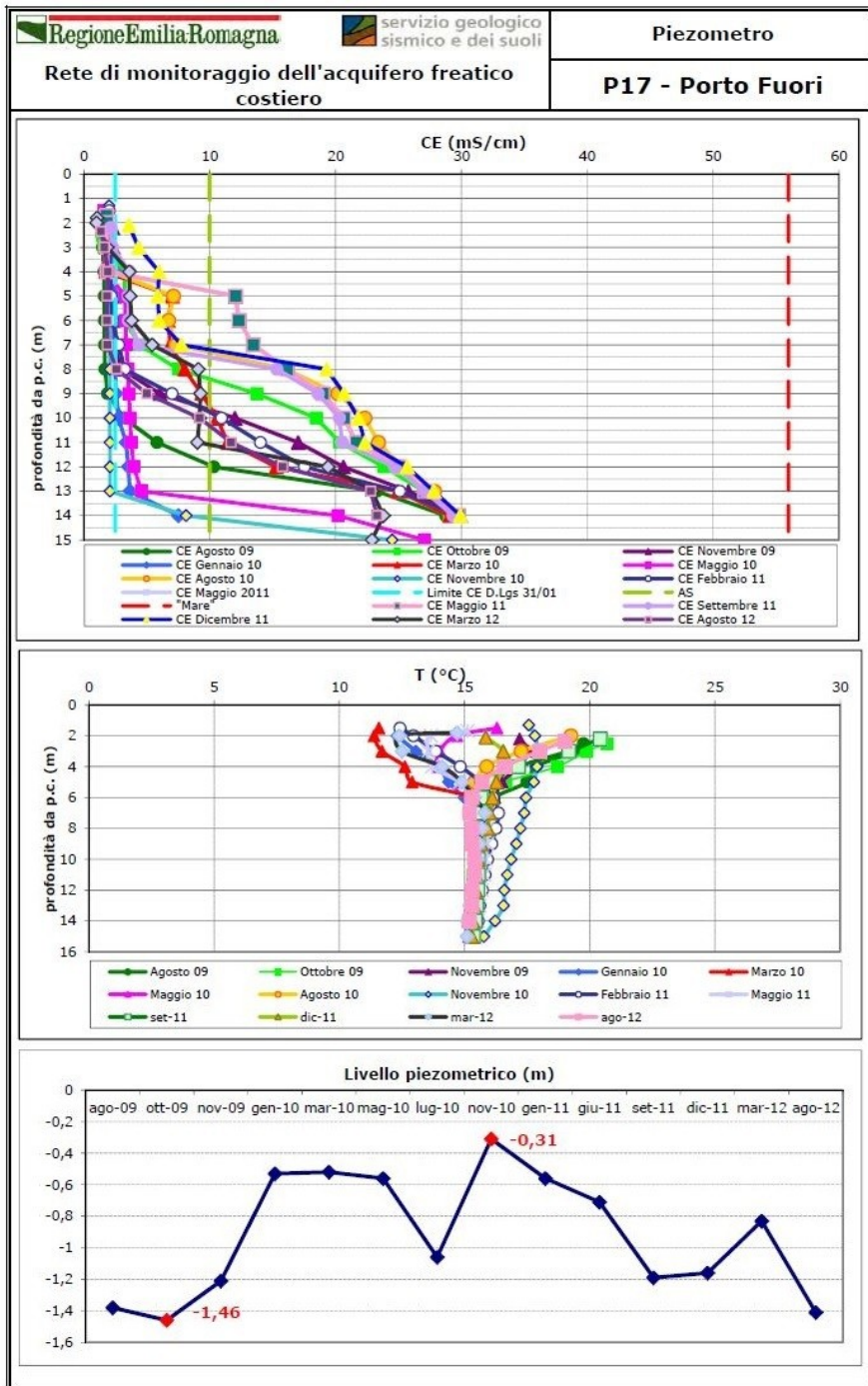
 		Piezometro
Rete di monitoraggio dell'acquifero freatico costiero		P19 - Punta Marina
UBICAZIONE		
Località: Punta Marina		X (UTM*) 762628,2153
Comune: Ravenna		Y (UTM*) 925732,6436
Provincia: RAVENNA		Quota (m s.l.m.): 1.38
1:100.000		1:5.000
		
SITO		DATI TECNICI
		Data di perforazione: 4 giugno 2009
		Profondità (m): 7.5
		Allestimento: primo metro cieco; fino a fondo foro fessurato
		Diametro: 2"
		Sezione geologica di riferimento Sez. 2
		Foglio CARG 223 - Ravenna



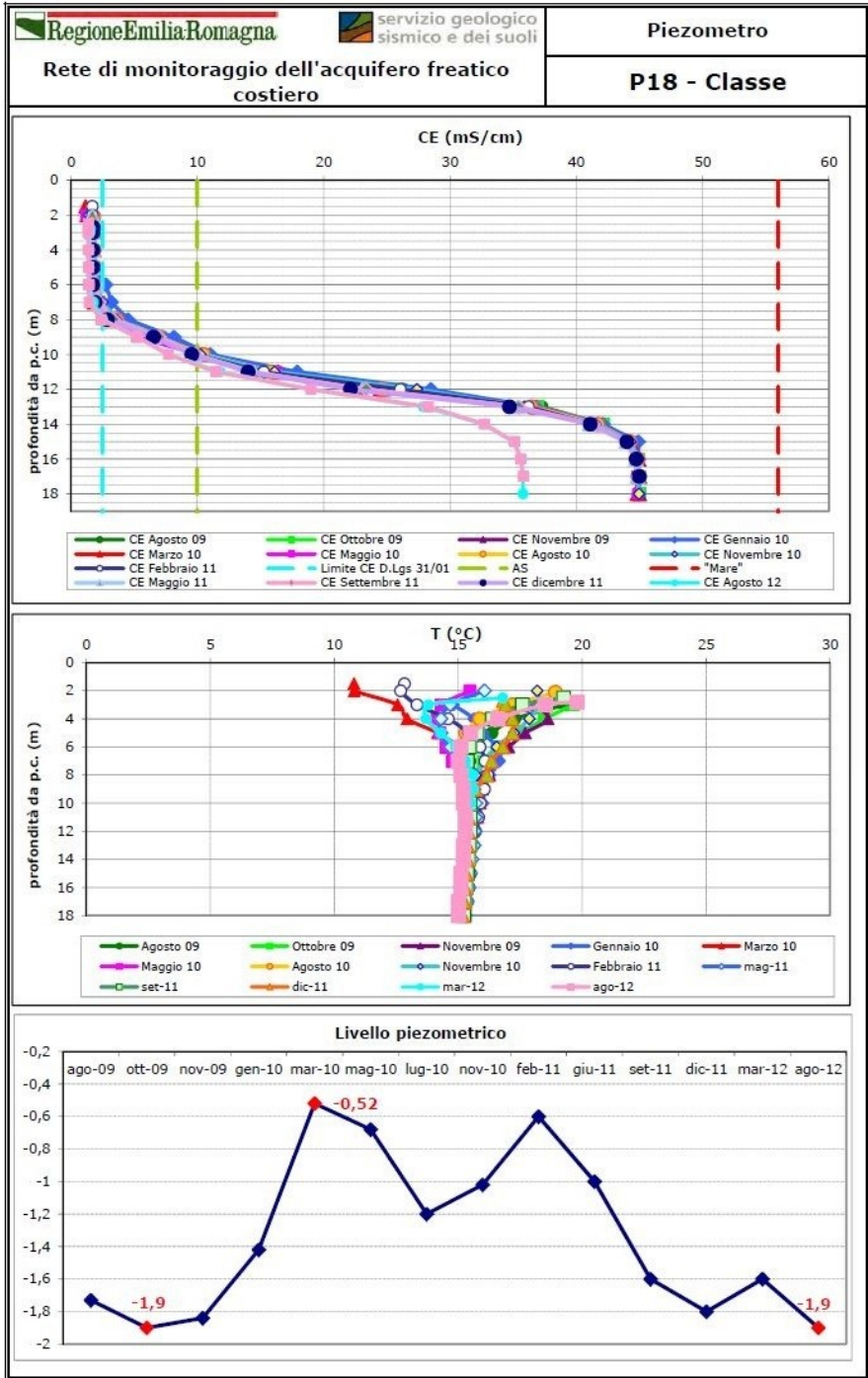
 		Piezometro	
Rete di monitoraggio dell'acquifero freatico costiero		P31 - Ravenna Est	
UBICAZIONE			
Località: Porto Fuori		X (UTM*) 759752,625	
Comune: Ravenna		Y (UTM*) 923068,98	
Provincia: RAVENNA		Quota (m.s.l.m.): 0,92	
1:100.000		1:5.000	
			
SITO		DATI TECNICI	
		Data di perforazione: maggio 2011	
		Profondità (m): 11,5	
		Allestimento: primo metro cieco; fino a fondo foro fessurato	
		Diametro: 2"	
		Sezione geologica di riferimento Sez. 2	
		Foglio CARG 223 - Ravenna	


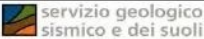





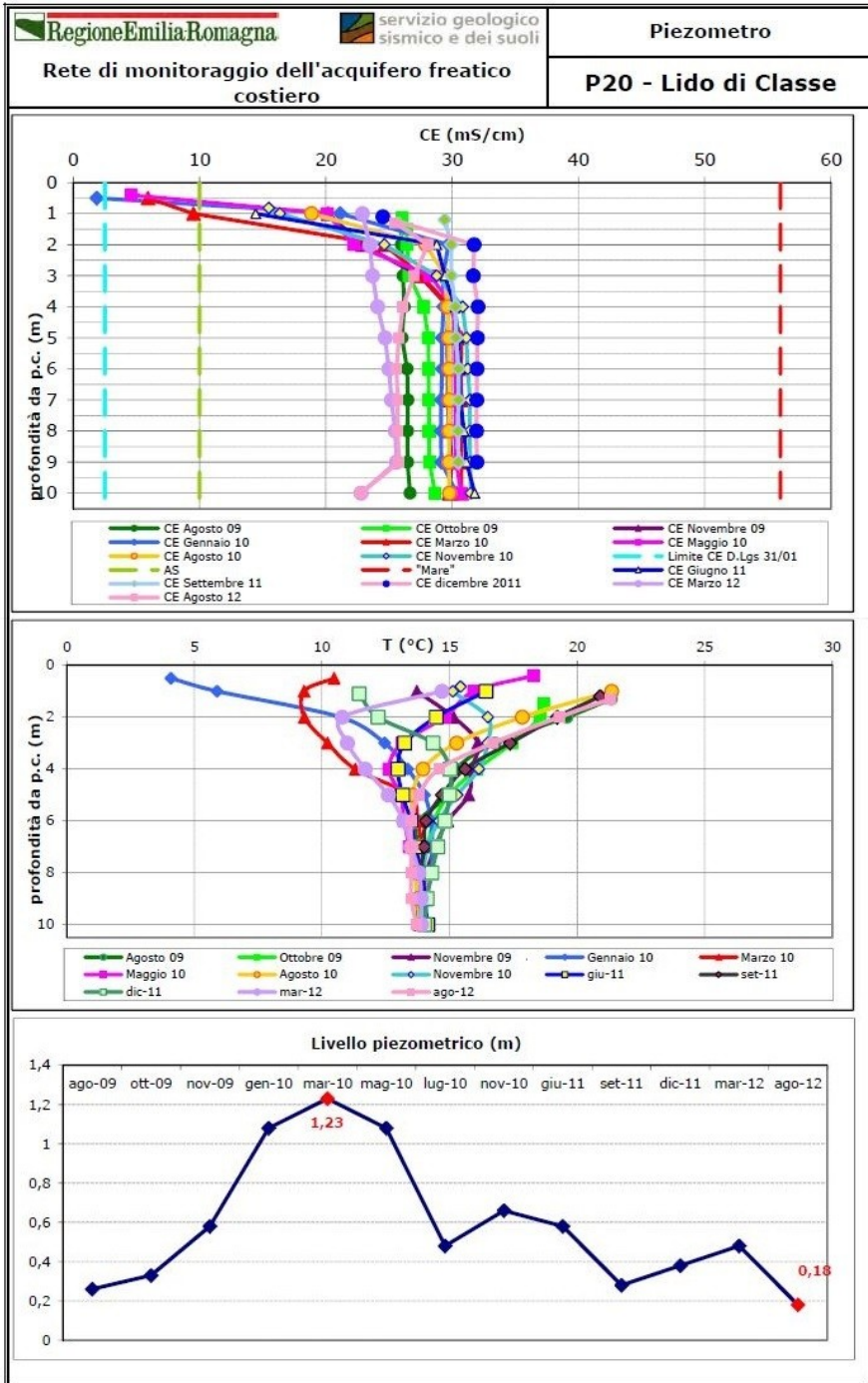
 		Piezometro
Rete di monitoraggio dell'acquifero freatico costiero		P17 - Porto Fuori
UBICAZIONE		
Località: Porto Fuori		X (UTM*) 758891,4754
Comune: Ravenna		Y (UTM*) 921992,3775
Provincia: RAVENNA		Quota (m s.l.m): 0.94
1:100.000	1:5.000	
		
SITO	DATI TECNICI	
	Data di perforazione: 3 giugno 2009	
	Profondità (m): 15	
	Allestimento: primo metro cieco; da un metro a fondo foro fessurato e rivestito da geotessuto	
	Diametro: 2"	
	Sezione geologica di riferimento Sez. 2	
	Foglio CARG 223 - Ravenna	





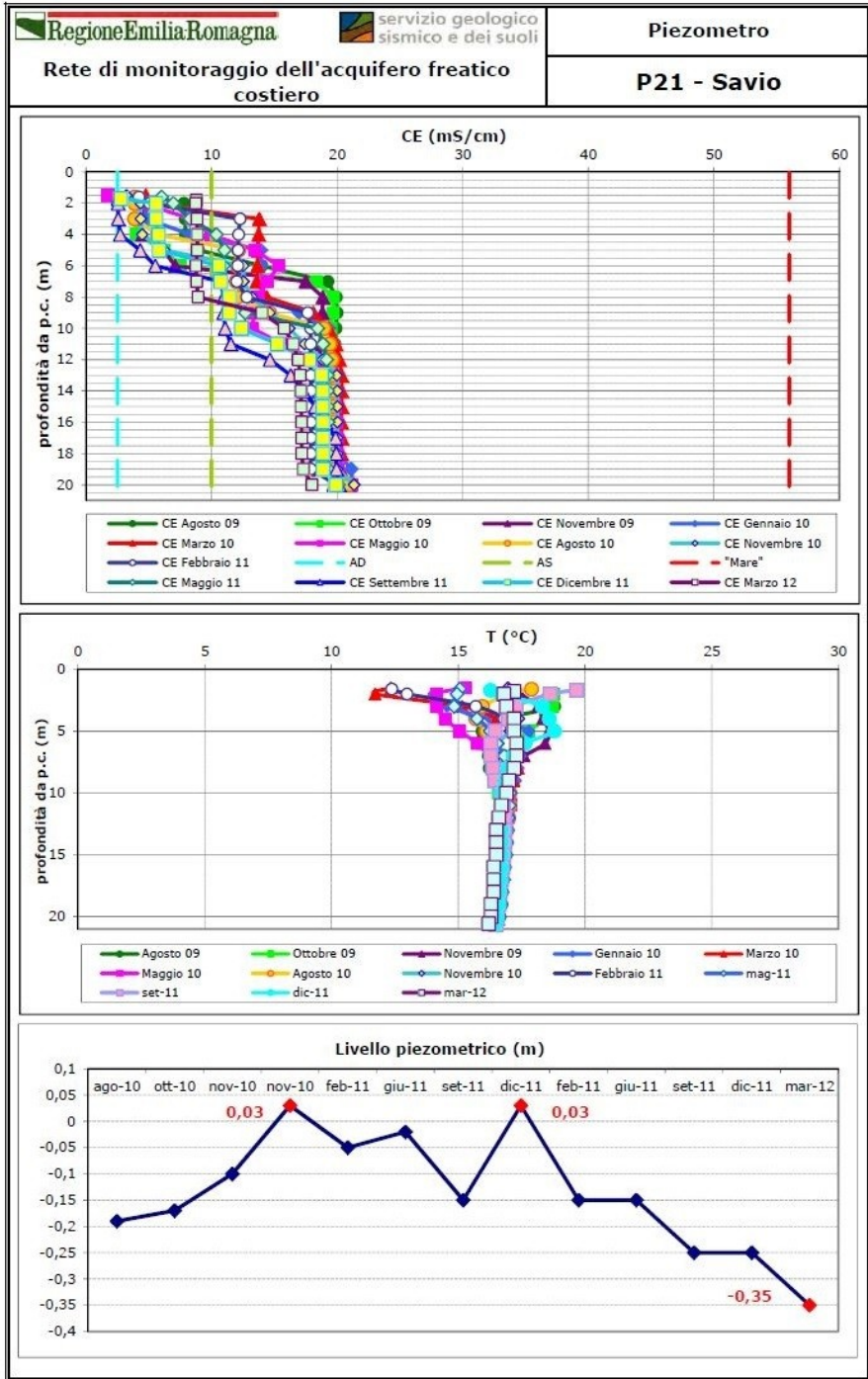
 Regione Emilia Romagna		 servizio geologico sismico e dei suoli		Piezometro	
Rete di monitoraggio dell'acquifero freatico costiero				P18 - Classe	
UBICAZIONE					
Località: Classe			X (UTM*) 757632,8498		
Comune: Ravenna			Y (UTM*) 920262,5082		
Provincia: RAVENNA			Quota (m s.l.m): 0.9		
1:100.000			1:5.000		
					
SITO			DATI TECNICI		
			Data di perforazione: 3 giugno 2009		
			Profondità (m): 18		
			Allestimento: fessurato per tutta la lunghezza		
			Diametro: 2"		
			Sezione geologica di riferimento Sez. 2		
			Foglio CARG 240 - Forlì		



 		Piezometro
Rete di monitoraggio dell'acquifero freatico costiero		P20 - Lido di Classe
UBICAZIONE		
Località: Lido di Classe		X (UTM*) 765433,5158
Comune: Ravenna		Y (UTM*) 915409,9074
Provincia: RAVENNA		Quota (m s.l.m.): 1.48
1:100.000	1:5.000	
		
SITO	DATI TECNICI	
	Data di perforazione: 4 giugno 2009	
	Profondità (m): 10.5	
	Allestimento: primo metro cieco; fino a fondo foro fessurato	
	Diametro: 2"	
	Sezione geologica di riferimento Sez. 3	
	Foglio CARG 240 - Forlì	



 		Piezometro
Rete di monitoraggio dell'acquifero freatico costiero		P21 - Savio
UBICAZIONE		
Località: Savio di Ravenna		X (UTM*) 762737,4452
Comune: Ravenna		Y (UTM*) 913968,7934
Provincia: RAVENNA		Quota (m s.l.m): 1.45
1:100.000	1:5.000	
		
SITO	DATI TECNICI	
	Data di perforazione: 5 giugno 2009	
	Profondità (m): 21	
	Allestimento: primo metro cieco; fino a fondo foro fessurato	
	Diametro: 2"	
	Sezione geologica di riferimento Sez. 3	
	Foglio CARG 240 - Forlì	



UNIVERSITY OF BOLOGNA NETWORK

Piezometer	Distance from sea (m)	Distance from Fosso Ghiaia (m)	Top seal	Land Use coefficient	Aquifer thickness	K sand (m/d)	Sand/shale	Subsidence (mm/y)
<i>PZLD1</i>	748	5252	0.00	0.05	8.0	48	1.00	10
<i>PIS</i>	1039	4841	0.00	0.25	8.0	58	0.80	10
<i>PZLD3</i>	938	4809	0.00	0.25	8.0	52	1.00	10
<i>P2S</i>	960	4623	0.00	0.25	8.2	58	0.75	9
<i>PZLD2</i>	1086	4501	0.00	0.25	8.0	62	1.00	10
<i>PZBEV2A</i>	766	4805	0.00	0.05	6.6	80	1.00	8
<i>PZBEV2B</i>	749	4838	0.00	0.05	6.6	80	1.00	8
<i>PZBEV1F</i>	678	5090	0.00	0.05	6.60	80	1.00	8
<i>PZBEV2F</i>	706	5063	0.00	0.25	6.60	80	1.00	8
<i>PZBEV3F</i>	882	4900	0.00	0.25	6.60	80	1.00	8
<i>PZBEV3G</i>	798	5239	0.00	0.25	6.60	80	1.00	8
<i>P15S</i>	714	5566	0.00	0.25	9.70	58	0.90	8

Table B.1 Characteristics of the monitoring wells of University of Bologna, in the area 1 object of study [Greggio, 2013].

Area 1	Coordinates (WGS84)	
	Long	Lat
<i>PZLD1</i>	12.319866	44.379691
<i>MAR1</i>	12.314787	44.372915
<i>MAR2</i>	12.312661	44.372607
<i>PIS</i>	12.317126	44.375907
<i>PZLD3</i>	12.319317	44.372441
<i>P2S</i>	12.321196	44.364145
<i>PZLD2</i>	12.319516	44.364391
<i>PZBEV2A</i>	12.324804	44.359756
<i>PZBEV2B</i>	12.325607	44.357527
<i>PZBEV1F</i>	12.32875	44.348878
<i>PZBEV2F</i>	12.328409	44.348829
<i>PZBEV3F</i>	12.326281	44.348347
<i>PZBEV3G</i>	12.329001	44.341989
<i>P15S</i>	12.331315	44.337224

Area 2 north	Coordinates (WGS84)	
	Long	Lat
<i>PZCL1</i>	12.269276	44.373833
<i>PZCL2</i>	12.273749	44.368142
<i>P4S</i>	12.283248	44.361771
<i>P5S</i>	12.266372	44.359033
Area 2 south	Coordinates (WGS84)	
	Long	Lat
<i>P12S</i>	12.292823	44.341755
<i>P13S</i>	12.278649	44.336177
<i>P14S</i>	12.290956	44.328654
Area 3	Coordinates (WGS84)	
	Long	Lat
<i>EMS1</i>	12.235776	44.356483
<i>P6S</i>	12.24158	44.353901
<i>P10S</i>	12.250866	44.344894
<i>P11S</i>	12.250214	44.344574

Table B.2 Coordinates of the monitoring wells of University network, divided by the zone of interest.

References

Abramowitz M., Stegun I.A. (1970) Handbook of Mathematical Functions; Dover Publications: New York, NY, USA.

Almon S. (1965) The Distributed Lag Between Capital Appropriations and Expenditures. *Econometrica* 33 (1), 178-196.

Amorocho J., Orlob G.T. (1961) Nonlinear analysis of hydrologic systems. California University. Water Resources Center, contrib.40.

Amorosi A., Centineo M.C., Colalongo M.L., Fiorini F. (2005). Millennial-scale depositional cycles from the Holocene of the Po plain, Italy. *Marine geology*, 222-223, 7-18.

Amorosi A., Colalongo M.L., Fiorini F., Fusco F., Pasini G., Vaiani S.C., Sarti G. (2004) Palaeogeographic and palaeoclimatic evolution of the Po Plain from 150-ky core records. *Global and planetary change*, 40, 55-78.

Amorosi A., Centineo M.C., Colalongo M.L., Pasini G., Sarti G., Vaiani S. C. (2003) Facies Architecture and Latest Pleistocene–Holocene Depositional History of the Po Delta (Comacchio Area), Italy. *The Journal of Geology*, 111, 39–56.

Amorosi A., Centineo M.C., Dinelli E., Lucchini F., Tateo F. (2002) Geochemical and mineralogical variations as indicators of provenance changes in late Quaternary deposits of SE Po Plain. *Sedimentary Geology*, 151, 273–292

Amorosi A., Colalongo M.L., Pasini G., Preti D. (1999) Sedimentary response to late quaternary sea-level changes in the Romagna Coastal Plain (Northern Italy). *Sedimentology*, 46, 99–121.

Antonellini M., Mollema P.N. (2010) Impact of groundwater salinity on vegetation species richness in the coastal pine forests and wetlands of Ravenna, Italy. *Ecological Engineering*, 36, 1201–1211.

Antonellini M., Mollema P., Giambastiani B., Bishop K., Caruso L., Minchio A., Pellegrini L., Sabia M., Ulazzi E., Gabbianelli G. (2008) Saltwater intrusion in the coastal aquifer of the southern Po Plain, Italy. *Hydrogeology Journal*, 16, 1541–1556.

ARPA Agenzia Ambientale della Regione Emilia-Romagna, <http://www.arpa.emr.it/>

Bárdossy A. (1998) Generating precipitation time series using simulated annealing. *Water Resources Research*, 34, 1737–1744.

Battaglia F. (2007) *Metodi di previsione statistica*. Springer-Verlag Italia, Milano.

Bear J. (1979) *Hydraulics of Groundwater*. New York: McGraw Hill.

Bear J., Dagan G. (1964) Some exact solutions of interface problems by means of the hodograph method. *Journal of Geophysical Research*, 69, 1563–72.

Beck N., Katz J.N. (2011) Modeling Dynamics in Time-Series–Cross-Section Political Economy Data. *Annual Review of Political Science*, 14, 331–352.

Bondesan M., Favero V., Viñals M.J. (1995) New evidence on the evolution of the Po-delta coastal plain during the Holocene. *Quaternary International*, 29–30, 105–110.

Bolster D.T., Tartakovsky D.M., Dentz M. (2007) Analytical models of contaminant transport in coastal aquifers. *Advances in Water Resources*, 30, 1962–1972.

Bonzi L., Calabrese L., Severi P., Vincenzi V. (2010) L'acquifero freatico costiero dell'Emilia-Romagna: modello geologico e stato di salinizzazione. *Il Geologo dell'Emilia-Romagna*, 39, 21–34.

Box G., Jenkins G. (1976) *Time Series Analysis: forecasting and control*. Holden-Day, Oakland, California.

Box G.E.P. (1967) Models for forecasting seasonal and nonseasonal time series. In *Spectral Analysis of Time Series*, edited by: Harris, B., Wiley, New York, 271–311, 1967.

Capaccioni B., Didero M., Paletta C., Didero L. (2005) Saline intrusion and refreshing in a multilayer coastal aquifer in the Catania Plain (Sicily, southern Italy): Dynamics of degradation processes according to the hydrochemical characteristics of groundwater. *Journal of Hydrology*, 307, 1–16.

Carminati E., Martinelli G. (2002) Subsidence rates in the Po Plain, northern Italy: the relative impact of natural and anthropogenic causation. *Engineering Geology*, 66, 241 – 255.

Cheng A.H.D., Konikow L.F., Ouazar D. (2001) Preface to special issue of transport in porous media on seawater intrusion in coastal aquifers. *Transport in Porous Media*, 43:1–2.

Cheng A.H.-D., Ouazar, D. (1999) Analytical solutions. In *Seawater Intrusion in Coastal Aquifers—Concepts, Methods and Practices*, 1st ed.; Bear, J., Cheng, A.H.-D., Sorek, S., Ouazar, D., Herrera, I., Eds.; Springer: Dordrecht, the Netherlands, Volume 14, pp. 163–191.

Cheng A.H.-D., Halhal D., Naji A., Ouazar D. (2000) Pumping optimization in saltwater-intruded coastal aquifers. *Water Resources Research*, 36, 2155–2165.

Ciavola P., Armaroli C., Chiggiato J., Valentini A., Deserti M., Perini L., Luciani P. (2007) Impact of storms along the coastline of Emilia-Romagna: the morphological signature on the Ravenna coastline (Italy). *Journal of coastal research SI*, 50, 540-544.

Ciriello V., Di Federico V., Riva M., Cadini F., De Sanctis J., Zio E., Guadagnini A. (2013) Polynomial chaos expansion for global sensitivity analysis applied to a model of radionuclide migration in a randomly heterogeneous aquifer. *Stochastic Environmental Research and Risk Assessment*, 27(4), 945-954.

Ciriello V., Di Federico V. (2013) Analysis of a benchmark solution for non-Newtonian radial displacement in porous media. *International Journal of Non-Linear Mechanics*, 52, 46–57.

Coulibaly P., Baldwin C.K. (2005) Nonstationary hydrological time series forecasting using nonlinear dynamic methods. *Journal of Hydrology*, 307, 164-174.

Davison A.C., Ramesh N.I. (1996) Some models for discretized series of events. *Journal of the American Statistical Association*, 91, 434, 601-609.

De Barros F.P.J., Bolster D., Sanchez-Vila X., Nowak W. (2011) A divide and conquer approach to cope with uncertainty, human health risk, and decision making in contaminant hydrology. *Water Resources Research*, 47, W05508, doi:10.1029/2010WR009954.

De Luca A., Preziosi E., Giuliano G., Mastroianni D., Falconi F. (2004) First evaluation of the saltwater intrusion in the Tiber delta area (Rome, central Italy). In *Proceedings of 18th Salt Water Intrusion Meeting*, Cartagena, Spain, 31 May–3 June 2004; p. 34.

Enders W. (2004) *Applied Econometric Time Series* (Second ed.). Wiley, New York.

Engle R.F., Granger C.W.J. (1992) *Long-run Economic Relationships*. Oxford University Press, Oxford.

European Communities (EC). *Common Implementation Strategy for the Water Framework Directive (2000/60/EC); Guidance Document No. 11, Planning Processes, Working Group 2.9.*; Office for the Official Publications of the European Communities: Luxembourg, 2003.

Esca S., Venturini L. (2006). Hydrogeological impact of wellpoint dewatering upon unconfined coastal aquifer of the municipality of Cervia (Ravenna – Italy). *Proceedings 1st SWIM-SWICA Joint Saltwater intrusion Conference*, Cagliari-Chia Laguna, Italy – September 24-29, 2006, 71-77.

Felisa G., Ciriello V., Di Federico V. (2013) Saltwater Intrusion in Coastal Aquifers: A Primary Case Study along the Adriatic Coast Investigated within a Probabilistic Framework. *Water*, 5, 4: 1830-1847.

Fetter C.W. (2001) *Applied Hydrogeology*. Ed. Prentice Hall, Fourth Edition, 691 pp.

Gambolati G., Teatini P., Tomasi L., Gonella, M. (1999) Coastline regression of the Romagna region, Italy, due to natural and anthropogenic land subsidence and sea level rise. *Water Resources Research*, 35, 163-184.

Gambolati G., Teatini P. (1998) Numerical analysis of land subsidence due to natural compaction of the Upper Adriatic Sea basin. In: Gambolati G. (ed) CENAS, Coastal evolution of the upper Adriatic sea due to sea level rise and natural and anthropogenic land subsidence. Kluwer Academic Publishing, Water Science & Technology Library n. 28, 103-131.

Gambolati G., Ricceri G., Bertoni W., Brighenti G., Vuillermin E. (1991) Mathematical simulation of the subsidence of Ravenna. *Water Resources Research*, 27, 2899–2918.

Gargini A., Spensieri P., Rossi M. (2001). Monitoraggio dei parametri idrogeologici ed idrochimici della rete freaticometrica costiera della provincia di Ferrara nel periodo 1989-1999. Università degli Studi di Ferrara, Provincia di Ferrara. Italia tipolitografia (Fe).

Ghanem R.G., Spanos P.D. (1991) Stochastic finite elements-a spectral approach. Springer, Berlin.

Giambastiani B.M.S., Mollema P.N., Antonellini M. (2009) Groundwater management in the Northern Adriatic Coast (Ravenna, Italy): New strategies to protect the coastal aquifer from saltwater intrusion. In *Groundwater. Modeling, Management, and Contamination*; König, L.F., Weiss, J.L., Eds.; Nova Science Publishers: New York, NY, USA, pp. 203–230.

Giambastiani B.M.S., Antonellini M., Oude Essink G.H.P., Stuurman R.J. (2007) Saltwater intrusion in the unconfined coastal aquifer of Ravenna (Italy): A numerical model. *Journal of Hydrology*, 340, 91–104.

Graham M.H. (2003) Confronting multicollinearity in ecological multiple regression. *Ecology*, 84, 2809–2815.

Greggio N.(2013) Individuazione di tecniche di gestione idrica-agronomica e di ricarica dell'acquifero freatico costiero per limitare la salinizzazione delle acque sotterranee e dei suoli. Tesi di dottorato in Scienze Ambientali: tutela e gestioni delle risorse naturali, ciclo XXV, Università di Bologna.

Haan C.T. (1977) Statistical Methods in Hydrology. Iowa State University Press, Iowa, USA.

Hamilton J.D. (1994) Time Series Analysis. Princeton, N.J.: Princeton University Press.

Hanson R.T., Dettinger M.D., Newhouse M.W. (2006) Relations between climatic variability and hydrologic time series from four alluvial basins across the southwestern United States. *Hydrogeology Journal*, 1122-1146.

Hantush M.S. (1964) Hydraulics of wells. In *Advances in Hydrosience*, Vol. 1, Ed.: V. T. Chow, Academic Press, New York,. 281–432.

Henry C.M., Allen D.M., Huang J. (2011) Groundwater storage variability and annual recharge using well-hydrograph and GRACE satellite data. *Hydrogeology Journal*, 19, doi: 10.1007/s10040-011-0724-3.

Henry H.R. (1964) Effects of dispersion on salt encroachment in coastal aquifers. Technical Report on Water Supply, Paper 1613-C, US Geological Survey.

Henry H.R. (1959) Salt intrusion into fresh-water aquifers. *Journal of Geophysical Research*, 64, 1911–1919.

Huppert H.E., Woods A.W. (1995) Gravity-driven flows in porous layers. *Journal of Fluid Mechanics*, 292, 55–69.

Hutchinson I. (1991) Salinity Tolerances of Plants of Estuarine Wetlands and Associated Uplands. Washington State Department of Ecology Report; Washington State Shorelands and Coastal Zone Management Program, Wetlands Section: Washington, DC, USA.

IPCC (2007) Climate Change 2007: The Physical Science Basis. Contribution of Working Group I to the Fourth Assessment Report of the Intergovernmental Panel on Climate Change [Solomon, S., D. Qin, M. Manning, Z. Chen, M. Marquis, K.B. Averyt, M. Tignor and H.L. Miller (eds.)]. Cambridge University Press, Cambridge, United Kingdom and New York, NY, USA.

Kacimov A.R., Obnosov Y.V. (2001) Analytical solution for a sharp interface problem in sea water intrusion into a coastal aquifer. *Proceedings of the Royal Society of London A*, 457, 2016, 3023–38.

Kadane J.B., Lazar N.A. (2004) Methods and criteria for model selection. *Journal of the American Statistical Association*, 99, 465, 279-290.

Konishi S., Kitagawa G. (2008) Information Criteria and Statistical Modeling. Springer.

- Kooi H., De Vries, J.J. (1998) Land subsidence and hydrodynamic compaction of sedimentary basins. *Hydrology and Earth System Sciences*, 2, 159-171.
- Koutsoyiannis D., Montanari A.(2007) Statistical analysis of hydroclimatic time series: Uncertainty and insights, *Water Resources Research*, 43 (5), W05429, doi:10.1029/2006WR005592.
- Jurado A., De Gaspari F., Vilarrasa V., Bolster D., Sanchez-Vila X., Fernandez-Garcia D., Tartakovsky D. M. (2012), Probabilistic analysis of groundwater-related risks at subsurface excavation sites, *Engineering Geology*, 125, 35-44.
- Langevin C.D., Thorne D.T.Jr., Dausman A.M, Sukop M.C., Weixing G. (2007) SEAWAT Version 4: A computer program for simulation of multi-species solute and heat transport. U.S. Geological Survey Techniques and Methods Book 6, Chapter A22, 39 p.
- Law A.G. (1974) Stochastic analysis of groundwater level time series in the Western United States. Hydrology Papers, 68, Colorado State University, Fort Collins, Colorado.
- Lu C., Chen Y., Luo J. (2012) Boundary condition effects on maximum groundwater withdrawal in coastal aquifers. *Ground Water*, 50, 386–393.
- Maas E.V. (1984) Salt tolerance of plants. In *Handbook of Plant Science in Agriculture*; CRC Press: Boca Raton, FL, USA, pp. 57–75.
- Machiwal D., Jha M.K. (2012) Hydrologic Time Series Analysis: Theory and Practice. Springer Netherlands, doi: 10.1007/978-94-007-1861-6.
- Manfreda S., Caylor K.K. (2013) On the vulnerability of water limited ecosystems to climate change. *Water*, 5, 819–833.
- Mantoglou A., Papantoniou M. (2008) Optimal design of pumping networks in coastal aquifers using sharp interface models. *Journal of Hydrology*, 361, 52–63.
- Mantoglou A. (2003) Pumping management of coastal aquifers using analytical models of saltwater intrusion. *Water Resources Research*, 39, 1335, doi:10.1029/2002WR001891.

- Marchesini L., Amorosi A., Cibin U., Zuffa G.G., Spadafora E., Preti D., (2000). Sand composition and sedimentary evolution of a late Quaternary depositional sequence, Northwestern Adriatic Coast, Italy. *Journal of Sedimentary Research*, 70, 829–838.
- Meckel T.A., Ten Brink U.S., Williams S.J. (2007) Sediment compaction rates and subsidence in deltaic plains: numerical constraints and stratigraphic influences, *Basin Research*, 19, 19-31.
- Mollema P.N., Antonellini M., Dinelli E., Gabbianelli G., Greggio N., Stuyfzand P.J. (2013) Hydrochemical and physical processes influencing salinization and freshening in Mediterranean low-lying coastal environments. *Applied Geochemistry*, 34, 207-221.
- Montanari A., Rosso R., Taqqu M.S. (1997). Fractionally differenced ARIMA models applied to hydrologic time series: identification, estimation and simulation. *Water Resources Research*, 33, 1035–1044.
- Naji A., Cheng A.H.-D., Ouazar D. (1998) Analytical stochastic solutions of saltwater/freshwater interface in coastal aquifers. *Stochastic Hydrology Hydraulics*, 12, 413–430.
- Najm H.N. (2009) Uncertainty Quantification and Polynomial Chaos Techniques in Computational Fluid Dynamics. *Annual Review of Fluid Mechanics*, 41, 35-52.
- Neuman S.P., Xue L., Ye M., Lu D. (2012) Bayesian analysis of data-worth considering model and parameter uncertainty. *Advances in Water Resources*, 36, 75-85.
- Neuman S.P. (2003) Maximum likelihood Bayesian averaging of uncertain model predictions. *Stochastic Environmental Research and Risk Assessment*, 17(5), 291– 305.
- NOAA - National Oceanic and Atmospheric Administration, www.noaa.gov/
- Oude Essink G.H.P., van Baaren E.S., De Louw P.G.B. (2010) Effects of climate change on coastal groundwater systems: A modeling study in the Netherlands. *Water Resources Research*, 46, W00F04, doi: 10.1029/2009WR008719.

Park C.H., Aral M.M. (2004) Multi-objective optimization of pumping rates and well placement in coastal aquifers. *Journal of Hydrology*, 290, 80–99.

Piccolo D. (1990) Introduzione all'analisi delle serie storiche. Ed. Carrocci, Roma, Italia.

Preti M., De Nigris N., Morelli M., Monti M., Bonsignore F., Aguzzi M. (2009) Stato del litorale emiliano-romagnolo all'anno 2007 e piano decennale di gestione; Agenzia regionale per la prevenzione e l'ambiente (ARPA): Emilia-Romagna, Italy; p. 270.

Preti M. (2000) Eustatismo, subsidenza e linee di intervento per la difesa del territorio costiero in Emilia-Romagna. Mare e cambiamenti globali, ICRAM, ARPA – Ingegneria Ambientale, Bologna, 167-179.

Rajabi M.M., Ataie-Ashtiani B., Simmons C.T. (2015) Polynomial chaos expansions for uncertainty propagation and moment independent sensitivity analysis of seawater intrusion simulations. *Journal of Hydrology*, 520, 101-122.

Regione Emilia-Romagna (2009) Foce bevano: l'area naturale protetta e l'intervento di salvaguardia. Pubblicazione a cura del Servizio difesa del suolo della costa e bonifica.

Rodriguez-Iturbe I., D'Odorico P., Laio F., Ridolfi L., Tamea S. (2007) Challenges in humid land ecohydrology: Interactions of water table and unsaturated zone with climate, soil, and vegetation. *Water Resources Research*, 43, W09301, doi:10.1029/2007WR006073.

Rodriguez-Iturbe I., Cox D.R., Isham V. (1987) Some Models for Rainfall Based on Stochastic Point Processes. *Proceedings of the Royal Society of London. Series A, Mathematical and Physical Sciences*, 410, 1839, 269-288.

Rubin Y. (2003) Applied Stochastic Hydrogeology. Oxford University Press, 1st ed.: New York, NY, USA; p. 416.

Rizzini A. (1974) Holocene sedimentary cycle and heavy mineral distribution, Romagna-Marche coastal plain, Italy. *Sedimentary Geology*, 11, 17-37.

Sanford W.E., Pope J.P. (2010) Current challenges using models to forecast seawater intrusion: lessons from the Eastern Shore of Virginia, USA. *Hydrogeology Journal*, 18, 73–93.

Sestini G. (1992) Implication of climatic changes for the Po Delta and Venice lagoon. *Climatic Change and the Mediterranean*, 429-491.

Servan-Camas B., Tsai F.T.-C. (2010) Two-relaxation-time lattice Boltzmann method for the anisotropic dispersive Henry problem. *Water Resources Research*, 46, W02515.

Shalev E., Lazar A., Wollman S., Kington S., Yechieli S., Gvirtzman H. (2009) Biased monitoring of fresh water-salt water mixing zone in coastal aquifers. *Ground Water*, 47 (1), 49-56

Sivakumar B. (2009) Nonlinear dynamics and chaos in hydrologic systems: latest developments and a look forward. *Stochastic Environmental Research and Risk Assessment*, 23, 7, 1027-1036.

Soize C., Ghanem R. (2004) Physical systems with random uncertainties: Chaos representations with arbitrary probability measures. *Journal of Scientific Computing*, 26(2), 395-410.

Solomatine D.P., Ostfeld A. (2008) Data-driven modelling: some past experience and new approaches. *Journal of Hydroinformatics*, 10.1, 3-22.

Stefani M., Vincenzi S. (2005) The interplay of eustasy, climate and human activity in the late Quaternary depositional evolution and sedimentary architecture of the Po Delta system. *Marine Geology*, 222-223, 19-48.

Strack O.D.L. (1976) A single-potential solution for regional interface problems in coastal aquifers. *Water Resources Research*, 12, 1165–1174.

Sudret B. (2008) Global sensitivity analysis using polynomial chaos expansions. *Reliability Engineering & System Safety*, 93, 964–979.

Tartakovsky D.M. (2012) Assessment and management of risk in subsurface hydrology: A review and perspective. *Advances in Water Resources*, 51, 247–260.

Tartakovsky D.M. (2007) Probabilistic risk analysis in subsurface hydrology. *Geophysical Research Letters*, 34, L05404, doi:10.1029/2007GL029245.

Teatini P., Ferronato M., Gambolati G., Gonella M. (2006) Groundwater pumping and land subsidence in the Emilia-Romagna coastland, Italy: Modeling the past occurrence and the future trend, *Water Resources Research*, 42, W01406, doi:10.1029/2005WR004242.

Teatini P., Ferronato M., Gambolati G., Bertoni W., Gonella M. (2005) A century of land subsidence in Ravenna, Italy. *Environmental Geology*, 47, 831-846.

Thomas A.J. (1972) Multiple Regression with Correlated Independent Variables. *Mathematical Geology*, 4, (3), 203-218.

Thomas J.J., Wallis K.F. (1971) Seasonal Variation in Regression Analysis. *Journal of the Royal Statistical Society. Series A (General)*, 134, 1, 57-72.

Ulazzi E., Antonellini A., Gabbianelli G. (2007) Coastal phreatic aquifer characterization of the Cervia Area. In *Stratigraphy and Sedimentology of Aquifers*; Vallone, R., Ed.; APAT: Parma, Italy.

US National Research Council. Review of Recommendations for Probabilistic Seismic Hazard Analysis: Guidance on Uncertainty and Use of Experts; National Academy Press: Washington, DC, USA, 1997; p. 84.

Vandenbohede A., Mollema P.N., Greggio N., Antonellini M. (2014) Seasonal dynamic of a shallow freshwater lens due to irrigation in the coastal plain of Ravenna, Italy. *Hydrogeology Journal*, 22, 893-909.

Venturini L. (2008) Impatto idrogeologico degli scavi sotto falda in ambito costiero (Dewatering dei terreni di fondazione). http://www.regione.emilia-romagna.it/wcm/geologia/canali/convegni_e_seminari/convegni_2008/2008_10_castell_arquato/06_venturini_catArq_2008.pdf. Presentazione orale in: Idrogeologia in Emilia-Romagna risorsa, applicazioni e tutela, 3 ottobre 2008 Palazzo del Podestà, Castell'Arquato, Piacenza.

Wang H.R., Wang C., Liu X., Kang J. (2014) An improved ARIMA model for precipitation simulations. *Non Linear Processes in Geophysics*, 21, 1159-1168.

Watson T.A., Werner A.D., Simmons C.T. (2010) Transience of seawater intrusion in response to sea level rise, *Water Resources Research*, 46, W12533, doi:10.1029/2010WR009564.

Webster M., Tatang M.A., McRae G.J. (1996) Application of the probabilistic collocation method for an uncertainty analysis of a simple ocean model. Technical report, MIT joint program on the science and policy of global change reports series no. 4, Massachusetts Institute of Technology.

Werner A.D., Bakker M., Post V.E.A., Vandenbohede A., Lu C., Ataie-Ashtiani B., Simmons C.T., Barry D.A. (2013) Seawater intrusion processes, investigation and management: Recent advances and future challenges. *Advances in Water Resources*, 51, 3–26.

Werner A.D., Bakker M., Post V.E.A., Vandenbohede A., Lu C., Ataie-Ashtiani B., Simmons C.T., Barry D.A. (2013) Seawater intrusion processes, investigation and management: Recent advances and future challenges. *Advances in Water Resources*, 51, 3–26.

Werner A.D., Ward J.D., Morgan L.K., Simmons C.T., Robinson N.I., Teubner M.D. (2012) Vulnerability indicators of sea water intrusion. *Ground Water*, 50, 48–58.

Werner A.D., Simmons C.T. (2009) Impact of sea-level rise on sea water intrusion in coastal aquifers. *Ground Water*, 47, 197–204, doi: 10.1111/j.1745-6584.2008.00535.x.

Wiener N.(1938) The homogeneous chaos. *American Journal of Mathematics*, 60, 897–936.

Winter C. L., Tartakovsky D.M. (2008) A reduced complexity model for probabilistic risk assessment of groundwater contamination. *Water Resources Research*, 44, W06501, doi:10.1029/2007WR006599.

Xiu D., Karniadakis G.E. (2002) The Wiener-Askey polynomial chaos for stochastic differential equations. *Journal of Scientific Computing*, 24(2), 619-644.

Yaglom A.M. (1962) An introduction to the theory of stationary random functions. Prentice-Hall, Inc., Englewood Cliffs, N.J.

Yang G., Bowling L. C. (2014) Detection of changes in hydrologic system memory associated with urbanization in the Great Lakes region. *Water Resources Research*, 50, doi:10.1002/2014WR015339.

Ringraziamenti

Questi tre anni di dottorato sono senza ombra di dubbio stati gli anni più intensi della mia vita, sotto tantissimi punti di vista. Mi hanno aiutato a crescere, mi hanno permesso di vivere l'esperienza della ricerca, con i suoi pro e i suoi contro. Ma soprattutto mi sono serviti per mettermi alla prova, e capire che nella ricerca quello che guida è la passione.

Vorrei ringraziare innanzitutto il mio supervisore, il Prof. Vittorio Di Federico, per la fiducia dimostrata nei miei confronti e il costante impegno dedicatomi durante lo svolgimento di questo dottorato.

Alla stessa maniera ringrazio il Prof. Daniel Tartakovsky, che nonostante la distanza, mi è stato vicino in questo percorso, sapendomi indirizzare con pazienza e costanza. Lo ringrazio anche per il periodo che mi ha permesso di vivere all'estero, riuscendo sempre a non farmi sentire mai sola, e per avermi permesso di conoscere tante persone che come me erano straniere in terra straniera, ma sentendosi a casa.

Un ringraziamento speciale va alla Dott.ssa Valentina Ciriello. Ci conosciamo da ormai tanti anni, eravamo compagne tra i banchi di Università. Anche nei momenti in cui ero giù di morale, è stata in grado di incoraggiarmi e starmi vicina, spronandomi a tirare fuori il meglio di me stessa. Per cui non solo vorrei ringraziarla, ma vorrei anche chiederle scusa, perché sicuramente tante volte sarò stata insopportabile per tanti motivi, ma per fortuna l'amicizia guarda oltre.

Ringrazio la mia famiglia per avermi sempre sopportato e supportato in qualsiasi momento della mia vita e di questo percorso, appoggiandomi in tutte le decisioni e lasciandomi libera nelle mie scelte.

Ringrazio i miei amici per essermi sempre vicini e per riuscire a farmi staccare la spina anche nei momenti difficili.

Last but not least, ringrazio Federico, la mia forza e il mio scoglio.